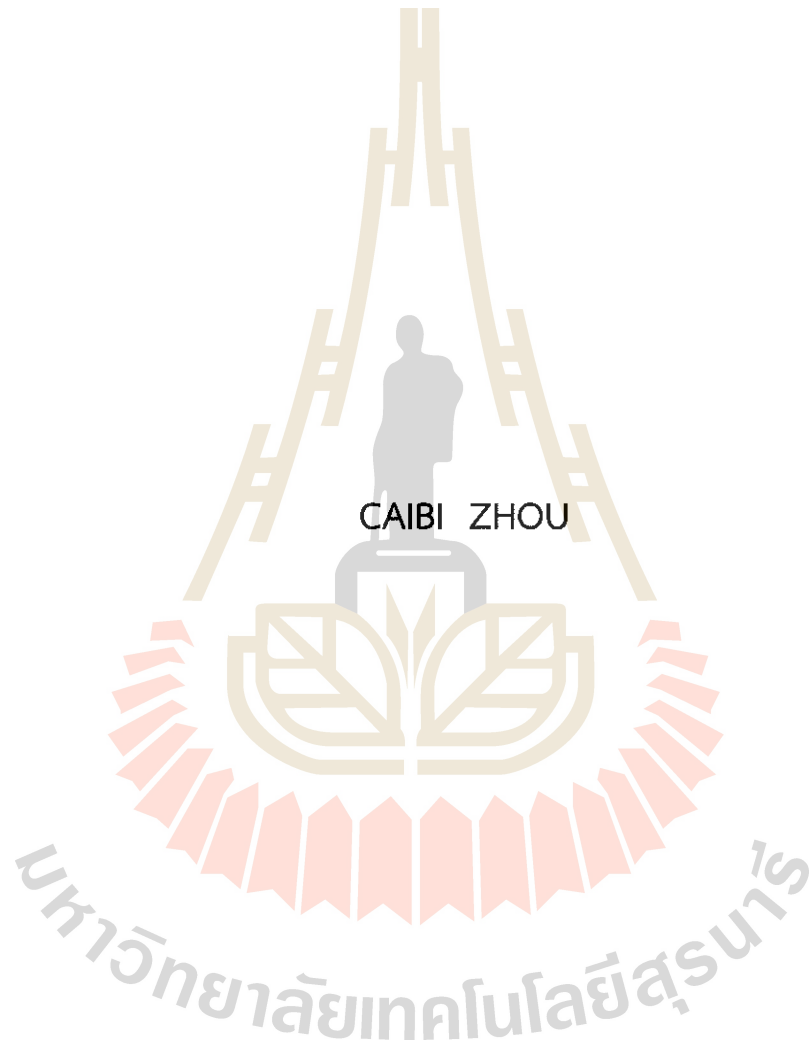
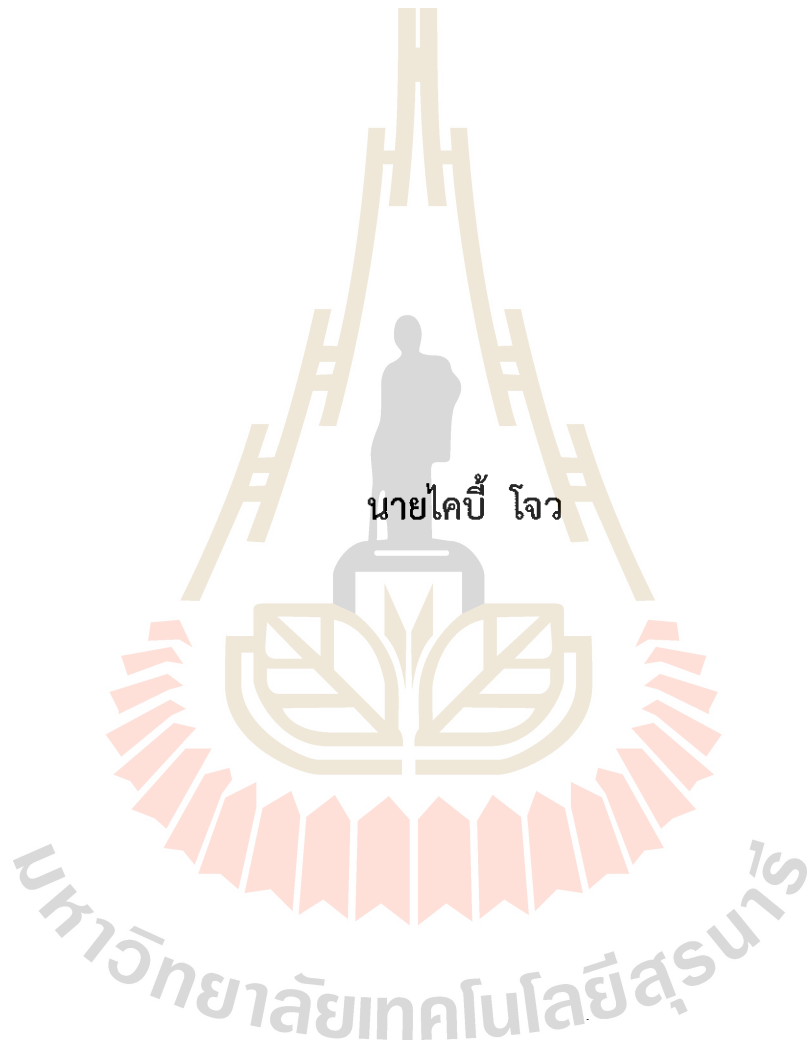


THE CHLOROPLAST GENOME ANALYSIS, METABOLITE PROFILES,
FLAVONOID BIOSYNTHESIS, HERBAL TEA ACUTE TOXICITY
EVALUATION, AND ANTIOXIDANT ACTIVITIES OF
Mussaenda pubescens



A Thesis Submitted in Partial Fulfillment of the Requirements for the
Degree of Doctor of Philosophy in Crop Science
Suranaree University of Technology
Academic Year 2023

การวิเคราะห์จีโนมของคลอโรพลาสต์ โปรไฟล์ของสารเมตาโบไลต์
การสังเคราะห์ฟลาโวนอยด์ การประเมินความเป็นพิษแบบเฉียบพลัน
และกิจกรรมการต้านสารอนุมูลอิสระของ *Mussaenda pubescens*

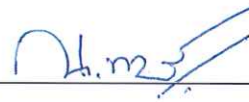


วิทยานิพนธ์นี้เป็นส่วนหนึ่งของการศึกษาตามหลักสูตรปรัชญาดุษฎีบัณฑิต
สาขาวิชาพืชศาสตร์
มหาวิทยาลัยเทคโนโลยีสุรนารี
ปีการศึกษา 2566

THE CHLOROPLAST GENOME ANALYSIS, METABOLITE PROFILES,
FLAVONOID BIOSYNTHESIS, HERBAL TEA ACUTE TOXICITY
EVALUATION, AND ANTIOXIDANT ACTIVITIES OF
Mussaenda pubescens

Suranaree University of Technology has approved this thesis submitted in partial fulfillment of the requirements for the Degree of Doctor of Philosophy.

Thesis Examining Committee



(Assoc. Prof. Dr. Nakorn Jongrunklang)

Chairperson



(Asst. Prof. Dr. Teerayoot Girdthai)

Member (Thesis Advisor)



(Asst. Prof. Dr. Piyaporn Chueamchaitrakun)

Member (Thesis Co-advisor)



(Prof. Dr. Piyada Alisha Tantasawat)

Member



(Asst. Prof. Dr. Thitiporn Machikowa)

Member



(Assoc. Prof. Dr. Yupaporn Ruksakulpiwat)

Vice Rector for Academic Affairs and
Quality Assurance

(Prof. Dr. Neung Teaumroong)

Dean of Institute of Agricultural
Technology

โคบี โจว : การวิเคราะห์จีโนมของคลอโรพลาสต์ โปรไฟล์ของสารเมตาโบไลต์ การสังเคราะห์ฟลาโวนอยด์ การประเมินความเป็นพิษแบบเฉียบพลันและกิจกรรมการต้านสารอนุมูลอิสระของ *Mussaenda pubescens*. (THE CHLOROPLAST GENOME ANALYSIS, METABOLITE PROFILES, FLAVONOID BIOSYNTHESIS, HERBAL TEA ACUTE TOXICITY EVALUATION, AND ANTIOXIDANT ACTIVITIES OF *Mussaenda pubescens*.) อาจารย์ที่ปรึกษา : ผู้ช่วยศาสตราจารย์ ดร.ธีรยุทธ เกิดไทย, 122 หน้า.

Mussaenda pubescens เป็นผลิตภัณฑ์จากธรรมชาติที่มีคุณค่าทางยา โดยเฉพาะลำต้นและใบที่นิยมใช้เป็นยารักษาโรคหรือตากแห้งเพื่อใช้แทนชา อย่างไรก็ตาม ยังไม่มีรายงานวิจัยเกี่ยวกับการเจริญและพัฒนาการหรือการใช้ประโยชน์จากพืชดังกล่าว งานวิจัยนี้ จึงเป็นการศึกษาที่ครอบคลุมครั้งแรก ซึ่งมีวัตถุประสงค์เพื่อตรวจสอบความสัมพันธ์ทางพันธุกรรม โปรไฟล์ของเมตาโบไลต์ การสังเคราะห์ฟลาโวนอยด์ และการประเมินการป้องกันความเป็นพิษแบบเฉียบพลัน และความสามารถในการต้านสารอนุมูลอิสระของ *M. pubescens* งานวิจัยประกอบด้วย 4 งานทดลองดังนี้ งานทดลองที่ 1. การทดลองนี้ ดำเนินการเพื่อศึกษาลักษณะทางสัณฐานวิทยาและจีโนมของคลอโรพลาสต์ ของ *M. pubescens* ทำการทดลองโดยการตรวจลำดับเบสของจีโนมในคลอโรพลาสต์โดยใช้ Illumina NovaSeq 6000 platform จากการศึกษาลักษณะทางสัณฐานวิทยาของ *M. pubescens* พบว่า *M. pubescens* และ *M. hirsutula* มีความสัมพันธ์ใกล้ชิดกัน ขนาดจีโนมของคลอโรพลาสต์ของ *M. pubescens* มีความยาวทั้งหมด 155,122 คู่เบส (bp) ผลการวิเคราะห์สายวิวัฒนาการแสดงให้เห็นว่าสปีชีส์ในสกุลเดียวกัน มีความใกล้ชิดกันทางพันธุกรรม นอกจากนี้ *M. hirsutula* ยังมีความเชื่อมโยงทางพันธุกรรมอย่างใกล้ชิดกับ *M. pubescens* โดยทั้งสองสปีชีส์มีการกระจายที่ทับซ้อนกันในพื้นที่ของประเทศจีน งานทดลองที่ 2. การศึกษานี้ใช้เทคนิค ultra-performance liquid chromatography-tandem mass spectrometry (UPLC-MS/MS) เพื่อตรวจสอบการเปลี่ยนแปลงของสารเคมี และศึกษาความสัมพันธ์ระหว่างสารเมตาโบไลต์และความสามารถในการต้านสารอนุมูลอิสระของใบ *M. pubescens* ผลการศึกษาพบว่าใบของ *M. pubescens* มีสารเมตาโบไลต์ถึง 957 ชนิด ซึ่งส่วนใหญ่เป็นกรดฟีนอลิก ไขมัน และเทอร์พีนอยด์ และพบว่า มีความแตกต่างของการสะสมสารเมตาโบไลต์ (DAMs) 317 ชนิดในใบ ความเข้มข้นของฟีนอล ฟลาโวนอยด์ และแอนโทไซยานินทั้งหมดลดลงเมื่อใบ *M. pubescens* เติบโตและพัฒนาในขณะที่เทอร์พีนอยด์เพิ่มขึ้นอย่างมีนัยสำคัญ สารฟีนอลิก ฟลาโวนอยด์ เทอร์พีนอยด์ และแอนโทไซยานินเป็นปัจจัยหลักที่มีอิทธิพลต่อปฏิกิริยาการต้านสารอนุมูลอิสระของใบ *M. pubescens* งานทดลองที่ 3. การศึกษานี้ใช้การวิเคราะห์เมตาโบลอมและทรานสคริปโตมเพื่อตรวจสอบสารเมตาโบไลต์และการแสดงออกของยีนที่สำคัญของตาใบ ใบอ่อนและใบแก่ของ *M. pubescens* ผลการทดลองพบสารฟลาโวนอยด์ทั้งหมด 81 ชนิดในใบของ *M. pubescens* และมีการแสดงออกของยีนที่เกี่ยวข้องกับการสังเคราะห์ฟลาโวนอยด์เพิ่มขึ้น (HCT, CHS, E5.5.1.6 และ PGT1) นอกจากนี้ ยังพบว่าการแสดงออกของยีนที่เกี่ยวข้องกับ flavonoid 3'-monooxygenase (CYP75B1), anthocyanidin synthase (ANS), naringenin 3-dioxygenase (F3H), bifunctional dihydroflavonol 4-reductase/flavanone 4-reductase (DFR) และ flavanone 7-O-glucoside 2"-O-beta-L-rhamnosyltransferase (C12RT1) มีความสัมพันธ์สูงกับสารเมตาโบไลต์ที่เกี่ยวข้องกับการสังเคราะห์ฟลาโวนอยด์ตลอดวงจรการเจริญเติบโตของใบ งาน

ทดลองที่ 4. ในการศึกษาครั้งนี้ ใบสดของ *M. pubescens* ถูกผลิตเป็นชาดำ (MpBT) โดยใช้กระบวนการแปรรูปชาดำแบบดั้งเดิม ตัวอ่อนของปลาหมึกนำมาใช้เพื่อศึกษาผลการป้องกันความเสียหายจากออกซิเดชันที่เกิดจากสาร CuSO_4 ผลการทดลองพบว่า MpBT สามารถเพิ่มอัตราการฟัก อัตราการรอดชีวิต ลักษณะทางสัณฐานวิทยา และลดอัตราการเกิดความผิดปกติอย่างมีนัยสำคัญ ($p < 0.05$) นอกจากนี้ MpBT ยังสามารถยับยั้งการสะสมของสาร reactive oxygen species (ROS) กระตุ้นการทำงานของเอนไซม์ต้านอนุมูลอิสระและทำงานของยีนที่เกี่ยวข้อง นอกจากนี้ MpBT ยังป้องกันไฮโดรโคโรนที่ทำให้เกิดการอักเสบ และส่งเสริมยีนที่เกี่ยวข้องกับการตายของเซลล์ที่ถูกกระตุ้นด้วยสาร CuSO_4 ในเอ็มบริโอของปลาหมึก ซึ่งรายงานนี้เป็นรายงานฉบับแรกเกี่ยวกับลักษณะทางสัณฐานวิทยา จีโนมของคลอโรพลาสต์ โปรไฟล์ของสารเมตาโบไลต์ของของ *M. pubescens* ซึ่งสามารถใช้เป็นข้อมูลอ้างอิงสำหรับกลไกการควบคุมระดับโมเลกุลของการเปลี่ยนแปลงสีในการพัฒนาการและการใช้ประโยชน์จาก *M. pubescens*



สาขาวิชาเทคโนโลยีการผลิตพืช
ปีการศึกษา 2566

ลายมือชื่อนักศึกษา... *Caibi Zhou*
ลายมือชื่ออาจารย์ที่ปรึกษา... *[Signature]*

CAIBI ZHOU : THE CHLOROPLAST GENOME ANALYSIS, METABOLITE PROFILES, FLAVONOID BIOSYNTHESIS, HERBAL TEA ACUTE TOXICITY EVALUATION, AND ANTIOXIDANT ACTIVITIES OF *Mussaenda pubescens*. THESIS ADVISOR : ASST. PROF. DR. TEERAYOOT GIRDTHAI, 122 PP.

Morphological characteristics/*Mussaenda pubescens*/Chloroplast genomes/
Phylogenetic relationship/Metabolome/Antioxidants/Quality traits/
Transcriptome/Flavonoids biosynthesis/Acute Toxicity/*Zebrafish*

Mussaenda pubescens is a valuable source of medicinal natural products, particularly stems and leaves, which have been used medicinally or dried as a tea substitute. However, no research on their growth and development or their utilization has been reported. This was the first comprehensive research aimed to investigate the genetic relationship, metabolite profiles, flavonoid biosynthesis, and evaluation of its protective effect from acute toxicity and antioxidant properties of *M. pubescens*. This research included four experiments. Experiment 1: This experiment was conducted to investigate the morphological characteristics and complete chloroplast (cp) genome of *M. pubescens*. The cp was sequenced using the Illumina NovaSeq 6000 platform. According to the morphological characteristics of *M. pubescens*, there is a close relationship between *M. pubescens* and *M. hirsutula*. The cp genome of *M. pubescens* spanned a total length of 155,122 bp. The results of phylogenetic analyses demonstrated that species within the same genus displayed a tendency to group closely together. Furthermore, *M. hirsutula* showed a close genetic connection to *M. pubescens*, with the two species having partially overlapping distributions in China. Experiment 2: This study used ultra-performance liquid chromatography-tandem mass spectrometry (UPLC-MS/MS) technique to investigate substance changes and the relationship between metabolites and antioxidant capacity in *M. pubescens* leaves. The results showed that *M. pubescens* leaves contained 957 metabolites, the majority of which were phenolic acids, lipids, and terpenoids. A total of 317 differentially accumulated metabolites (DAMs) in leaves were screened. Total phenolics, flavonoids, and anthocyanin concentrations decreased as *M. pubescens* leaves grew and developed, whereas terpenoids increased significantly. Phenolics, flavonoids, terpenoids, and anthocyanins were the primary factors influencing the antioxidant activity of leaves. Experiment 3: This study used metabolome and transcriptome analyses to investigate the key metabolites and genes from bud leaves, tender leaves, and mature leaves in *M. pubescens*. The results showed a total of 81 individual

flavonoids in *M. pubescens* leaves. The expression of flavonoid biosynthesis genes (HCT, CHS, E5.5.1.6, and PGT1) were up-regulated. Additionally, the expression of genes involved in flavonoid 3'-monooxygenase (CYP75B1), anthocyanidin synthase (ANS), naringenin 3-dioxygenase (F3H), bifunctional dihydroflavonol 4-reductase/flavanone 4-reductase (DFR), and flavanone 7-O-glucoside 2"-O-beta-L-rhamnosyltransferase (C12RT1), exhibited a highly correlative relationship with metabolites in the flavonoid biosynthesis across the whole growth cycle of *M. pubescens* leaves. Experiment 4: In this study, the fresh leaves of *M. pubescens* were produced into black tea (MpBT) using traditional black tea processing procedures. Zebrafish embryos were used to study the protective effects of CuSO₄-induced oxidative damage. The results showed that MpBT significantly improved hatching, survival rates, morphological characteristics, and decreased malformation rates ($p < 0.05$). Furthermore, MpBT inhibited the generation of reactive oxygen species (ROS), recovered the activities of antioxidant enzymes, and increased oxidative stress-associated genes. Other than that, MpBT also prevented pro-inflammatory cytokines and improved apoptosis-associated genes induced by CuSO₄ in *zebrafish* embryos. This first report on the morphological characteristics, *cp genome*, and metabolite profiles of *M. pubescens* provides a reference value for the molecular regulation mechanism of leaf color alteration and the development and utilization of *M pubescens*.



School of Crop Production Technology
Academic Year 2023

Student's Signature.....*Ceibi Zhou*
Advisor's Signature.....*Teenyoot Aisalmaj*

ACKNOWLEDGEMENT

I would like to express my sincere gratitude to my thesis advisor, Asst. Prof. Dr. Teerayoot Girdthai, for providing me the opportunity to study toward my doctor's degree in Crop Science at Suranaree University of Technology. Without her well-designed plan and careful review of the draft, this thesis would have never been possible. Her kind supervision, valuable advice and enthusiastic encouragement are invaluable for me.

I would like to thank Asst. Prof. Dr. Piyaporn Chueamchaitrakun for guidance, supporting and providing knowledge on the experiment.

I am very grateful to Assoc. Prof. Dr. Nakorn Jongrunklang, Prof. Dr. Piyada Alisha Tantasawat and Asst. Prof. Dr. Asst. Prof. Thitiporn Machikowa committee members of this thesis, for their valuable comments and suggestions during my qualifying, proposal and thesis examination.

I sincerely thank my lab members, all teachers and staff in the School of Crop Production Technology, Suranaree University of Technology for their help and taking care while I was studying in Thailand.

Finally, I would like to express my special thanks to my family for their encouragement, supports and understandings.

Caibi Zhou

มหาวิทยาลัยเทคโนโลยีสุรนารี

CONTENTS

	Page
ABSTRACT (THAI)	I
ABSTRACT (ENGLIST).....	III
ACKNOWLEDGEMENT	V
CONTENTS.....	VI
LIST OF TABLES.....	X
LIST OF FIGURES.....	XI
LIST OF ABBREVIATIONS.....	XIII
CHAPTER	
I INTRODUCTION	1
II LITERATURE REVIEW	6
2.1. <i>M. pubescens</i> germplasm.....	6
2.1.1 Genetic characterization	6
2.1.2. Microsatellite markers.....	8
2.1.3. <i>cp genome</i>	8
2.2. Compounds and metabolite profiles.....	9
2.2.1. Compounds.....	10
2.2.2. Metabolite profiles.....	11
2.3. Leaf color change and flavonoid biosynthesis.....	13
2.3.1. Leaf color change	13
2.3.2. Flavonoid biosynthesis.....	14
2.3.3. Transcriptomics and metabolomics	16
2.4. Toxicology and pharmacology.....	17
2.4.1. Efficacy in vitro.....	17
2.4.2. <i>Zebrafish</i>	19
III MATERIALS AND METHODS	22
3.1. The complete <i>cp genome</i> of <i>M. pubescens</i> and phylogenetic analysis.....	22
3.1.1. Plant samples	22
3.1.2. Complete <i>cp genome</i> sequence	22
3.1.3. Phylogenetic analysis	22

CONTENTS (continued)

	Page
3.2. Metabolomics reveals the importance of metabolites in <i>M. pubescens</i>	23
3.2.1. Materials.....	23
3.2.2. Metabolome analysis	23
3.2.3. Chemical components and antioxidant analysis.....	25
3.3. Metabolomic and Transcriptomic Profiling Reveals the Flavonoid Components and Discoloration Mechanism of <i>M. pubescens</i> Leaves.....	26
3.3.1. Plant materials.....	26
3.3.2. Chemical composition	27
3.3.3. Metabolite profiles analysis	27
3.3.4. Transcriptome sequencing analysis.....	27
3.3.5. Correlation analysis of metabolites and genes.....	28
3.3.6. Quantitative real-time PCR (qRT-PCR) validation.....	28
3.4. The Acute Toxicity Assessment and Protective Effects of <i>M. pubescens</i>	28
3.4.1. <i>M. pubescens</i> tea processing.....	28
3.4.2. Preparation and extraction of MpBT	29
3.4.3. <i>Zebrafish</i> breeding and experimental conditions	29
3.4.4. The median lethal concentration (LC50)	30
3.4.5. Exposure of <i>zebrafish</i> embryos to MpBT.....	30
3.4.6. Oxidative-stress-related biochemical analyses	31
3.4.7. Protein expression analysis	32
3.4.8. RNA extraction and gene expression analysis	32
3.4.9. Statistical analyses	32
IV RESULTS AND DISCUSSION.....	33
4.1. The complete <i>cp genome</i> of <i>M. pubescens</i> and phylogenetic analysis.....	33
4.1.1 Morphological characteristics of <i>M. pubescens</i>	33
4.1.2 <i>cp genome</i> features of <i>M. pubescens</i>	38
4.1.3 Phylogenetic analysis	47
4.2. Metabolomics reveals the importance of metabolites in <i>M. pubescens</i>	49

CONTENTS (continued)

	Page
4.2.1 Metabolomic profiling of Mp leaves at different developmental stages.....	49
4.2.2 PCA and OPLS-DA for Mp	51
4.2.3 Differentially accumulated metabolites screening, functional annotation, and enrichment analysis among the Mp leaves at different developmental stages.....	53
4.2.4 Evaluation of the different metabolites during the Growth and development of Mp leaves.....	58
4.2.5 Total phenolics, flavonoids, terpenoids, anthocyanins, and antioxidant activity.....	63
4.2.6 Correlation analysis between DAMs and antioxidant activity	65
4.3. Metabolomic and Transcriptomic Profiling Reveals the Flavonoid Components and Discoloration Mechanism of <i>M. pubescens</i> Leaves.....	67
4.3.1 Differences in biological phenotypes, pigment and functional components	67
4.3.2 Metabonomic analysis.....	69
4.3.3 Transcriptomic analysis	72
4.3.4 Correlation analysis of transcriptome and metabolome... ..	76
4.3.5 TFs related to metabolomic biosynthesis	80
4.3.6 qRT-PCR validation of DEGs in transcriptome sequencing.....	82
4.4. The Acute Toxicity Assessment and Protective Effects of <i>M. pubescens</i>	84
4.4.1 Sensory evaluation and components analysis of MpBT....	84
4.4.2 Acute toxicity assessment of MpBT.....	84
4.4.3 Morphological and developmental effects of <i>zebrafish</i> embryos exposure to MpBT.....	86
4.4.4 Analysis of oxidative-stress-related biochemical indicators.....	89
4.4.5 Protein expression levels.....	90

CONTENTS (continued)

	Page
4.4.6 Effects on antioxidant, inflammation, and apoptosis related gene expression	91
V CONCLUSION	95
5.1. The complete <i>cp genome</i> of <i>M. pubescens</i> and phylogenetic analysis.....	95
5.2. Metabolite profiles of <i>M. pubescens</i>	95
5.3. Metabolomic and Transcriptomic Profiling Reveals the Flavonoid Components and Discoloration Mechanism of <i>M. pubescens</i>	96
5.4. The Acute Toxicity Assessment and Protective Effects of <i>M. pubescens</i>	96
REFERENCES	98
BIOGRAPHY	122

LIST OF TABLES

Table	Page
4-1-1. Morphological comparison of <i>M. pubescens</i> and <i>M. hirsutula</i>	34
4-1-2. Characteristics of <i>M. pubescens</i> cp genome.....	39
4-1-3. The nucleotide composition of the complete cp genomes of <i>M. pubescens</i>	41
4-1-4. Lists of annotated genomic genes for <i>M. pubescens</i>	42
4-1-5. Characteristics and sizes of the intron and exon genes from..... <i>M. pubescens</i>	44
4-1-6. Codon usage of <i>M. pubescens</i> cp genome from RSCU tools.....	45
4-4-1. Acute toxicity assessment of MpBT.....	85
4-4-2. Significance analysis of <i>zebrafish</i> morphological index of MpBT at different concentrations.....	88

LIST OF FIGURES

Figure	Page
4-1-1. Morphological characters of <i>M. pubescens</i>	33
4-1-2. The <i>cp genome</i> maps of <i>M. pubescens</i>	40
4-1-3. The phylogenetic tree of <i>M. pubescens</i>	47
4-2-1. Phenotypes of the leaves surface and back of MP at the different growth stages.....	49
4-2-2. Abundance and differential expression of metabolites in the leaves of Mp.....	50
4-2-3. Orthogonal partial least squares-discriminant analysis scores of Mp leaves.....	52
4-2-4. Differential metabolites present in Mp leaves.....	55
4-2-5. Trend analysis of differential metabolites during the development of Mp leaves.....	56
4-2-6. KEGG pathways analysis in Mp leaves.....	57
4-2-7. Pie chart of the number of different types in Mp leaves.....	59
4-2-8. The content of total phenolics, flavonoids, terpenoids, anthocyanin, and antioxidant activities of DPPH, ABTS and FRAP assays during three different stages of Mp leaves.....	64
4-2-9. Correlation analysis between DAMs and antioxidant activity.....	66
4-3-1 Phenotypes and colour of the leaves surface (A) and back (B) of MP at the different growth stages.....	67
4-3-2 Difference of color and functional components in different leaves of Mp.....	68
4-3-3 Quantitative analysis of metabolite components in Mp leaves.....	69
4-3-4 Differential accumulated flavonoids metabolites in Mp leaves.....	70
4-3-5 Overview of transcriptome analysis of Mp leaves.....	74
4-3-6 KEGG enrichment analyses of DEGs in Mp leaves.....	76
4-3-7 Integrated analysis of DAMs and DEGs.....	77
4-3-8 Transcript profiling of genes in the phenylpropanoid and flavonoid biosynthetic pathways in MpBud, MpTea, and MpMat.....	79
4-3-9 qRT-PCR validation of candidate genes associated with phenylpropanoid, flavonoid and anthocyanidin biosynthesis in Mp leaves.....	82
4-4-1. <i>Mussaenda pubescens</i> black tea (MpBT)	84

LIST OF FIGURES (continued)

Figure	Page
4-4-2. Effects of MpBT on CuSO ₄ -induced developmental damage in <i>zebrafish</i> embryos at 24-144 hpf.....	87
4-4-3. The morphological features of <i>zebrafish</i> embryos exposed to CuSO ₄	88
4-4-4. Effects of on CuSO ₄ -induced oxidative damage in <i>zebrafish</i> embryos at 120 hpf.....	90
4-4-5. Effects of MpBT on CuSO ₄ -induced protein expression level in <i>zebrafish</i> embryos at 120 hpf.....	91
4-4-6. Effects of MpBT on CuSO ₄ -induced antioxidant-, inflammation- and apoptosis-related gene expression in <i>zebrafish</i> embryos at 120 hpf.....	92



LIST OF ABBREVIATIONS

Mp	=	<i>Mussaenda pubescens</i>
TCM	=	traditional Chinese medicine treatment
SSC	=	short single-copy
LSC	=	large single-copy
IR	=	inverted repeats
UPLC-MS/MS	=	ultra-performance liquid chromatography-tandem mass spectrometry
ROS	=	reactive oxygen species
L	=	long-styled
S	=	short-styled
cp	=	Chloroplasts
BI	=	Bayesian inference
QNUN	=	Qiannan Normal University for Nationalities
PCA	=	Principal component analysis
HCA	=	hierarchical cluster analysis
DMAs	=	Differential metabolites analysis
SD	=	standard deviation
TPTZ	=	2,4,6-Tri(2-pyridyl)-S-triazine
OPLS-DA	=	orthogonal partial least squares-discriminant analysis
NR	=	NCBI non-redundant protein database
COG	=	Clusters of Orthologous Groups of proteins
KOG	=	EuKaryotic Orthologous Groups of proteins database
Pfam	=	Pfam protein families database
GO	=	Gene Ontology
KEGG	=	Kyoto Encyclopedia of Genes and Genomes
FDR	=	false discovery rate
DEGs	=	differentially expressed genes
qRT-PCR	=	Quantitative real-time PCR
PVDF	=	Polyvinylidene fluoride
LC50	=	The median lethal concentration
DCFDA	=	2',7'- dichlorofluorescein diacetate
qRT-PCR	=	quantitative real-time polymerase chain reaction

LIST OF ABBREVIATIONS (Continued)

SE	=	standard error
CDS	=	Protein-coding genes
POD	=	anthocyanin, peroxidase
CAT	=	catalase
SSC	=	soluble solid content
TEAC	=	trolox equivalent capacity
FRAP	=	ferric reducing capacity
DPPH	=	2,2-diphyl-1-pic-rylhydrazyl
TFs	=	transcription factors
HSV-1	=	Herpes Simplex Virus type 1
IC50	=	50% inhibition concentrations
SI	=	selective indices
GE	=	<i>Gelsemium elegans</i>
RA	=	Rotundine acid
GSH	=	glutathione
LPO	=	lipid peroxidation
ROS	=	reactive oxygen species
MpBT	=	<i>Mussaenda pubescens</i> black tea
hpf	=	hour post-fertilization
CAT	=	catalase
SOD	=	superoxide dismutase
MDA	=	malondialdehyde
DCFDA	=	2',7'- dichlorofluorescein diacetate
qRT-PCR	=	quantitative real-time polymerase chain reaction
H ₂ O ₂	=	hydrogen peroxide
HSP70	=	heat shock protein 70
PCD	=	programmed cell death
Bcl-2	=	B-cell lymphoma-2
Bax	=	Bcl-2-associated X protein
Mn-sod	=	manganese-containing superoxide dismutase
IL-1 β	=	interleukin-1 β
TNF- α	=	tumor necrosis factor- α
INF- γ	=	interferon- γ

CHAPTER I

INTRODUCTION

Mussaenda pubescens (Mp), a member of the *Rubiaceae* family (Deng & Zhang, 2006), is a liana-like shrub that is distributed in a shady hillside, valley, and shrub jungle of eastern, southern, and southwestern China. The stems and leaves of Mp, with a sweet and cool taste, have been used for medicine or dried instead of tea in China's ethnic minority areas (Li et al., 2017). We found Mp at the general survey of plants germplasm resources in Guizhou Province. There are several interesting questions about the plant: (1) as the maturity of blades, the leaf color of Mp gradually changes from purple to green. (2) Mp has been used as medicine or a substitute for tea in ethnic minority areas of China, but it has not been widely developed and utilized.

The natural compounds of plants have been particularly important because of their applications in the chemical, food, and pharmaceutical industries (Yang et al., 2016). Most of the research about Mp have concentrated on the identification of bioactive components. Many components involved in saponins (e.g., mussaendosides D, E, H, S (Zhao et al., 1996), I, J (Zhao et al., 1996)), monoterpenes (e.g., mussaenins A, B, C (Zhao et al., 1994)), and triterpenoid saponins (e.g., mussaendosides U, V (Zhao et al., 1997), R, S (Zhao et al., 1995), G, K (Zhao et al., 1996), P, Q (Zhao et al., 1994), F (WM et al., 1995)), cycloartane saponin (e.g., mussaenoside X, O, G (Huong et al., 2021), M, N (XU et al., 1992)), phenolic glycoside (e.g., mussaenoside L (Zhao et al., 1996)), and shanzhiside methylester, barlerin, (6S, 9R)-roseoside and coniferin (Việt & Trung, 2017). The main aromatic constituents in the leaves of Mp are monoterpenoids and sesquiterpenes involved in β -ionone, linalool, and limonene, with 7.2%, 5.6%, and 3.6%, respectively.

Many special metabolites, also known as natural products, are synthesized, and accumulated in plants, providing an abundant source for modern pharmacy (Yang et al., 2016). Especially, traditional Chinese medicine treatment (TCM) provides valuable potentiality for discovering natural products with bioactive and developing new modern pharmaceuticals (Fidan et al., 2022). Medicinal plants have been widely used in treating diseases and infections throughout history as traditional healing remedies due to their broad therapeutic spectrum and minimal or no side effects. Mp, with the most significant number of compounds, was found in *Mussaenda*, which has been applied in TCM. The extracts of Mp showed immunoprotective, hemolytic (Xu et al.,

1996), anti-RSV activity (Li et al., 2004), and inhibition β -hematin formation, osteoclast formation (Huong et al., 2021) and HSV-1 activity (Huong et al., 2021). In addition, Mp detoxified the *Gelsemium elegans* (Xu et al., 2012) and improved prominently analgesic effect (Wang et al., 2017). The whole plants of Mp have been applied to TCM for laryngopharyngitis, acute gastroenteritis, and dysentery (Chen et al., 2013) as a diuretic, antiphlogistic, diaphoretic, antipyretic, detoxify poisons and contraceptive agent (Qin & Xu, 1998). In summary, there were not reported that the genetic relationship, metabolite profiles and flavonoid biosynthesis of *M. pubescens*, as well as acute toxicity assessment and protective effects of its tea products.

The genus *Mussaenda* L., which belongs to the family *Rubiaceae* belonging to *Rubiaceae*, consists of approximately 120 species primarily found in Africa, the Pacific islands, and Asia, including 31 species, 1 variety, and 1 variant in China. The morphology of trichomes and the shape of calyx and corolla are valuable characteristics for species identification (Grecebio et al., 2016). The species of *Mussaenda* can be easily distinguishable from other genera due to their expanded petaloid calycophylls, terminal umbel inflorescence, and fleshy berries. *M. pubescens*, a liana-like shrub belonging to the genus *Mussaenda* (Deng et al., 2006), is categorized into two forms known as *M. pubescens* f. *pubescens* and *M. pubescens* f. *clematidiflora*, which are identified as the same species through 'the Key to Dioecious Species of *Mussaenda* in China'.

In general, the chloroplast is a semi-autonomous replication organelle (Xue et al., 2019) and contains independent cpDNA (Choi & Park, 2015). Some species exhibit a circular structure consisting of one short single-copy (SSC) region, one large single-copy (LSC) region, and two inverted repeats (IR) regions that serve as a separator between the LSC and SSC regions (Xue et al., 2019). The contraction and expansion of the IR, LSC, and SSC regions are common phenomena in the process of evolution (Huang et al., 2014), which regions constitute the primary factors that contribute to the differences in size observed in cp genomes (Yao et al., 2015). SSRs identified in cp genomes exhibit high conservation in terms of types and numbers, and many mono-nucleotide repeats consist of base A or T, making them particularly well-suited as genetic markers for plant molecular studies (Khan et al., 2019). The cp genome offers valuable insights for various scientific fields such as species identification, population genetics, phylogenetics, and genetic engineering research due to its similar structure (Luo et al., 2021; Wu et al., 2021), large genetic information, highly conserved sequences (Dobrogojski et al., 2020), high-valuable information (Li et al., 2019), and stable maternal inheritance (Wu et al., 2020). Therefore, the cp genome has become an ideal resource for species and higher-order phylogenetic inference (Fan et al., 2021),

serving as a molecular marker in taxonomic research (Han et al., 2022). The complete *cp genomes* of various plant species within the same genus were sequenced using the Illumina NovaSeq 6000 platform, thus providing valuable insights for species identification, evolutionary analysis, and phylogenetic studies of these plants (Wang et al., 2022). In the present study, the complete *cp genomes* of Mp were sequenced using the Illumina NovaSeq 6000 platform, elucidated the morphology and phylogeny of Mp, and explored the genetic relationship of Mp. This research will serve as a valuable resource for the species identification, evolution, population genetics, and phylogenetic analyses of *Mussaenda*.

Plants produce and accumulate many secondary metabolites, or natural products, which are a rich source of pharmaceuticals. TCM has great potential for utilizing bioactive natural products and developing new pharmaceuticals (Fidan et al., 2022). The genus *Mussaenda* contains medicinal natural substances such as flavonoids, triterpenes, saponines, and iridoids (Vidyalakshmi et al., 2008), of which the abundance and wide availability of the iridoids make this plant a potential target for researching this drug's activity (Việt et al., 2017). Mp contained the greatest quantity of compounds among *Mussaenda*. Triterpenoids, triterpenes, iridoid glycosides, saponins, and organic acids were reported to be the essential ingredients in Mp based on phytochemical research (Wang & Kang, 2013).

However, few studies have provided a comprehensive overview of the chemical components and functional properties of Mp at various stages of leaf development, which have been used in tea production and pharmaceutical applications. Furthermore, the dynamic analysis of metabolites at various growth stages of Mp leaves is largely unknown. Utilizing biochemical analysis and widely targeted metabolomics analysis based on ultra-performance liquid chromatography-tandem mass spectrometry (UPLC-MS/MS), it is possible to detect a broad spectrum of metabolites simultaneously and obtain valuable chemical information rapidly. Understanding metabolite-induced bioactivity differences in Mp is critical for utilizing and developing Mp plants with improved nutritional properties. The present study utilized a widely targeted metabolome approach to analyze the species and relative contents of metabolomic profiles in Mp leaves at different stages. This method enables the investigation of the dynamic changes that occur in metabolites within Mp leaves, as well as the qualitative and quantitative determination of the nutrient composition. Therefore, this study aimed to determine the specific components responsible for the antioxidant properties and health benefits of Mp, including total phenolics, flavonoids, terpenoids, and anthocyanins. This research will offer valuable insights for the utilization and development of Mp resources.

Our initial investigations and observations have uncovered an intriguing phenomenon: As the increase of elongation, the leaf color of Mp gradually transitions from purple to green. This might be caused by the metabolism of different components, which could be inferred that mature leaf probably contains more chlorophyll, while bud leaf contains more anthocyanins. Flavonoids are a significant class of plant secondary metabolites. The Mp leaves used in previous studies were collected solely from one developmental stage, and the majority of analyzed compounds in Mp leaves fall into four categories involved in flavonoids, polyphenols, saponins triterpenic, and organic acids. Flavonoid compounds, especially anthocyanins, are responsible for leaf color and physiological and biochemical processes (Zhou et al., 2016). Additionally, leaf color is closely associated with the structural genes of pigments. The genes involved in flavonoid biosynthesis (PAL, CHS, CHI) along with their transcription factors (MYB, HD-Zip, bHLH) exhibited specific and increased expression during the purple-red periods (Jiao et al., 2020; Shi et al., 2020). Leaf color is related to some key structural genes in flavonoid and anthocyanin biosynthesis such as PAL, CHS, CHI, F3H, DFR, ANS and UFGT and regulatory factors such as MYB, MADS-box, bHLH, WD40, bZIP and WRKY (Li et al., 2021; Lu et al., 2021). Combined transcriptomics and metabolomics can not only result in a greater understanding of the expression of specific genes but also result in the identification of functional genes related to biological characteristics from the changes in the level of metabolites and reveal the regulatory mechanisms of specific genes (Chu et al., 2020). However, comprehensive and dynamic research on the metabolites present in Mp leaves at various stages of development is currently lacking. The metabolomic and transcriptomic profiles of the apical bud, tender leaf, and mature leaf of Mp were investigated in this study. The expression of associated genes, and biochemical components involved in anthocyanins, chlorophyll, carotenoids, total flavonoids, polyphenols, flavanols, and terpenoids were further determined to reveal the differences in leaves at three distinct developmental stages. This study elucidated the dynamic changes in metabolites and the molecular regulatory mechanisms underlying leaf color change in Mp.

Oxidative stress, which is a constant buildup of reactive oxygen species (ROS), is a disruption of the balance between the pro-oxidation and anti-oxidation systems caused by an increase in free radicals and a decrease in the antioxidant defense system's activity (Shashni et al., 2023). ROS commonly serves as a biomarker of oxidative stress. When oxidative stress occurs, the excessive generation of ROS can induce inflammation by up-regulate the expression of pro-inflammatory gene, resulting in apoptosis (Félix et al., 2020; Lite et al., 2022) and the occurrence of various chronic diseases (Biswas, 2016). CuSO_4 has been acted as an inducer in studies of the anti-

oxidation, anti-inflammation, and anti-apoptosis of some bioactive substances in vivo (Ai et al., 2023). Previous studies have reported that CuSO_4 -induced *zebrafish* larvae model evaluated the potential protective effects of surfactin on anti-inflammatory and antioxidation, indicating that surfactin decreased the migration of neutrophils, as well as reduced the levels of oxidative stress and inflammatory factors (Wang et al., 2021). In addition, methanolic extracts of *Mussaenda pubescens* leaves has been demonstrated to have significant anti-osteoclastogenic activity (Huong et al., 2021).

Zebrafish genes are homogenous with human genes (Ma et al., 2022). The embryonic development of *zebrafish* is transparent, with advantages such as small size and short development cycle (Teame et al., 2019). The simplicity and multifunctionality of *zebrafish* were one of the optimum spinal animal models for various types of research involved in toxicology, pharmacology, and developmental biology (SoussiYanicostas, 2022). Therefore, a CuSO_4 -induced *zebrafish* model was performed to evaluate the protective effects of Mp against oxidative damage and inflammation during the development stage of *zebrafish* larvae, and provided available information for the development and utilization of *M. pubescens* germplasm resources.



CHAPTER II

LITERATURE REVIEW

2.1. *M. pubescens* germplasm

M. pubescens is a plant of the genus *Musaenda* L., generally grouped into *M. pubescens* f. *pubescens* and *M. pubescens* f. *clematidiflora* according to their origin, habitat, and biological characteristics. According to the **Key to Dioecious Species of *Musaenda* in China**, *M. pubescens* Ait. f. var. is a new variety of the genus *M. pubescens*, which are same species and exactly like *M. pubescens* var. *pubescens* with yellow flowers (Deng et al., 2006).

2.1.1 Genetic characterization

Although recognition of *Mussaenda* as a species genus has been widely accepted, its generic circumscriptions have always been controversial. The forms of trichomes and morphology of the calyx and corolla are valuable characters for species identification (Grecebio et al., 2016). For example, an African origin of the newly delimited *Mussaenda* is diagnosed by reduplicate-valvate aestivation and glabrous styles, whereas *Bremeria* can be distinguished from the remaining *Mussaendae* genera through reduplicate- and induplicate-valvate aestivation as well as densely pubescent styles (Alejandro et al., 2005).

2.1.1.1 Heterostyly

Heterostyly is a type of floral polymorphism that increases inter-morph pollen transfer and promotes disassortative mating. The germination rate of hybrid seeds is very low, and naturally occurring hybrids exhibit pollen sterility. Intercourse hybridization resulted in significantly reduced fruits set and seed germination rates (Chen et al., 2014). *Mussaenda* is an ideal system to study the evolution of floral traits and their relationship with sexual system shifts, as its genus possesses diverse sexual systems involved in distyly, dioecy, floral monomorphism, and homostyly (Yuan et al., 2017). Distyly is the most likely ancestral state in *Mussaenda*. Dioecy originates from homosexuality in these species, while unisexual flowers preserve specific characteristics of consummate flowers, which are morphologically perfect and functionally unisexual (Judkevich et al., 2022). Reproductive isolation is a fundamental requirement for speciation, which plays a crucial role in maintaining species (Luo et al., 2015). For the species with closer phylogenetic relationships, the mechanisms of pre-zygotic and post-zygotic reproductive segregation play an important role in limiting gene exchange

between co-occurring species and maintaining species integrity in areas of sympatry (Chen et al., 2014).

2.1.1.2 Dioecy

The dioecy is a rare sexual system that is thought to represent an “evolutionary dead end”. Dioecy has independently evolved at least four times from distyly, and has reversed to homostylous hermaphroditism at least two times, which does not support the hypothesis of an “evolutionary dead end” (Duan et al., 2018). Hermaphroditic flowers typically exhibit no significant differences in the growth of reproductive organs between the male and female structures in the floral form (Li et al., 2010). *M. pubescens* exhibits the presence of perfect hermaphroditic flowers and populations with two distinct styles of morphs; however, there exists weak differentiation in the anther position (stigma-height dimorphism). Although the physical characteristics of the species are hermaphroditic, their sexual functions are dioecious (Li et al., 2010). In *Mussaenda*, a significant correlation was found between the evolutionary development of dioecy and climbing growth form, and a strong association was observed between high net diversification rates and dioecy, while there is no correlation between the diversification rate and climbing habits (Duan et al., 2018).

2.1.1.3 Distyly

Distyly is a genetic-controlled floral dimorphism (Chen et al., 2013), which has subsequently given rise to dioecy, short-styled floral monomorphism, and long-styled floral monomorphism, associated with divergence in the functional gender between long- and short-styled individuals (Pannell, 2018). Self- and intra-morph pollinations of the S-morph are consistent with those expected from dimorphic incompatibility. Dimorphism in style height has evolved repeatedly in flowering plants, with some individuals possessing short styles while others possessing long styles; in the case of distylous species, the stigma position varies reciprocally with that of the anthers. In *M. pubescens*, cryptic dioecy has evolved from stigma-height dimorphism due to more specific sterility mutations (Li et al., 2010). The long-styled (L) morph possesses sterile pollen and functions as a female, whereas the short-styled (S) morph is female sterile and functions as a male. In the L-morph, the microspore nucleus degenerated during the tetrad stage resulting in male sterility, while microsporogenesis and male gametophyte development are normal in the S-morph. The failure to form megaspore mother cells and/or the development of megagametophytes resulted in female sterility in the S-morph compared with the normal megasporogenesis in the L-morph.

2.1.1.4 Pollinators

In addition, there are a total of 26 species of *M. pubescens* flower-visiting insects with different characteristics in the daily activity rhythms of *Lepidoptera*,

Hymenoptera, and *Diptera*, with 21 species from *Lepidoptera*, two species from *Hymenoptera*, and three species from *Diptera*. The distribution ranges and flowering times of *M. pubescens* var. *alba*, *M. shikokiana*, and *M. kwangtungensis* partially overlap, while the principal pollinators differed strikingly for them, with *M. pubescens* visited more commonly by bees and *M. shikokiana* frequently by butterflies (HE et al., 2016).

2.1.2. Microsatellite markers

The sexual system of the genus *Mussaenda* is highly diverse, which makes it possible to study the patterns of population differentiation, speciation, and evolution of the sexual system in this genus. In *Rubiaceae* phylogenetics, the number of markers has been frequently demonstrated as a limitation due to the inadequacy of supporting well-resolved trees at the tribal and generic levels.

Microsatellite markers are valuable tools for analyzing gene flow and hybridization. *M. pubescens* was amplified successfully for 19 microsatellites, of which 17 were polymorphic. At the population level, it was found that the average number of alleles in each locus among 68 individuals was eight. The observed and expected heterozygosities varied from 0 to 1.000 and 0 to 0.882, respectively (Duan et al., 2012). The newly developed microsatellite markers will facilitate the reconstruction of the phylogenies, gene flow analysis, hybridization detection among sympatric species, as well as the determination of genetic differentiation patterns among populations between two ecologically distinct subspecies, that is, *M. pubescens* with yellow flowers and *M. pubescens* var. *alba* with white flowers (Duan & Zhang, 2016).

2.1.3. cp genome

Genome sequencing has been widely used to analyze the genetic variability and evolution of species. Chloroplasts, mitochondria, and nuclei contain independent genomes, which can provide important genetic information for phylogenetic analysis.

The cp has a complete cp genome independent of the nuclear genome (Shinozaki et al., 1986). Compared with the mitochondrial genome, variations in cp genome size in different plants are relatively low (the mitochondrial genome size is 300-600 kb, and the cp genome size is 115-165 kb) (Shaw et al., 2005). As a semi-autonomous replication organelle (Xue et al., 2019), cp contained independent cpDNA (Choi et al., 2015), which has a circular structure that includes one large single-copy (LSC) region, one short single-copy (SSC) region, and two inverted repeat (IR) regions, with the IR region separating the LSC and SSC regions (Xue et al., 2019). The contraction and expansion of the IR, LSC and SSC regions is a common phenomenon in the process of evolution (Huang et al., 2014), which are the main reason that leads to the size difference in cp genomes (Yao et al., 2015). In addition, SSRs detected in cp genomes

are highly conserved in types and numbers, and most mono-nucleotide repeats comprise base A or T, which is ideal genetic markers in plant molecular studies (Khan et al., 2019).

Considering the similar structures, large genetic information, highly conserved sequences (Dobrogojski et al., 2020), high-valuable information (Li et al., 2019), and stable maternal heredity (Wu et al., 2020), the cp genome provides valuable information for species identification, as well as population genetics, phylogenetic, and genetic engineering studies (Luo et al., 2021; Wu et al., 2021)

Therefore, cp genome has become an ideal resource for phylogenetic inference at species and higher orders (Fan et al., 2021; Ly et al., 2020), may be used as molecular markers in taxonomic studies (Han et al., 2022). The complete *cp genomes* of different species plants from the same genus were sequenced using the Illumina NovaSeq 6000 platform, which could provide valuable information for further species identification, evolution, and phylogenetic studies of the plants (Wang et al., 2022). Duan et al researched showed that the information of TPs and hypervariable regions would provide reliable molecular resources for identification, phylogenetic resolution, population structure and biodiversity of *Taxodium* (Duan et al., 2020). Han et al researched showed that the genes *trnG-GCC*, *matK*, *petL*, *ccsA*, and *rpl32* showed significant nucleotide diversity in the complete *cp genomes* of five typical species of the *Agropyron* genus, which may be used as molecular markers in taxonomic studies (Han et al., 2022). Liang et al analysis of the cp genome of *F. longipetiolata* would provide important genetic information for further research into the classification, phylogeny and evolution of *Fagus* (Liang et al., 2022).

2.2. Compounds and metabolite profiles

Many specialized metabolites, also known as natural products, are synthesized and accumulated in plants, providing a rich source for modern pharmacy (Yang et al., 2016). TCM provides a precious potential for discovering bioactive natural products and developing novel modern medicines (Fidan et al., 2022). The genus *Mussaenda* is an important source of medicinal natural products (Vidyalakshmi et al., 2008). Some species of *Mussaenda* have been used in traditional medicine, and the species in which the largest number of compounds has been identified is *M. pubescens*. Phytochemical research showed that triterpenes, triterpenoid saponins, iridoid glycosides, and organic acids are the primary components in *M. pubescens* (Wang et al., 2013).

2.2.1. Compounds

2.2.1.1 Saponins

Saponins are ubiquitous phytochemicals widely reported to be present in many species of plants and animals. The three new saponins were isolated from the hydrophilic fractions of aerial parts in *M. pubescens*, named mussaendosides D, E, and H (Zhao et al., 1996), along with a known saponin, mussaendoside S. Two new saponins named mussaendoside I and J (Zhao et al., 1994) were isolated from the aerial parts of *M. pubescens* Ait.f. Based on chemical and spectral methods involved in 2D NMR technique, their structures were elucidated as 3-O- β -D-glucopyranosyl (1 \rightarrow 2)-O- β -D-glucopyranosyl pomolic acid 28-O- β -D-glucopyranosyl ester and 3 β -O- α -L-rhamnopyranosyl (1 \rightarrow 2)-O- β -D-glucopyranosyl oleanolic acid 28-O- β -D-glucopyranosyl ester, respectively.

Three new monoterpenes named mussaenins A, B, and C (Zhao et al., 1994), together with a known monoterpene, argyol, were isolated from the aerial parts of *M. pubescens*. Three triterpenoid saponins, named mussaendosides U, V (Zhao et al., 1997), and F (WM et al., 1995), were isolated from the aerial part of *M. pubescens*. Zhao et al isolated seven new triterpenoid saponins named mussaendoside R, S (WM et al., 1995), G, K (Zhao et al., 1996), O, P, and Q (ZHAO et al., 1994) from the whole plant of *M. pubescens*.

One new cycloartane saponin, mussaendoside X was isolated from *M. pubescens* (Huong et al., 2021). Xu et al isolated two new cycloartane-type triterpenoidal saponins from whole plants of *M. pubescens* (XU et al., 1992), named mussaendosides M and N. A new phenolic glycoside named mussaendoside L (Zhao et al., 1996), along with four known iridoidal glycosides, were isolated from the aerial parts of *M. pubescens*.

2.2.1.2 Aromatic compounds

Twenty-nine compounds in the leaves of *M. pubescens* were identified (Wang et al., 2013), which comprised 97.2% of the volatile fraction. The main aromatic constituents were monoterpenoids and sesquiterpenes, such as β -ionone (7.2%), linalool (5.6%), and limonene (3.6%). The main constituents of the oil were (E)-hexenoic acid 2-butyl ester (25.23%), (E, E)- 2-hexenoic acid 2-hexenyl ester (15.1%), and β ionone (7.2%).

2.2.1.3 Other compounds

From the water extract of *M. pubescens*, six compounds, shanzhiside methylester (1), barlerin (2), mussaenoside (3), (6S, 9R)-roseoside (4), mussaendoside L (5) and coniferin (6) were isolated (Viêt et al., 2017).

2.2.2. Metabolite profiles

Metabolites have their origin in plant metabolic process, eliciting desired health beneficial effects in animals and humans. Metabolites have the unique chemical structures, could modulate biological and physiological conditions to favorable bioavailability and biochemical function (Pham & Lee, 2012), to effectively quench ROS for redox balance (NavaneethaKrishnan et al., 2019), and inhibited inflammation, oxidative stress, and metabolic disorders (Hyunju Kang, 2023). ROS were negatively correlated with flavonol, anthocyanin, peroxidase (POD), catalase (CAT), soluble solid content (SSC), trolox equivalent capacity (TEAC), ferric reducing capacity (FRAP), 2,2-diphenyl-1-picrylhydrazyl (DPPH) as well as hydroxyl radical scavenging ability (James et al., 2022).

2.2.2.1 Secondary metabolites

Secondary metabolites affect the quality, flavor, and immune function of agricultural products and have medicinal value or promote human health (Huang et al., 2021). Plants produce a wide range of secondary metabolites (e.g. flavonoids, terpenoids, phenolics or alkaloids) that play vital roles for their primary functions such as growth, defence, adaptations or reproduction. In addition, some of the plant secondary metabolites are beneficial to mankind as nutraceuticals and pharmaceuticals (Devi et al., 2023).

Flavonoids, the most described phenolic secondary metabolites, are widely distributed in plant, which can be classified into six categories involved in flavonols, flavanones, flavones, flavanols, isoflavones and anthocyanidins (Montoro et al., 2005). Flavonoids are important coloring substances in tea infusions (Wang et al., 2004). The grade related biomarkers of green tea are eight metabolites, such as gallic acid, catechin, gallic acid, catechin, gallic acid, catechin, salicylic acid, theasinensin B, theasinensin C, kaempferol 3-(6"-rhamnosylsoporoside) and l-linalool 3-[xylosyl-(1->6)- glucoside] (Li et al., 2022). The levels of catechin, epicatechin, and epigallocatechin increased with tea shoot maturity, whereas those of epicatechin gallate, epigallocatechin gallate, and total catechins decreased (Xu et al., 2021). The thermal hydrolysis of flavonoid glycosides leads to the production of aglycones and sugar bodies during fixation (Bedrni et al., 2020). A reduction in the glycoside content can reduce the astringency and bitterness of tea soup. Flavonoid aglycones are absorbed relatively easily, which enhances their functional activity (Ye et al., 2022). In addition, several compounds with high accumulation, such as kaempferol, quercetin, naringenin and their glycosides (Li et al., 2021), have been proved to have beneficial bioactivities including antioxidant, anticancer and anti-inflammatory (Kashyap et al., 2017).

Phenolic compounds, omnipresent in plant cell walls as an integral entity

with polysaccharides, are a crucial part of the human diet (Jakobek & Blesso, 2023) and are of considerable interest due to their antioxidant properties and other potential beneficial health effects (Sunantha et al., 2022). The composition and contents of phenolic acids varied greatly among different varieties and tissue, which were related to their antioxidant and enzyme inhibitory activities (Shen et al., 2018). The accumulation of the phenolic acid (i.g. hydroxybenzoic acid, hydroxycinnamic acid and their derivatives), especially Trans-4-Hydroxycinnamic Acid Methyl Ester in the bud leaves were consistent higher than those of the old leaves (Liu et al., 2020).

Terpenoids, included monoterpenoids, sesquiterpenoids, triterpene and triterpene saponin, possessed antibacterial, anti-inflammatory and antioxidant effects (Gunasekaran et al., 2017). Poncirin had anti-inflammatory, anti-tumor, anti-osteoporotic activity and anticolic properties (Afridi et al., 2019) and luteolin-4'-O-glucoside showed a potent clinical effect in treating hyperuricemia and gout (Lin et al., 2018).

Alkaloids are considered the primary bioactive components in plant chemicals, which possess various bioactivities because of their properties (Kuang et al., 2021). The health benefits of tea plant are associated with its abundant content of caffeine. The content of black tea processed by the fresh and tender buds or leaves from spring was higher than that of mature leaves from monsoon and autumn seasons (Bhandari et al., 2019).

2.2.2.2 Primary metabolites

Primary metabolites involved in amino acids, organic acids, lipids or sugars are essential for maintaining the life activities of cells and function as an important energy resource and some small molecular compounds for secondary metabolism (Hounsome et al., 2008). The carotenoids, lipids, amino acids, and glycosides are important precursors in terms of green tea aroma formation (Feng et al., 2019).

Amino acids are important components responsible for the brisk and sweetness tastes, while soluble sugars are the main source of sweetness. They are not only key precursors for enhancing the aroma (Cui et al., 2019; Zhang et al., 2020), but also contribute to nutritional and functional ingredients (Saeed et al., 2017).

Organic acids function as the important intermediate products of carbohydrate catabolism, which contribute to the vinegar taste and fruity flavor of tea (Das et al., 2019), simultaneously restrain the bitterness and sourness (Chen et al., 2023). The content of organic acids in fresh leaves was obviously higher than that in mature leaves. The contents of common organic acids (i.g. anchoic acid, citric acid, and quinic acid) showed significant increases during the tea production process ($p < 0.05$), while that of L-malic acid significantly decreased after fixation. Such changes

play an important role in reconciling the taste of the green tea soup (Ayabe & Aoshima, 2007).

Lipids in fresh tea leaves were responsible for the production of flavor and aroma substances (Chen et al., 2022). The compounds of lipids in new shoots were higher than that in mature leaves, and highly abundance of lipid metabolites contributed to the formation of tea aroma (Liu et al., 2017). Most lipids and lipid-like molecules, organic acids, amino acids, and flavonoids increased significantly after processing (Jiang et al., 2023).

2.2.2.3 Metabolomics

Widely targeted metabolomics using ultra-performance liquid chromatography-tandem mass spectrometry (UPLC-MS/MS) has increased in popularity in analyzing and identifying metabolites from medicine, agriculture, and food due to its high throughput, fast separation, high sensitivity, and wide coverage (Chu et al., 2020; Wang et al., 2019). Sun et al reveal metabolic profiles, bioactive compounds and antioxidant activity of rosehips from Xinjiang using extensively targeted metabolomics, provided references for improving their utilization, introduction, and breeding (Sun et al., 2023). Li et al (2021) research showed that considerable difference between varieties was observed in accumulation of phenolic acids and flavonoids, which might lead to difference in antioxidant activities, revealed metabolites important for antioxidant properties and quality trait, provide useful information for further investigation of proso millet food chemistry and for sufficient utilization of this special crop.

2.3. Leaf color change and flavonoid biosynthesis

The genus *Mussaenda* is an important source of medicinal natural products, particularly flavonoids, iridoids, triterpenes, and saponines, isolated from Mp (Viêt et al., 2017). While flavonoids, include anthocyanins, contributed to leaf color change from red to purple. With leaf development, the leaf color of Mp will gradually change from purple to green, which may be caused by flavonoids metabolism different.

2.3.1. Leaf color change

Leaves are the main photosynthetic organs and are also involved in responses to biotic and abiotic stresses (Aude & Laufs, 2018). The formation of leaf color is closely correlated with the types and proportions of pigment in plants (Li et al., 2021). The color change could be attributed to three major pigments: chlorophylls, carotenoids, and flavonoids (Lightbourn et al., 2008; Shen et al., 2018), which provide the foundation for coordinated regulation of plant tissue color (Zhang et al., 2020).

2.3.1.1 Chlorophylls

Chlorophyll plays a key role in photosynthesis (Zheng et al., 2021). Leaves appeared green mainly due to high concentrations of chlorophylls, which were influenced by natural environmental factors, including light duration, light intensity, and temperature fluctuations (Zhang et al., 2016). Tea leaves present an albino or chlorina phenotype due mainly to altered chlorophyll metabolism (Li et al., 2016).

2.3.1.2 Carotenoids

Carotenoids are generally responsible for the yellow and red pigments in leaves. Flavonoids / anthocyanins are generally responsible for the red, blue, and purple pigments in leaves (Winkel-Shirley, 2001). The combination of flavonoids, anthocyanins and carotenoids increased the diversity of leaf color (Luiza et al., 2022). The ratio of carotenoids or anthocyanins to chlorophyll can result in the leaves turning yellow or red (Cheng et al., 2015).

Carotenoids are a group of important isoprenoids involved in photosynthesis and synthesized in the chloroplast membrane, which could play an important role in the regulation of leaf color, participate in the auxiliary function of photosynthesis (Chen et al., 2017; Yuan et al., 2015), and help ensure efficient photosynthesis and the removal of various reactive oxygen species (Rezaei et al., 2016; Shen et al., 2018). As cellular senescence, the reduction of chlorophyll content, the leaves color change from green to yellow.

2.3.1.3 Anthocyanins

Abundant accumulation of anthocyanins is the fundamental substance for the reddening of colorful plant leaves (Zhang et al., 2019). The leaves color changed from yellow to red or purple with the presence of anthocyanin pigments (Sharma et al., 2021). The purple leaves have a higher content of flavonoids compared to the green leaves, while their content of chlorophyll and carotenoids is relatively low (Shen et al., 2018). There is a significant negative correlation between the content of anthocyanins and chlorophyll in colored tree species (Ren et al., 2019). In addition, the accumulation of anthocyanins varies in different colored leaves, as well as the increase of malvidin 3-O-glucoside (violet) and pelargonidin 3-O-glucoside (orange red) is significantly correlated with the change in leaf color from green to purple red (Li et al., 2021).

2.3.2. Flavonoid biosynthesis

2.3.2.1 Flavonoid

Flavonoids could be classified into six categories involved in flavonols, flavanones, flavones, flavanols, isoflavones and anthocyanidins (Montoro et al., 2005).

Flavonoid biosynthesis is a crucial secondary metabolism process for tea plants (Shi et al., 2020). Flavonoids metabolites concentrations in purple leaves and green leaves were significantly influenced by the genes involved in flavonoid biosynthesis, transcriptional regulation, transport, and hormone response. Meanwhile, genes including CsPAL, Cs4CL, CsCHS, CsFLS, CsDFR, CsANS, CsLAR, CsANR, and CsUFGT determined to be responsible for the flavonoid biosynthesis. In addition, transcription factors (TFs) including CsMYBT1, CsMYBT2, NAC008, MYB23, and bHLH96 and transporters such as ABC transporter I might be responsible for the flavonoid and anthocyanins accumulation in purple leaves (Song et al., 2022). Flavonoid compounds, especially anthocyanins, are responsible for leaf color and physiological and biochemical processes (Zhou et al., 2016).

2.3.2.2 Anthocyanin biosynthesis

Anthocyanins are a class of flavonoid compounds with special molecular structures and strong water solubility. They are synthesized through the shikimate pathway in the cytoplasm (Hu et al., 2016), which is an important branch of the flavonoid biosynthesis pathway and serves as one of the primary routes for the synthesis of secondary metabolites in plants (Zhao et al., 2023). They are further modified by acylation, methylation and glycosylation until being eventually stored in vacuoles. Anthocyanins can be classified into six categories including pelargonidin, cyanidin, delphinidin, peonidin, petunidin and malvidin, which are widely distributed in the leaves, flowers, fruits and seeds of numerous plants (Martens et al., 2014), contributing to color maintenance and safeguarding photosynthesis, as well as providing antioxidant protection and moderate stress adaptation. In addition, anthocyanins exhibit anti-aging properties by scavenging free radicals and inhibiting tumor formation.

Additionally, leaf color is closely associated with the structural genes of pigments. The genes involved in flavonoid biosynthesis (PAL, CHS, CHI) along with their transcription factors (MYB, HD-Zip, bHLH) exhibited specific and increased expression during the purple-red periods (Jiao et al., 2020; Shi et al., 2020). Leaf color is related to some key structural genes in flavonoid and anthocyanin biosynthesis such as PAL, CHS, CHI, F3H, DFR, ANS and UFGT and regulatory factors such as MYB, MADS-box, bHLH, WD40, bZIP and WRKY (Li et al., 2021; Lu et al., 2021). MYB and HD-Zip positively regulate flavonoids/anthocyanins biosynthetic genes during the fruit ripening process (Zhang et al., 2020). MYB and the heterogenous bHLH TFs activate key structural genes for anthocyanin biosynthesis in blueberry (Plunkett et al., 2018). Some protein complexes negatively regulate key genes in the flavonoid pathway in plants (Huang et al., 2019). bHLH TFs are mainly involved in the regulation of anthocyanin accumulation

in early jujube fruit development (Shi et al., 2019). R2R3-MYB is a core transcription factor of anthocyanin biosynthesis in plants, which can activate PAL, the initial gene of phenylpropanoid biosynthesis, and consequently increases the abundance of anthocyanins (Chen et al., 2021). Particularly, R2R3-MYB interacts with bHLH and WD40 to form the MYB-bHLH-WD40 regulatory complex (MBW) to further induce anthocyanin biosynthesis and accumulation in plants (Zhao et al., 2019). ANS genes play essential roles in anthocyanin biosynthesis because they directly convert leucoanthocyanidins into colored anthocyanidins (Wan et al., 2020). However, the lack of ANS and DFR activity results in the loss of pigmentation (Jiao et al., 2020). The UFGT gene can convert anthocyanins to a more stable water-soluble state as the last step of flavonoid pathway (Gao et al., 2020). With high expression of two UFGT genes (Cluster-24837.111509 and Cluster-24837.123865), the leaf color gradually turns purple red. Chlorophyll metabolism is of great significance to plant leaf color change. The accumulation of chlorophyll results in green leaves, while a small amount of chlorophyll was etiolated. Two CLH genes (Cluster-24837.1383 and Cluster-24837.8715) and one CHL-G gene (Cluster-24837.111895) may negatively regulate chlorophyll biosynthesis in purple-red leaves (Lu et al., 2020), exhibiting high-level expression in green leaves, followed by purple and purple-red leaves, consistent with the chlorophyll content data.

2.3.3. Transcriptomics and metabolomics

Transcriptomics is the study of the transcriptome—the complete set of RNA transcripts that are produced by the genome, under specific circumstances or in a specific cell—using high-throughput methods, such as microarray analysis. Comparison of transcriptomes allows the identification of genes that are differentially expressed in distinct cell populations, or in response to different treatments. Transcriptomics has increased in popularity in analyzing and identifying genes from animal, plants, and microorganisms due to its high real-time, high throughput, high sensitivity, wide coverage, relatively low cost. Combined transcriptomics and metabolomics can not only result in a greater understanding of the expression of specific genes but also result in the identification of functional genes related to biological characteristics from the changes in the level of metabolites and reveal the regulatory mechanisms of specific genes (Chu et al., 2020).

Li et al (2021) analyzed the anthocyanins accumulation of the leaf colors in *Ziziphus jujuba mill* that determine by transcriptome and metabolome. The results showed that the flavonoid biosynthesis genes (PAL, CHS and CHI) and their transcriptional regulators (MYB, HD-Zip and bHLH) exhibited specific increased expression during the purple-red periods. The anthocyanin biosynthetic genes (UFGT

and BZ1) were substantially higher than in leaves of other colors and may be related to the purple-red color change. The flavonoids were the major differentially accumulated metabolites, and anthocyanins determined the leaf coloration. Compared with the green-leaf cultivars, the leaf buds of the purple-leaf cultivars contained higher anthocyanin content. These results improve the understanding of the chemical components and medicinal value of jujube leaf and provide theoretical support for the development of jujube leaf as a functional food.

2.4. Toxicology and pharmacology

China has accumulated a wealth of empirical knowledge regarding using medicinal plants to treat various ailments throughout its long history. Plant natural products have been particularly important because of their applications in the food, cosmetic and pharmaceutical industries (Yang et al., 2016). Medicinal plants have been used widely throughout history to treat diseases and infections as traditional healing remedies due to their broad therapeutic spectrum and minimal or no side effects.

The genus *Mussaenda* is an essential source of medicinal natural products, particularly iridoids, triterpenes, saponines, and flavonoids isolated from *M. pubescens*. The abundance and widespread availability of iridoids made this plant a potential target for investigating the activity of this drug (Viêt et al., 2017). The whole plants of *M. pubescens* have been used in TCM against laryngopharyngitis, acute gastroenteritis, and dysentery, as a diuretic, antiphlogistic, diaphoretic, antipyretic, detoxify poisons, and contraceptive agent (Chen et al., 2013).

2.4.1. Efficacy in vitro

2.4.1.1 Antiviral activity

M. pubescens is a Chinese folk medicine that has been used as a detoxifying poisons agent and has also been employed to detoxify mushroom poisons. Herb medicinal products derived from plants have long been considered as an alternative option for treating various diseases, and natural products represent an important source of new antiviral activity. Herpes Simplex Virus type 1 (HSV-1) is a common pathogen that causes disease worldwide. The extracts of *Mussaenda pubescens* exhibited potential antiviral activity by maintaining cell viability, with an inhibition rate of 80% on HSV-1 (House, 2013).

The eighteen saponins were identified from *M. pubescens*, which were believed to be an antagonist of the M-Ach receptor and were presumed to be responsible for the detoxification activity against certain medicinal plants and mushroom toxins. *Mussaendoside O*, the most abundant saponin from *M. pubescens*,

with immunopromotive and hemolytic activities, can significantly inhibit the secretions of the lachrymal and salivary glands induced by galanthamine, as well as suppress the contraction of the isolated longitudinal muscle strip from guinea pig ileum evoked by an M-Ach receptor agonist (carbachol, 10^{-6} M) at concentrations of 10^{-4} and 10^{-5} M (Xu et al., 1996). Furthermore, the extracts of *M. pubescens* exhibited anti-RSV activity with 50% inhibition (IC₅₀) concentrations ranging from 12.5 to 32 µg/mL, and selective indices (SI) ranging from 11.2 to 40 (Xu et al., 1996).

2.4.1.2 Detoxification

Gelsemium elegans (GE) belongs to the family *Loganiaceae*, which is widely distributed in Northern America, East Asia, and Southeast Asia (Dutt et al., 2010). GE contains a series of active constituents such as alkaloids, triterpenes, iridoid, and phenylpropanoids (Zhang et al., 2012), which has been used as a Chinese folk medicine for the treatment of malignant tumors, pain, rheumatic arthritis, psoriasis, and immune function (Xu et al., 2012). The prominent analgesic effect members in GE were gelsemine and koumine, with gelsemine consistently serving as the main urinary marker for *Gelsemium* exposure (Lai & Chan, 2009). GE is a well-known toxic plant that contains highly dangerous toxins such as gelsenicine, humantenidine and gelsevirine. Among these, gelsenicine serves as the most toxic component, capable of causing severe respiratory depression and impact on neural transmission without leaving any damage (Li et al., 2022). Due to the efflux transporters participation, a decrease in absorption and an increase in efflux of indole alkaloids from the detoxification herbal formula involved in GE and MP were discovered in Caco-2 cells monolayer model (Wang et al., 2017).

2.4.1.3 Antitumor activity

TCM has demonstrated an impact on the pathways leading to the death of tumor cells, which provided novel insights that may aid in guiding clinical decision-making for tumor treatment (Gerber, 2008). Compounds derived from natural medicines with unique and diverse chemical entities still constitute a considerable resource for developing novel medicaments.

Rotundine acid (RA) has the potential for development as a new drug that is used in combination with radiation therapy for treating human breast cancer (Wang et al., 2018). RA belongs to the pentacyclic triterpenoid family, isolated from *M. pubescens* and *Guettarda platypoda* of the *Rubiaceae* family (Bhattacharyya & de Almeida, 1985; Zhao et al., 1997). In addition, RA, one of several isolated compounds, demonstrated anticancer activity and induced apoptosis in MCF-7 cells (Kim et al., 2012). Furthermore, RA relieved oxidative stress and liver damage, significantly improved the defense system through enhancing their enzymatic antioxidant

properties (SOD, CAT and GPx), glutathione (GSH) level, and decreased the elevated lipid peroxidation (LPO) content intoxicated rats, effectively suppress and terminates hepatotoxicity induced through HgCl₂ (Revathi & Jagadeesan, 2022).

2.4.1.4 Inhibition osteoclast formation

The compounds from *M. pubescens*, with the new cycloartane (mussaendoside X), acts as potential effective inhibitors of osteoclastogenesis, significantly decreasing the number of osteoclasts in a concentration-dependent manner and positively suppressing osteoclast formation (Huong et al., 2021).

2.4.1.5 Hepatoprotective activity

The two iridoids such as sanshiside-D and lamalbide were isolated from the ethyl acetate fraction of *Mussaenda "dona aurora"* (sepals), observed the highest activity of hepatoprotective and antioxidant. Sanshiside-D exhibited a hepatoprotective activity greater than silimarin as was evidenced by significant reduction of ALT and AST in the serum enzyme levels (Vidyalakshmi et al., 2009).

2.4.2. Zebrafish

Zebrafish genes have high homology with human genes (Ma et al., 2022). The embryonic development of *zebrafish* is transparent, with advantages such as small size and short development cycle (Teame et al., 2019). *Zebrafish* embryos, as a model organism (Xu et al., 2022), were an effective alternative model for biomedical research and toxicology (Nadia, 2022), offering an analyzable endpoint for studying toxicological effects from acute to developmental toxicity (Strähle et al., 2012). Hatching is a crucial developmental process in the life cycle in which embryos are digested by the chorion from the egg through chlorolytic enzymes (Li et al., 2022). The body length of *zebrafish* is crucial for evaluating their growth status and biomass (Zhao et al., 2022). The postponement in hatchability of *zebrafish* embryos exposed to CuSO₄ might be due to the interference of hatching enzymes digested by the chorionic membrane or the delay of embryonic development induced by hypoxia (Nipun et al., 2021).

CuSO₄ has acted as an inducer to investigate the anti-oxidation, anti-inflammation, and anti-apoptosis of some bioactive substances in vivo (Ai et al., 2023). CuSO₄-induced oxidative damage caused cellular injuries and excessive production of free radicals as well as many health problems (Park et al., 2016), while antioxidants contributed to the prevention such oxidative stress-associated diseases (Lanzarin et al., 2021; Rajiv et al., 2021). Surfactin could decrease the migration of neutrophils in CuSO₄-induced *zebrafish* larvae model, as well as reduced the levels of oxidative stress and inflammatory factors (Wang et al., 2021).

Oxidative stress is a continuous state of the accumulated reactive oxygen species (ROS), leading to the excessive formation of free radicals, disturbance in the

balance of anti-oxidation systems, and decrease in the activity of the antioxidant defense system (Shashni et al., 2023), which might contribute to the pathogenesis of many diseases, including atherosclerosis, diabetes, and cancer (Bhagat et al., 2021; Gong et al., 2020). Excessive free radicals can induce oxidative damage of biomacromolecules in cells to break the balance between oxidation and antioxidant defense system as well as induce oxidative stress (Nipun et al., 2021) cause endothelial dysfunction and tissue damage, and lead to inflammatory response and oxidative stress (Bhagat et al., 2021; Gong et al., 2020). ROS commonly serves as a biomarker of oxidative stress, when oxidative stress occurs, the excessive generation of ROS can induce inflammation by up-regulating the expression of pro-inflammatory gene, which causes apoptosis (Félix et al., 2020; Lite et al., 2022) and the occurrence of various chronic diseases (Biswas, 2016) due to the destruction of various biomolecules involved in DNA, proteins and cell membrane lipids. MDA, a common biomarker for identifying oxidative damage in organisms (Wang et al., 2021), is initiated lipid peroxidation by the attack of ROS on polyunsaturated fatty acids that are present in biofilms. The oxidative stress was enhanced with the increase in MDA content (Xu et al., 2022). The endogenous antioxidant defense is proved to be capable of preventing ROS-induced damage (Hahn et al., 2015). SOD and CAT are the crucial endogenous antioxidant enzymes (Pessina et al., 2021; Velayutham et al., 2021), acted as crucial roles in the antioxidant defense system, and could alleviate oxidative stress by increasing the expressions of antioxidant enzymes (Wang et al., 2021), and protect cells from damage caused by potentially harmful molecules known as free radicals (Mao et al., 2022).

Oxidative stress can stimulate the generation of pro-inflammatory cytokines and induce inflammatory responses (Gong et al., 2020; Nipun et al., 2021). The inflammatory response is a defense response that is a common pathological phenomenon during severe disturbances to the homeostasis, which eliminates the harmful stimuli by killing microbes and removing stimulators (Gong et al., 2020; Zhou et al., 2020).

Apoptosis is an evolutionarily conserved form of programmed cell death that plays a critical role in maintaining a balance between proliferation and death for development and tissue homeostasis in animals (D'Arcy, 2019; Fen et al., 2018). Oxidative stress and inflammation are crucial factors in inducing apoptosis (Wang et al., 2022). In the process of the cellular stress response, heat shock protein 70 (HSP70) plays an important role in protecting against oxidative stress, resisting copper toxicity, and maintaining intracellular homeostasis, and is involved in responding to various pressures (Nguyen et al., 2020). Bax and bcl-2 are intracellular apoptotic protein and anti-apoptotic protein, respectively (Wang et al., 2021). However, under stress

conditions, induced-expression or overexpression of HSP70 can reduce the muscle atrophy induced by unloading (Isao et al., 2009), increase the expression of Bcl-2 and inhibit cell apoptosis (Li et al., 2010), which protective effects are achieved by repairing damaged proteins in the cytoplasm and preventing cell apoptosis (M, 2004). Quercetin, an important natural flavonoid (Wach et al., 2007), could regulate the expression levels of apoptosis-associated genes (Bax, bcl-2) in *zebrafish* induced by TAA, and be able to possess an anti-apoptosis effect (Wang et al., 2021).

The toxicity evaluation (such as neurotoxicity, cardiotoxicity, hepatotoxicity and nephrotoxicity), associated with human consumption (Rao et al., 2022) is crucial for the development and utilization of plant resources (Murugesu et al., 2019). Determining LC50 is a vital preliminary step in evaluating the toxicological characteristics of any given chemical substance, defined as the concentration of a substance that causes death in 50% of the exposed population in a defined period (Nipun et al., 2021). This measure is widely used to determine the potential hazards and lethal effects of chemicals in various fields, including pharmaceutical, agricultural and industrial sectors (Ajuru et al., 2019). Therefore, the LC50 value is a critical parameter in determining safe exposure levels and acceptable risk levels of chemical substances for both humans and the environment. New compounds or drugs are safe with a high therapeutic index (Shetty et al., 2007). The LC50 for the n-hexane fraction of *Clinacanthus nutans* was 75.49 μ g/mL, and embryos exposed to over 500 μ g/mL showed spinal curvature and edema defects (Murugesu et al., 2019). *Zebrafish* heart is frequently used as a model system in toxicity studies (Zoupa et al., 2017). The changes in gene expression associated with cardiotoxicity are the primary determinants of alterations in cardiac function (Wang et al., 2021), among which Gata4 and Bmp4 play crucial roles in heart development, especially in the proliferation of myocardial cells (Arceci et al., 1993). Nanoplastics have significantly modulated the expression changes of Gata4 and Bmp4 in *zebrafish* induced by pyrrole (Bhagat et al., 2021). Ache is involved in the development and maturation of cells and promotes nerve system development (Wang et al., 2019); while Wnt signaling pathway plays a key role in the development process and may be responsible for positive and negative regulation (Hu et al., 2018).

CHAPTER III

MATERIALS AND METHODS

3.1. The complete *cp genome* of *M. pubescens* and phylogenetic analysis

3.1.1. Plant samples

All the materials were collected from the Third Botanical Resources Survey in Libo County (Guizhou, China, 26°12'N, 107°30'E) in September 2020. The species has been officially identified as '*M. pubescens*' by a professor of plant taxonomy at Qiannan Normal University for Nationalities, which would be compared with the specimens of Chinese *Mussaenda*. The specimen (DZ20210505) was deposited in the herbarium of Qiannan Normal University for Nationalities in Duyun City, Guizhou Province, China. Morphological features of *M. pubescens* involved in branches, leaves, stipules, inflorescences, calyx lobes, corolla tubes, florescences, and fruits were observed to compare their differences (Figure 4-1-1).

3.1.2. Complete *cp genome* sequence

The leaves of *M. pubescens* were collected on September 15, 2020 (Figure 4-1-1) and stored immediately at -80°C. The isolation of total genomic DNA was performed using a modified CTAB method (Zhou et al., 2021). Library construction and sequencing were conducted by Novogene Bioinformatics Technology Co. Ltd. (Guangzhou, China) using the Illumina NovaSeq 6000 platform with a Paired-End 150 (PE150) strategy.

The FastQC software was employed to trim low-quality reads and adapters, and the genome was *de novo* assembled using SPAdes v3.9 (Bankevich et al., 2012), and subsequently annotated using Plann software (Zhou et al., 2021). The accuracy of the preliminary annotation results was verified by comparing them with the proteins and rRNA sequences from previously reported *cp genomes* of relevant species using the methods of blastn and blastp. The complete *cp genome* was submitted to the Database Resources of the National Genomics Data Center, China National Center for Bioinformatics (Genome Sequence Archive accession number: CRA013306; <https://ngdc.cncb.ac.cn/gsa>). The circular structure of the *cp genome* was visualized using CPGView (<http://www.1kmpg.cn/cpgview/>).

3.1.3. Phylogenetic analysis

A total of 28 complete *cp genome* sequences spanning across 24 *Rubiaceae* species were acquired from the NCBI GenBank to ascertain the phylogenetic positions

of *M. pubescens* within the *Rubiaceae* lineages. The Bayesian inference (BI) tree was constructed following standard protocols. The alignment of 28 cp genomic sequences was generated using the MAFFT online version (Kato & Standley, 2013) with default parameters. The software tools MAFFT, Ultrafast bootstrap, IQ-TREE, ModelFinder, and MrBayes were employed within the PhyloSuite framework (Zhang et al., 2020). FigTree was employed to illustrate the phylogenetic relationships (<http://tree.bio.ed.ac.uk/software/figtree/>).

3.2. Metabolomics reveals the importance of metabolites in *M. pubescens*

3.2.1. Materials

The plants obtained from Guilan Shui Nationality Township in Duyun, China (26°12'N, 107°30'E) were cultivated in the germplasm resource nursery of Qiannan Normal University for Nationalities (QNUN) in Duyun, Guizhou province, China. The nursery provided nutrient-rich humus soil, efficient drainage, and sufficient sunlight. The voucher specimen (QNSY202106003) was deposited at the Botanical Museum of QNUN. Fresh leaves from 3-year-old plants that grow normally without pests and pathogens under favorable lighting conditions were selected in September 2021 and divided into three stages based on their growth status and utilization: bud leaf (Stage 1, MpBud), tender leaf (Stage 2, MpTen), and mature leaf (Stage 3, MpMat) (Figure 4-2-1). Leaf samples were collected at three distinct developmental stages, frozen in liquid nitrogen, and stored at -80°C for subsequent metabolome and biochemical analysis. At each stage, three biological replicates of leaf samples were collected, with each replicate comprising 15 bushes. Subsequently, 50 leaves were harvested from 15 bushes per replicate to create a mixture sample with a minimum total weight of 3 g.

3.2.2. Metabolome analysis

3.2.2.1 Preparation and extraction of plant samples

The samples were quickly freeze-dried and crushed at 30 Hz for 1.5 min by using a mixer mill (MM 400, Retsch, Shanghai, China) with zirconia beads. Fifty milligrams of powder was accurately weighed and then extracted with 0.50 mL of methanol/water/hydrochloric acid (799:200:1, V/V/V). The extracts were subjected to vortex and sonication for 10 min, respectively. The solution was subsequently centrifuged at 4 °C and 12,000 × g for 3 min to collect the supernatants, followed by filtration (PTFE, 0.22 μm) (ANPEL, Shanghai, China) before UPLC-MS/MS analysis performed by Wuhan MetWare Biotechnology Co., Ltd.

3.2.2.2 UPLC and ESI-Q TRAP-MS/MS conditions

The extract was analyzed using a UPLC-ESI-MS/MS system (UPLC, SHIMADZU Nexera X2, <https://www.shimadzu.com.cn/>, accessed on 9 November 2021;

MS, Applied Biosystems 4500 Q TRAP, <https://www.thermofisher.cn/cn/zh/home/brands/applied-biosystems.html>, accessed on 9 November 2021) with the analytical conditions described by Zhou et al. (Zhou et al., 2022). The effluent was alternately connected to the ESI-triple quadrupole-linear ion trap (QTRAP)-MS. The ion spray voltage (IS) was set to 5500 V and -4500 V in positive and negative ion modes. Other ESI source operation parameters were the same as the Zhou et al. (2022) protocol.

3.2.2.3. Qualitative and quantitative analysis

The public metabolite database and self-built MWDB were used to perform qualitative and quantitative analysis of metabolites by mass spectrometry. The substances detected in the samples were displayed by MRM metabolite detection multi-peak diagram. The peak area of each chromatographic peak manifests the relative content of the corresponding metabolites.

3.2.2.4. PCA, HCA, and OPLS-DA analysis

Principal component analysis (PCA) was performed using statistics function `prcomp` in R to measure the separation trends of metabolite between groups, indicating whether there were differences in metabolites among groups. To further identify the differences among all samples, hierarchical cluster analysis (HCA) and orthogonal partial least-squares discriminant analysis (OPLS-DA) were performed by the R-package. The prediction parameters of OPLS-DA involve R^2X , R^2Y and Q^2 , where R^2X and R^2Y express the explanation ratio of the model to X and Y matrices, respectively; Q^2 indicates the model's predictability. A permutation test (200 permutations) was performed by R package `MetaboAnalystR` to avoid overfitting.

3.2.2.5. Differential metabolites analysis (DMAs)

The screening for differential metabolites was determined by variable importance in projection (VIP) values ($VIP \geq 1$) based on the results in OPLS-DA and \log_2FC (fold change) ≥ 2 or ≤ 0.5 (Chu et al., 2020). The obtained metabolites were annotated using the KEGG compound database (<http://www.kegg.jp/kegg/compound/>, accessed on 9 November 2021), and then mapped to the KEGG pathway database (<http://www.kegg.jp/kegg/pathway.html>, accessed on 9 November 2021).

3.2.3. Chemical components and antioxidant analysis

3.2.3.1. Total phenolics, flavonoids, terpenoids, and anthocyanin

The determination of total phenolics were performed referred to the methods described by Afonso et al (2020). Twenty microliters of extract solution were mixed with a phenol reagent of Folin Ciocalteu and 7.5% Na_2CO_3 (100/80) in a 96-well microplate. The microplate reader (Multiskan GO Microplate Spectrophotometer, Thermo Scientific, Vantaa, Finland) was incubated in the dark at 45°C for 15 min. After that, the absorbance value was adjusted to 765 nm. A standard curve for various concentrations of gallic acid was performed, with the amount of total phenolic content being represented as mg/g DW.

The total flavonoids (Zhang et al., 2020) were determined using the $\text{NaNO}_2\text{-AlCl}_3\text{-NaOH}$ method by the biochemicals kit (NMKD0120, Norminkoda Biotechnology Co., Ltd., Wuhan, China). Twenty-five microliters of extract solution was blended with distilled water (100 μL) and 5% NaNO_2 (10 μL) in a 96-well microplate. The microplate reader was subsequently incubated in the dark condition at room temperature. Five minutes later, 10% AlCl_3 (15 μL) and NaOH (50 μL) were added to the mixture and finally mixed with 50 μL of distilled water. The absorbance value was determined at a wavelength of 510 nm against a blank. A standard curve for various concentrations of catechin was performed, the value of which was represented as mg/g DW.

Approximately 0.25 g of dry powder was weighed and then soaked in the NaCl solution for 6 h at a ratio of 1:18. After distillation for 8 h, the volatile oil layer was collected and dried overnight with an appropriate amount of Na_2SO_4 to obtain a volatile oil. One milliliter of volatile oil was blended with 9 mL of absolute ethanol and subsequently shaken well. After that, 1 mL of the extraction was distilled to a final volume of 5 mL with absolute ethanol. The extract solution (1 mL) was mixed with 5% vanillin glacial-acetic acid (3 mL), and subsequently with 3.5 mL of perchloric acid. Then, the solution was kept in a 71°C water bath for 28 min and rapidly cooled to room temperature. After cooling, 1.5 mL of glacial acetic acid was added to bring the final volume to 8 mL and then shaken well. The absorbance value was adjusted at the wavelength of 600 nm against a blank, and the total terpenoids content was expressed as mg/g DW.

For total anthocyanin content, extractions were performed according to pH differential method described by Lee et al (2016). About 0.1 g of powder was added into 1 mL of mixture with 8.5 % aqueous formic acid and an acetonitrile/methanol mixture (85/15) at a ratio of 9:1. The solution was vibrated at 75°C for 25 min, and

subsequently adjusted to a final volume of 1 mL with the mixture. After that, the solution was centrifuged for 10 min at 12,000 × g to collect the supernatant. The absorbance of the extract solution diluted with aqueous buffer (pH 1.0) and sodium acetate buffer (pH 4.5) was recorded at wavelengths of 530 nm and 700 nm, respectively.

3.2.3.2. Antioxidant activity

The biochemicals kit (NMKD0109, NMKD0110, NMKD0111, Norminkoda Biotechnology Co., Ltd. Wuhan, China) was used to measure the 2,2-diphenyl-1-picrylhydrazyl (DPPH) free radical scavenging ability, ferric reducing activity power (FRAP), and 2,20-azino-bis(3-ethylbenzothiazoline-6-sulfonic) acid (ABTS) radical scavenging activity, as described by Afonso et al. (Afonso et al., 2020).

For DPPH radical-scavenging activity, 0.1 g of plant powder was mixed with 80% methanol to obtain the diluted phenolic concentrations (0, 5, 10, 15, 20, and 25 µg/mL). One hundred microliters of solution were added to the 0.15 mL of DPPH methanolic solution and then standardized to a final volume of 1 mL with 80% methanol. After centrifugation for 10 min at 12,000 × g and room temperature, the supernatant was collected for detection. The absorbance value was recorded at 517 nm and expressed as mean values ± standard deviation (SD).

For the FRAP assay, 10 mM 2,4,6-Tri(2-pyridyl)-S-triazine (TPTZ) was added to the 40 mM HCl, followed by mixing with 20 mM FeCl₃·6H₂O and a 10-fold volume of acetate buffer (pH 3.6). After that, 5 µL of the extract solution was blended with 170 µL of Fe³⁺-TPTZ solution and 25 µL of distilled water. The absorbance value was recorded at 590 nm and FRAP was expressed as µmol Trolox/g DW.

For the ABTS method, 7 mM ABTS (pH 7.4) and 2.5 mM potassium persulfate were mixed to acquire the ABTS radical solution. Afterward, it was diluted with ethanol to obtain the absorbance value at the wavelength of 414 nm. Ten microliter of extract solution was added into 190 µL of ABTS radical solution and subsequently incubated in the dark at 23°C for 10 min. The absorbance value was recorded at 414 nm, and ABTS was expressed as µmol Trolox/g DW.

3.3. Metabolomic and Transcriptomic Profiling Reveals the Flavonoid Components and Discoloration Mechanism of *M. pubescens* Leaves

3.3.1. Plant materials

The materials from the same samples as the previous experiment were used to perform metabolomics and transcriptomics analyses with three biological replicates

for each treatment. Before analysis, the leaves were stored at - 80 °C for refrigeration.

3.3.2. Chemical composition

3.3.2.1. Extraction procedure

Extraction was conducted by vigorously mixing 40 mg (dry weight) of Mp leaves samples with 1 mL of 70% methanol in a vortex to homogenize the solution. The mixtures were heated at 70°C for 30 min and subsequently centrifuged at 13,000 rpm and 1°C for 15 min using an Eppendorf Centrifuge 5804R (Hamburg, Germany) to collect supernatants for filtration.

3.3.2.2. Determination of chlorophyll a, b, and total carotenoids

For chlorophyll a, b and total carotenoids quantification, a determination was performed as referred by Lichtentaler (1983), Warren (2008) and Pompelli et al (2013), with modifications. The concentration of each pigment was calculated from 1 cm corrected pathlength using the following formulas:

$$\text{Chlorophyll a } (\mu\text{g/mL}): \text{Chl a} = (11.75 \times \text{Abs662}) - (2.350 \times \text{Abs645})$$

$$\text{Chlorophyll b } (\mu\text{g/mL}): \text{Chl b} = (18.61 \times \text{Abs645}) - (3.960 \times \text{Abs662})$$

$$\text{Total Carotenoids } (\mu\text{g/mL}): ((1000 \times \text{Abs470}) - (2.270 \times \text{Chl a}) - (81.4 \times \text{Chl b}))/227$$

3.3.2.3. Total flavanol and flavonoids

The total flavanol contents (Jiao et al., 2019) were determined using the biochemicals kit (NMKD0262, Norminkoda Biotechnology Co., Ltd. Wuhan, China).

The methods for total flavonoids were determined using the $\text{NaNO}_2\text{-AlCl}_3\text{-NaOH}$ method by biochemicals kit in accordance with Zhang et al (Zhang et al., 2020).

3.3.3. Metabolite profiles analysis

The methods for metabolome analysis were in accordance with those of 3.2.3.

3.3.4. Transcriptome sequencing analysis

Total RNA was extracted from 1.0 g of leaves from the MpBud, MpTen, and MpMat samples using the Sangon Total RNA Purification Kit in accordance with the manufacturer's instruction (Shanghai Sangon Biotechnology Co., Ltd., Shanghai, China). The RNA sequencing (RNA-seq) and assembly were performed by the Biomarker Technologies Corporation in Beijing, China. The library was constructed and sequenced using the Illumina HiSeq 2500 platform. After discarding low-quality sequence reads, clean reads were aligned to the reference genome sequence using the HISAT2 program, available at http://www.plantkingdomgdb.com/tea_tree/.

To annotate the assembled unigenes, we performed homology searches against a set of seven databases involved in NR (NCBI non-redundant protein database), COG (Clusters of Orthologous Groups of proteins), KOG database (EuKaryotic Orthologous Groups of proteins database), UniProtKB/Swiss-Prot (UniProt

Knowledgebase), Pfam (Pfam protein families database), Ortholog database and GO (Gene Ontology) database, and KEGG (Kyoto Encyclopedia of Genes and Genomes). Gene expression levels were estimated using the FPKM method, which calculates the number of fragments per kilobase of transcript per million mapped fragments.

For differential expression analysis, the count matrix for each comparison group was obtained using the DESeq2 R package (version 1.10.0). The resulting p-values were adjusted using the false discovery rate (FDR) method developed by Benjamini and Hochberg. Genes with an adjusted p-value < 0.05 and $|\log_2FC| \geq 1$ were considered differentially expressed genes (DEGs). GO analysis of DEGs was analyzed using the Goseq R package, utilizing the Wallenius non-central hypergeometric distribution. The KOBAS 2.0 software was utilized to assess the statistical enrichment of DEGs within the KEGG pathways.

3.3.5. Correlation analysis of metabolites and genes

Pearson correlations were calculated to analyze the relationship between metabolites and genes involved in the biosynthesis of phenylalanine, phenylpropanoids, and flavonoids in Mp leaves. Correlations between the metabolome and transcriptome were identified as significant if they had a coefficient (r) value greater than 0.8 or less than -0.8, and a p-value less than 0.05.

3.3.6. Quantitative real-time PCR (qRT-PCR) validation

The expression levels of nine DEGs identified from transcriptome data were evaluated with qRT-PCR analysis (each treatment with three biological replicates). cDNA was synthesized by using MonScript™ RTIII All-in-One Mix with dsDNase (Monad Biotechnology Co., Ltd, Wuhan) according to the manufacturer's instructions. qRT-PCR was performed on the QuantiNova SYBR Green PCR Kit (QIAGEN, German). Gene expression relative analysis was computed utilizing $2^{-\Delta\Delta Ct}$ with β -actin serving as the reference gene. All primer sequences were designed for qRT-PCR using Primer Premier 6 software.

3.4. The Acute Toxicity Assessment and Protective Effects of

M. pubescens

3.4.1. *M. pubescens* tea processing

A bud with four leaves of *M. pubescens* were collected in May 2021 in Guilan Shui Nationality Township (Duyun, Guizhou province, China, 26°12'N, 107°30'E), which was employed in the current study. The voucher specimen (QNSY202106003) was deposited in the Botanical Museum of Qiannan Normal University for Nationalities (Fig. 1A). Mp leaves were subsequently cleaned and made into Mp black tea (MpBT) using

the manufacturing process of conventional black tea.

Approximately 2 kg of fresh Mp leaves were withered on bamboo sieves for 10 h at a temperature of $22 \pm 2^\circ\text{C}$ with a relative humidity of 60-70% until the water loss rate reached 35%. The withering leaves were performed to roll in a rolling machine (RCJ-32949 type; Shandong Pinjia Machinery Technology Co., Ltd., Jining, China) for 10 min at 45-55 r/min, with the rolling sequence being light-, heavy-, and light-pressures; afterwards, the leaves were then rolled for 20 min according to the previous conditions with the broken cell rate reaching 70-80% and the rolled twig rate reaching 80-90%. Subsequently, the rolled leaves (8 cm-thick) were fermented for 4 h at $25 \pm 5^\circ\text{C}$ with a relative humidity $< 90\%$ until the leaf redness rate reached 70% with floral fragrance. Finally, 1-cm-thick leaves were dried at 115°C for 10 min until the water content was 20-25%; after spreading out for 40 min, 3-cm-thick leaves were dried at 70°C for 1 h until complete dryness. The processed tea was further used for sensory evaluation and biochemical analysis.

3.4.2. Preparation and extraction of MpBT

The dried MpBT was crushed into a fine powder with the size smaller than 0.5 mm, and then extracted with E3 medium consisting of 3.5 g/L NaCl, 0.5 g/L KCl, 0.025 g/L NaHCO_3 and 0.1 g/L CaCl_2 at 85°C for 90 min with a ratio of 1:20 as an optimal extraction condition. The extract was further filtered with 0.22 μm Polyvinylidene fluoride (PVDF) or 20 μm membrane filter, diluted with E3 medium at 50 mg/mL, and then stored at -20°C before use. For the protective experiments of *zebrafish* embryos and larvae, aqueous extract was prepared every day extemporaneously.

3.4.3. *Zebrafish* breeding and experimental conditions

The adult *Zebrafish* (wild-type AB) provided by Shanghai Fish Biotechnology Co. Ltd. (Shanghai, China) was maintained in a recirculating culture system at a constant temperature of 28°C with a light/darkness cycle of 14/10 h and fed with sterilized brine shrimps three meals per day. The males and females (2/1) of *Zebrafish* were kept separately in spawning tanks overnight, and the baffle was dismantled the following day to allow light exposure to *Zebrafish* to induce spawning and fertilization. Approximately 1 h post-fertilization (hpf), all the obtained fertile eggs were evaluated by electron microscopy to collect normal developmental embryos and then maintained in E3 medium until 4 hpf. All the protocols were conducted in compliance with relevant legal rules and approved by the Laboratory Animal Ethics Committee of Qiannan Normal University for Nationalities (College of biological science and agriculture).

3.4.4. The median lethal concentration (LC50)

Toxicity assessment of MpBT extracts in *Zebrafish* embryos were carried out according to the method by Rashid et al. (Abd et al., 2022), and Velaithan et al. (Velaithan et al., 2017). Healthy *zebrafish* larvae was distributed into twenty-four well cell culture plates (1 larvae/well in 1 mL of solution), and exposure groups were divided into 11 groups, including a control group (medium), and 10 treated groups (0.2, 0.4, 0.8, 1.0, 2.0, 4, 8, 10, 20 and 50 mg/mL MpBT). For each exposure group, at least three parallel replicates were performed and incubated at 28.5°C for 48 h. The treatment solutions were updated every 24 h.

3.4.4.1. Mortality

The mortality of the larvae exposed to different concentrations were recorded, and dead larvae was removed in each concentration of the solution after 24 h and 48 h. *Zebrafish* larvae whose bodies have melted, hearts have stopped, and with no activity was considered dead. The dead larvae were timely removed to safeguard the exposure solutions from bacterial infections. The number of dead larvae in each treatment group with varying concentrations were compared to the initial number of larvae placed in the containers; then, the percentage mortality rate was calculated over time and accumulated to determine the relative mortality rate in comparison to the control group (Hu et al., 2011). The data was used to estimate LC50 at 24 h and 48 h using probability analysis (Pamanji et al., 2015).

3.4.4.2. Morphological and developmental effects

Phenotypic defect in *Zebrafish* larvae was observed within 48 h of hatching through a CZM4 stereo microscope under magnification of 40 x, and photographs were taken. Phenotypic defect (in percentage) was the number of embryos with phenotypic defects divided by the total number of normal embryos (without phenotype defects) and multiplied by 100 (Abd Rashid et al., 2022). After 48 h of embryos exposure in all treatment groups, their body length, eye length, and SV-BV was measured using ImageJ software, and their heart rates (beats/min) were observed under a stereomicroscope.

3.4.5. Exposure of *zebrafish* embryos to MpBT

To evaluate the protective effect of MpBT, healthy *Zebrafish* embryos (4-5 hpf) were assigned to a 24-well cell culture plate with 1 embryo/well in 1 mL of the solution following a method described by Li et al (2022) and divided into five groups involved in the control group (medium), CuSO₄-treatment group (3 µM), and three co-treatment groups (3 µM CuSO₄ + MpBT of 0.5, 1.0 and 1.5 mg/mL). MpBT extract solution was diluted to different concentrations using fresh embryo or larva medium

to obtain final concentrations of 0.5, 1.0, and 1.5 mg/mL in each experimental well, equivalent to 1/10 to 1/2 the LC50 value. For each exposure group, at least three bio replicates were performed and incubated for 144 h at 28.5°C. Furthermore, the treatment solutions were updated every 24 h.

During the exposure, *Zebrafish* larvae was randomly chosen to record the hatching rate and survival rate at an interval of 24 h, ranging from 24 hpf to 144 hpf, as well as malformation rate and heart rate at 144 hpf and overall morphological changes. The hatching rate was calculated as the proportion of the larvae hatched to the total number of initial living larvae between 24 and 144 hpf. The survival rate was expressed as the percentage of the survival larvae number to the total number of living larvae from 24 hpf to 144 hpf. The malformation rate was calculated as the ratio of the total number of malformed larvae to the total number of living larvae at 144 hpf. After 144 h of embryos exposure to all treatments, body length, eye length, and the distance from venous sinus to arterial bulb (SV-BA) of the larvae was measured using ImageJ software, and the larvae heartbeats were recorded under an electron microscope.

3.4.6. Oxidative-stress-related biochemical analyses

To evaluate the effect of MpTB on the oxidation and antioxidant levels of *Zebrafish* larvae, reactive oxygen species (ROS), catalase (CAT), superoxide dismutase (SOD) and malondialdehyde (MDA) were measured according to the manufacturer's instructions of Jiancheng Bioengineering Institute (Nanjing, China).

The generation of ROS was determined using a fluorescent dye, 2',7'-dichlorofluorescein diacetate (DCFDA), following the methods described by Bhagat et al. (Bhagat et al., 2021) and Wang et al. (Kexin et al., 2021). After 120 hpf of exposure, ten *Zebrafish* larvae randomly chosen from each group was processed with 20 μ M DCFDA for 30 min at a temperature of 28°C in the dark condition and then washed with medium three times. After anesthesia with 0.16% tricaine and fixation with 1% low-melting-point agarose, the *Zebrafish* larvae was observed under a fluorescence microscope (XK-DL005, Shenzhen, China) with 488 nm excitation and 527 nm emission, which the images for the fluorescence intensity was quantified using the Image J software. The thirty *Zebrafish* larvae (at 120 hpf) collected from each treatment was homogenized in 1 mL of cold phosphate buffer solution at pH 7.4, and then centrifuged for 15 min at 4,000 \times g and 4°C to collect supernatants for the determination of enzyme activity. The contents of CAT, SOD, and MDA were determined using the corresponding kits, and the absorbances were adjusted to the wavelength of 540 nm, 460 nm, and 540 nm, respectively, with a microplate reader (SpectraMax ABS Plus, Molecular Devices, USA).

3.4.7. Protein expression analysis

To evaluate the developmental toxicity caused by CuSO₄ of MpBT, the four protein expressions involved in heat shock protein 70 (HSP70), B-cell lymphoma-2 (Bcl-2) and Bcl-2-associated X protein (Bax) in the whole zebrafish larvae at 120 hpf was performed in compliance with the manufacturer's instructions from Jiancheng Bioengineering Institute (Nanjing, China).

3.4.8. RNA extraction and gene expression analysis

RNA extraction and quantitative real-time polymerase chain reaction (qRT-PCR) was conducted following the method described by Li et al (2022) with slight modifications. The total RNA of ten *Zebrafish* larvae selected from each treatment was extracted with Trizol reagent (Tiangen, China) to quantify using a NanoDrop-1000 spectrophotometer (Thermo Scientific, USA). 500 ng of total RNA was reverse transcribed into cDNA with ReverTra Ace qPCR RT Kit (Toyobo, Osaka, Japan). qRT-PCR of the antioxidant-related genes (Mn-sod, cat, Gpx1 α), inflammatory cytokines (1L-1 β , TNF- α , INF- γ), and apoptotic phase genes (Bax, bcl-2) was subsequently performed using StepOne Real-Time PCR System (USA) and PowerUp SYBR Green Master Mix (ABI, USA), with β -Actin as a conserved gene. The relative gene expression was evaluated using the method of relative fold differences ($2^{-\Delta\Delta Ct}$) with three replicates for each treatment.

3.4.9. Statistical analyses

All the obtained data were performed using SPSS 23.0 software (Chicago, USA) and presented as mean \pm standard error (SE). The comparisons among groups were conducted using one-way analysis of variance (ANOVA) with a Dunnett's tests. A value of $p < 0.05$ was accepted statistically significant.

CHAPTER IV RESULTS AND DISCUSSION

4.1. The complete *cp genome* of *M. pubescens* and phylogenetic analysis

4.1.1 Morphological characteristics of *M. pubescens*

The collected specimens of *M. pubescens* were compared with Chinese *Mussaenda* specimens for this research study (Table 4-1-1). The morphological features of *M. pubescens*, including branches, leaves, stipules, inflorescences, calyx lobes, corolla tubes, florescences, and fruits, were presented in Figure 4-1-1.



Figure 4-1-1. Morphological characters of *M. pubescens*.

(A) *M. pubescens* plant stand; (B) Fruit; (C) The longitudinal section of the fruit; (D) Transection of the fruit; (E) A fruiting branch (2 cm); (F) Enlarged Calyxlobes (2 cm); (G) Stipule (1 cm); (H) A long-styly branch (Scale bar: 5 cm); (I) Calyxlobes (1 cm); (J) A flowering short-styly branch (2 cm); (K) long-styly stigma (1 cm); (L) Long-styly corolla (1 cm); (M) Long-styly flower (1 cm).

Table 4-1-1. Morphological comparison of *M. pubescens* and *M. hirsutula*

Taxa	<i>M. pubescens</i>	<i>M. hirsutula</i>
Habitat	Climbing shrub, often extensively twining.	Climbing shrubs
Branches	Branchlets, appressed pubescence	Branchlets, densely ferruginous- or gray villosulous.
Leaves	Opposite or rarely whorled; obvious petiolate (3-15 mm), densely strigose; membranous or thin papery, ovoid oblong, ovoid lanceolate, 5-8 × 2-5 cm; apex abruptly acuminate or acute, base cuneate; with strigose sparsely on adaxially, densely on abaxially and veins; tertiary venation reticulate, secondary veins 4-7 pairs.	Opposite; petiole 3-5 mm, densely pilose; papery, elliptic or oblong, subovate, 7-13 × 2.5-4 cm, apex mucronate or acuminate, base cuneate, sparsely pilose on both sides, denser on below and veins; secondary veins 6-7 pairs, tertiary venation visible and reticulate.
Stipules	Triangular, 5-7mm, densely strigillose; deeply 2-lobed, segments subulate, 4-6mm long.	Triangular, 3-5 mm, densely pilose, deeply 2-lobed or 2-lobed; lobes lanceolate, 3-5mm long.
Inflorescences	Terminal, subcapitate, mostly unbranched, cyme, 4-6×2-7 cm, dense flowered, densely strigillose to villosulous; peduncles (sessile to nearly sessile, although fruits may have stalks) 0.1-1.4 cm; bracts, linear, 3-5 mm.	Terminal, cymose, 1.5-4 × 1.5-4 cm, densely grayish yellow villosulous; peduncle 0.3-1.5 cm; bract linear lanceolate, 4-5 mm.
Corollas	Corolla yellow, outside pubescent; corolla tube gyro-shaped, 3-4 mm long, uniformly cylindrical or inflated just below or at throat and densely clavate pubescent; corolla lobes, 4 mm long, oblong-lanceolate, acuminate.	Corolla yellow, outside densely strigillose; corolla tube, 26-28 mm, constricted at throat and inside orange-yellow clavate pubescent; corolla lobes, ellipsoid, mucronate.

Table 4-1-1. Morphological comparison of *M. pubescens* and *M. hirsutula* (continue)

Taxa	<i>M. pubescens</i>	<i>M. hirsutula</i>
Calyxes	Calyx lobe, non-leaflike, linear or triangular, less than 1.5 mm wide, longer than corolla tube twice, densely pilose on base, becoming sparser upward; 1 lobes on 1-3 flowers per inflorescence expanded into calycophyll, broadly elliptic, 2.5-5 × 2-3.5 cm, blunt or mucronate on apex, narrow on base strigillose on both surfaces, with 5-7 longitudinal veins.	Calyx lobe elliptic, 4-5mm long, densely pilose; lobe, linear, 7-10 mm long, densely pilose; 1 lobe on 1-3 flowers per inflorescence expanded into calycophyll, broadly elliptic, 4-4.5 × 3-3.5 cm, round or short pointed on apex, nearly rounded on base, pilose, with 7 longitudinal veins.
Flower period	April-July	April-June
Fruits	Fruit period, Jun to Dec; berry subglobose, 8-10 × 6-7.5 mm in diameter, smooth, fleshy or stiffly papery, sparsely pilose; stipitate 4-5 mm; black after drying.	Fruit period, July to next January; berry ellipsoid or subglobose, 14-20 × 9-12 mm in diameter; brown after dry with small light brown spots.
Identification	Inflorescence from congestion to relaxation. Flowers with stalks 1-5 mm. Corolla tube, gyro-shaped (3-4 mm long). Calyx lobes, non-leaflike, linear or triangular, less than 1.5 mm wide, 3-6 mm long, longer than corolla tube twice. Leaves with distinctly petiolate, were ovate-oblong or ovate-lanceolate.	Inflorescences densely congested. Flowers sessile or subsessile. Calyx lobes longer than corolla tube, twice. Calyx lobes, linear; corolla tube, elliptic; corolla lobes, elliptic. Leaves, elliptic or oblong, rarely obovate.

Type: China. Guizhou, Libo County, Maolan National Nature Reserve, 22°5' N, 107°56' E, ca. 980 m a.s.l., on forest edge, 26 Sep 2020, S. Wang 161915 (Holotype, IBSC!).

Distribution and habitat: Currently, *M. pubescens* is known from the provinces of Zhejiang, Hainan, Yunnan, Guizhou, Sichuan, Guangxi, Guangdong, Hubei, Fujian, Hunan, Jiangxi, and Taiwan in China. This plant species is commonly found in dense thickets located in ravines, on slopes of hills, and along village boundaries or roadsides, typically thriving at elevations ranging from 100 to 900 m a.s.l.

Phenology: Flowering from April to July, and fruiting from June to November.

Description: *M. pubescens*, climbing shrub, often extensively twining. Branchlets appressed pubescence, the stems are often accompanied by axillary short shoots that bear small leaves. Leaves with distinctly petiolate (3-15 mm), were ovate-oblong or ovate-lanceolate (5-8 × 2-5 cm), opposite or perhaps rarely whorled, membranous or thinly papery, densely strigillose. The stipules were triangular, densely strigillose, deeply 2-lobed, segments subulate (4-6mm long). Inflorescences were cyme with sessile to subsessile (0.1-1.4 cm, though the fruit may be stipitate), primarily unbranched, densely strigillose to villosulous. Calyx lobes were non-leaflike, linear or triangular, less than 1.5 mm wide, longer than corolla tube twice, densely pilose on base, becoming sparser upward; 1 lobe on 1-3 flowers per inflorescence expanded into calycophyll, broadly elliptic (2.5-5 × 2-3.5 cm), narrow on base, strigillose on both surfaces, with 5-7 longitudinal veins. Corolla tubes were gyro-shaped (3-4 mm long), uniformly cylindrical, or inflated just below or at the throat with dense clavate pubescence; corolla lobes were oblong-lanceolate (4 mm long) and acuminate. The flower period was Apr-Jul. Fruit period was Jun to Dec, were berry subglobose, 8-10 × 6-7.5 mm in diameter, smooth, fleshy or stiffly papery, sparsely pilose; stipitate 4-5 mm; black after drying.

Similar species: The breeding system of *M. pubescens* is characterized by functional dioecy. A Key to Dioecious Species of *Mussaenda* in China is provided below. The forms of trichomes, as well as the morphology of the calyx and corolla, are important characteristics for identifying species (Grecebio et al., 2016). *M. pubescens* is easily distinguished by its corolla tube 11-20 mm, with stems frequently having axillary short shoots containing small leaves (Li et al., 2010; Luo et al., 2015), flowers sessile to pedicellate and range in color from white to yellow, despite bearing morphological similarities to *M. hirsutula* (Deng & Zhang, 2006). Differences among these two species are provided in Table 4-1-1.

Etymology: The specific epithet is derived from the shape of the corolla.

Paratypes: China, Guangxi: Liu Jun 1235399 (PPBC), Zhang Dianxiang 0153214 (IBSC), Deng Liang 0659417 (IBSC), Rong County Census Team 0205196 (GXM); Guangdong: Li Guangmin 149045 (PPBC), Deng Xiaotong 012602 (SN), Liu Na 012311 (SN), Yang Yuying 010881 (SN); Hunan: Yu Xunlin 1236160 (PPBC), Ran Jing 0007240 (GNUG); Yunnan: Chen Yousheng 449219 (PPBC), Li Yongliang 1450785 (KUN), Yu Xunlin 064698 (CSFI); Fujian: Qu Hua 068014 (AU), Ching H.H. 0659418 (IBSC), Guo Zhizhao 076512 (AU); Jiangxi: Cao Lan 0001459 (JXCM), Chen Gongxi 00197444 (SYS); Gui zhou: Li Qirui 0101386 (GZTM), Chen Jianxiang 0099290 (GZTM), Wu Shiyan 0102818 (GZTM); Taiwan: Masakazu 0768530 (IBSC), Bartholomew B. 00793088 (PE); Hong Kong: Shiu Ying 00793108 (PE), Chen Huanyong 00793121 (PE); Sichuan: Zhu Dahai 02115800 (PE), Fang Wenpei 0472099 (IBSC); Hubei: Fu Guoxun 0472100 (IBSC); Zhejiang: Qin Renchang 0472098 (IBSC).

Key to dioecious species of *Mussaenda* in China

- 1a. Individual flowers with all calyx lobes enlarged into petaloid calycophylls *M. anomala*
- 1b. Individual flowers with only 1 calyx lobes enlarged into petaloid calycophylls, or without calycophylls (2)
 - 2a. Normal calyx lobes subleaflike, lanceolate, 1.5-5 mm wide (3)
 - 3a. Branches, calyx, and corolla, covered villosulous *M. macrophylla*
 - 3b. Branches, calyx and corolla, appressed strigillose *M. esquirolii*
 - 2b. Normal calyx lobes, non-leaflike, linear or triangular, less than 1.5 mm wide (4)
 - 4a. Leaves, sessile or subsessile, < 3 mm
 - 4b. Leaves, distinctly petiolate, 3-15 mm (5)
 - 5a. Normal calyx lobes (at anthesis) 1-15 mm, shorter than calyx tube
 - 5b. Normal calyx lobes (at anthesis) 25-30 mm, longer than calyx tube (6)
 - 6a. Calyx lobes longer than calyx tube, but not more than twice (7)
 - 7a. Cymes, dense
 - 7b. Cymes, Loose (8)
 - 8a. Calyx lobes, linear
 - 8b. Calyx lobes, subulate (9)
 - 9a. Corolla lobes, triangular-ovate; leaves, elliptic *M. elliptica*
 - 9b. Corolla lobes, ovate; leaves, elliptic or ovate-elliptic, with pubescent on abaxially *M. divaricata*
 - 6b. Calyx lobes longer than calyx tube, more than twice and more (10)

- 10a. Calyx lobes longer than calyx tube, more than twice
- 10b. Calyx lobes longer than corolla tube, twice (11)
- 11a. Corolla tube, elliptic; leaves, elliptic or oblong, rarely obovate (12)
- 12a. Corolla lobes, triangular-ovate; calyx lobes, linear-lanceolate
M. hainanensis
- 12b. Corolla lobes, elliptic; calyx lobes, linear *M. hirsutula*
- 11b. Corolla tube, gyro-shaped, 3-4 mm long; leaves, ovate-oblong or
ovate-lanceolate; corolla lobes, oblong-lanceolate, acuminate
M. pubescens

4.1.2 *cp genome features of M. pubescens*

cp DNA sequences, characterized by their highly conserved structure, minimal recombination events, and predominantly uniparental inheritance, have traditionally served as preferred markers for reconstructing plant phylogeny. A robust phylogeny is essential to investigate the evolutionary patterns of traits across varying taxonomic levels. The *cp genome* yields essential information for various scientific disciplines, including species identification, population genetics, phylogenetics, and genetic engineering research (Daniell et al., 2016; Luo et al., 2021; Wu et al., 2021). The filtering process obtained 20,928,581 paired end reads from the Illumina NovaSeq platform, all meeting the required quality standards. The values for Q20 and Q30 were determined to be 97.53% and 92.98%, respectively. The complete *cp genome* sequence of *M. pubescens* was constructed *de novo* and subsequently submitted to the Database Resources of the National Genomics Data Center (GSA accession number: CRA013306).

The *cp genomes* of plants consisted of photosynthetic genes, genes related to chloroplast transcriptional expression, and additional protein-coding genes (Jansen et al., 2005). Expansion and contraction of the boundaries of the inverted region (IR) are the primary factors contributing to changes in the size of the *cp genomes*, playing a crucial role in species evolution (Yen et al., 2023). As was common with other angiosperms, the *cp genome* of *M. pubescens* consisted of a circular genome measuring 155,122 bp in length and possessing the typical quadripartite structure. This structure included a pair of reverse repeats, namely IRA and IRB, which spanned 25,871 bp, a small single copy region (SSC) measuring 18,010 bp, and a large single copy region (LSC) spanning 85,370 bp (Table 4-1-2 and Figure 4-1-2). The expansion and contraction observed in the IR regions might serve as the primary mechanism for generating

variations in the length of the *cp genomes* in both *M. pubescens* and its closely related species (Asaf et al., 2016; Xue et al., 2019).

Table 4-1-2. Characteristics of *M. pubescens* *cp genome*.

Category	Item (bp)	Describe
cp genome structure	Total length	155122
	LSC length	85370
	SSC length	18010
	IRA length	25871
	IRB length	25871
Gene composition	Genes	128
	Protein-coding genes (CDS)	86
	tRNA genes	34
	rRNA genes	8

Genes situated on the inner side of the circle are transcribed in a clockwise direction, whereas those on the outer side are transcribed in a counterclockwise direction. The inner circle of a darker gray represents the GC content, while the lighter gray indicates the AT content. Different colors represent different functional genes.

The GC content varied across different regions of the *cp genomes*, with the IR regions particularly exhibiting high GC content, likely due to the presence of rRNAs (Abdullah et al., 2020). Our findings indicated that the GC contents in the IR and SSC regions were measured to be 43.17% and 31.89%, respectively, with the average GC content of the whole genome being 37.67% (Table 4-1-3). Notably, the GC content of DNA in the IR regions was higher than that in other regions (LSC, SSC) (Figure 4-1-2), which aligned with similar patterns observed in other flowering plants (Hu et al., 2016; Liu et al., 2018). Furthermore, the GC skewness has been identified as a crucial indicator of DNA leading chains, lagging chains, and replication origins and terminals, which in turn serves as an important determinant of species affinity (Necşulea & Lobry, 2007).

Gene functions were subsequently assigned to all the genes (Table 4-1-2), with these genes being classified into four types: genes related to self-replication, genes related to photosynthesis, unknown function genes, and specific genes, including maturase (*matK*), protease (*clpP*), and others. Out of the 128 identified genes, there

were 86 protein-coding genes, 34 transfer RNA (tRNA) genes, and 8 rRNA genes. The observed results were like those found in other *Mussaenda* species (Duan et al., 2017; Wang et al., 2019).

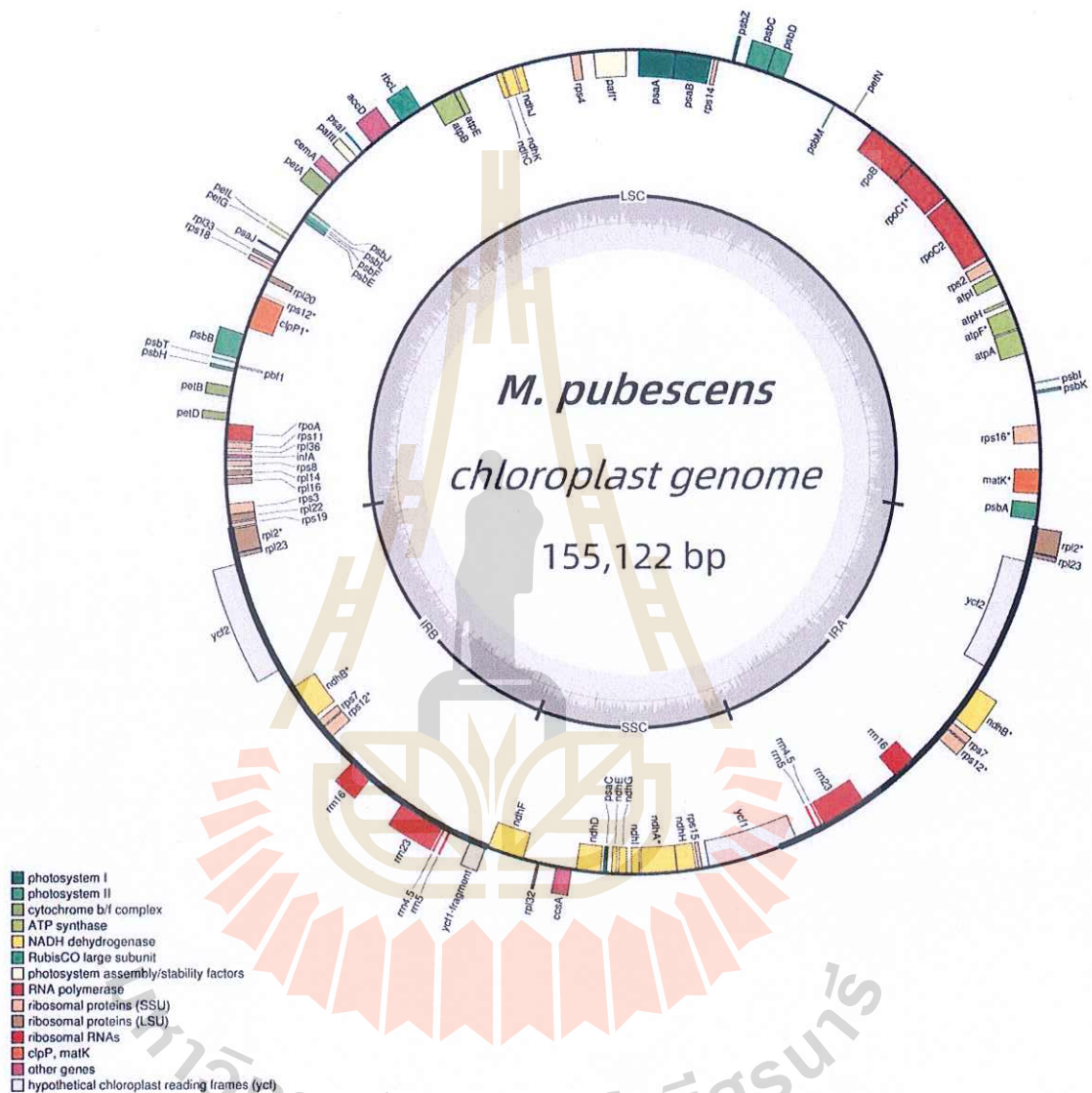


Figure 4-1-2. The *cp* genome maps of *M. pubescens*.

Table 4-1-3. The nucleotide composition of the complete *cp* genomes of *M. pubescens*

Region	A/%	T(U)/%	C/%	G/%	AT/%	GC/%
LSC	31.59	32.86	18.24	17.31	64.45	35.55
SSC	34.04	34.08	16.64	15.25	68.11	31.89
IR	28.42	28.42	21.58	21.58	56.83	43.17
Total	30.82	31.52	19.17	18.50	62.33	37.67

In total, 62 protein-coding genes and 22 tRNA genes were situated in the LSC region, while 11 protein-coding genes and 1 tRNA gene were assigned to the SSC region of the *cp* genome (Figure 4-1-2). Additionally, a total of 20 intron-containing genes, among which there were 17 genes (*e.g.*, *ndhA*, *ndhB*, *petB*, *petD*, *atpF*, *rpl16*, *rpl2*, and *rps16*) with 1 intron and only 3 genes (*rps12*, *clpP1*, and *trnH-GUG*) with 2 introns (Table 4-1-4). Among them, *ndhA* possessed the longest intron (1,115 bp), while the shortest intron (16 bp) was observed in *trnI GAU* (Table 4-1-5). It was noteworthy that *rps12* was classified as a trans-spliced gene consisting of two separated introns, with one exon positioned in the LSC region and the other two in the IR region (Figure 4-1-2). Besides that, the *rps12* gene of *M. pubescens* was comprised of an exon at the 5'-end located in the LSC region, while its 3'-end exons were positioned in the IR regions, as depicted in Figure 4-1-2, which was consistent with that of the homologous species *M. hirsutula* (Wang et al., 2019).

Table 4-1-4. Lists of annotated genomic genes for *M. pubescens*

Category	Gene Group	Gene Name
Photosynthesis	Subunits of Photosystem I	<i>psaA, psaB, psaC, psal, psaj</i>
	Subunits of Photosystem II	<i>psbA, psbB, psbC, psbD, psbE, psbF, psbH, psbI, psbJ, psbK, psbL, psbM, psbN, psbT, psbZ</i>
	Subunits of NADH dehydrogenase	<i>ndhA*, ndhB*(2), ndhC, ndhD, ndhE, ndhF, ndhG, ndhH, ndhI, ndhJ, ndhK</i>
	Subunits of Cytochrome b/f complex	<i>petA, petB*, petD*, petG, petL, petN</i>
	Subunits of ATP synthase	<i>atpA, atpB (2), atpE, atpF*, atpH, atpI</i>
	Large subunit of rubisco	<i>rbcl</i>
	Subunits photochlorophyllide reductase	-
	Large subunit ribosomal proteins	<i>rp114, rp116*, rp12*(2), rp120, rp122, rp123 (2), rp132, rp133, rp136</i>
	Small subunit ribosomal proteins	<i>rps11, rps12**(2), rps14, rps15, rps16*, rps18, rps19, rps2, rps3, rps4, rps7 (2), rps8</i>
	Subunits of RNA polymerase	<i>rpoA, rpoB, rpoC1*, rpoC2</i>
Ribosomal RNAs	<i>rrn16 (2), rrn23 (2), rrn4.5 (2), rrn5 (2)</i>	
Self-replication	Transfer RNAs	<i>trnA-UGC*(2), trnC-GCA, trnD-GUC, trnE-UUC, trnF-GAA, trnG-GCC*, trnH-GUG**(2), trnH-GUG, trnI-GAU* (2), trnL-CAA* (2), trnL-UAG, trnM-CAU (2), trnM-CAU* (2), trnN-GUU* (2), trnP-UGG, trnQ-UUG, trnR-ACG* (2), trnR-UCU, trnS-GCU, trnS-GGA, trnS-UGA, trnT-GGU, trnT-UGU, trnV-GAC* (2), trnW-CCA, trnY-GUA</i>
	Maturase	<i>matK</i>
Other genes	Protease	<i>clpP1**</i>
	Envelope membrane protein	<i>cemA</i>

Table 4-1-4. Lists of annotated genomic genes for *M. pubescens* (continue)

Category	Gene Group	Gene Name
Other genes (continue)	Acetyl-CoA carboxylase	<i>accD</i>
	c-type cytochrome synthesis gene	<i>ccsA</i>
	Translation initiation factor	<i>infA</i>
Unknown function genes	Other	-
	Conserved hypothetical chloroplast ORF	<i>pf1</i> , <i>pf2</i> , <i>pbf1</i> , <i>ycf1</i> , <i>#ycf1</i> , <i>ycf2</i> (2)

* , Gene with one intron; ** , Gene with two introns; #, Pseudogene; (2), Gene with two copies.

The codon usage bias in *cp genomes* may arise from a combination of natural selection and genetic mutation, which is important to investigate this phenomenon as it provides insights into the evolutionary processes and functional constraints shaping the genetic code of chloroplasts (Li et al., 2023). The relative frequency of synonymous codons in the coding sequence of *M. pubescens* cp demonstrated that all genes were represented by 19,850 codons. The study identified the four most utilized codons as ATT (Isoleucine), GAA (Glutamic acid), AAT (Asparagine), and AAA (Lysine), accounting for 843 (4.25%), 752 (3.79%), 723 (3.64%), and 715 (3.60%) codons, respectively. One of the most used amino acids was leucine, with 2155 hits; another one, cysteine, had the lowest content, with only 277 hits. Additionally, codons ending with 'A' and 'T' accounted for 69.13% of all codons (Table 4-1-6), which aligned with previous studies on angiosperms (Gao et al., 2023). The codon usage preferences encompassed within these features could actively contribute to a more in-depth understanding of exogenous gene expression and the mechanisms driving the evolution of the cp genome (Duan et al., 2021; Huo et al., 2022).

Table 4-1-5. Characteristics and sizes of the intron and exon genes from *M. pubescens*

Gene	Region (bp)	Exon I (bp)	Intron I (bp)	Exon II (bp)	Intron II (bp)	Exon III (bp)
<i>rps16</i>		36	840	231		
<i>atpF</i>		144	715	411		
<i>rpoC1</i>	LSC	430	756	1613		
<i>pafl</i>		124	717	228	768	155
<i>clpP1</i>		71	789	292	663	228
<i>rpl2</i>		391	659	434		
<i>ndhB</i>		777	684	756		
<i>rps12</i>	IRB	114	-	234	526	25
<i>trnI-GAU</i>		36	16	36		
<i>trnA-UGC</i>		37	40	28		
<i>ndhA</i>	SSC	553	1115	539		
<i>trnA-UGC</i>		37	40	28		
<i>trnI-GAU</i>		36	16	36		
<i>rps12</i>	IRA	234	526	25		
<i>ndhB</i>		777	684	756		
<i>rpl2</i>		391	659	434		

Table 4-1-6. Codon usage of *M. pubescens* cp genome from RSCU tools

Amino Acid	Symbol	Codon	Number	/1000	RSCU
*	Ter	TGA	13	0.65	0.57
*	Ter	TAG	21	1.06	0.93
*	Ter	TAA	34	1.71	1.50
A	Ala	GCG	100	5.04	0.37
A	Ala	GCA	301	15.16	1.11
A	Ala	GCT	480	24.18	1.77
A	Ala	GCC	201	10.13	0.74
C	Cys	TGT	176	8.87	1.55
C	Cys	TGC	51	2.57	0.45
D	Asp	GAT	652	32.85	1.62
D	Asp	GAC	153	7.71	0.38
E	Glu	GAG	267	13.45	0.52
E	Glu	GAA	752	37.88	1.48
F	Phe	TTT	672	33.85	1.23
F	Phe	TTC	420	21.16	0.77
G	Gly	GGG	252	12.7	0.72
G	Gly	GGA	580	29.22	1.66
G	Gly	GGT	437	22.02	1.25
G	Gly	GGC	127	6.4	0.36
H	His	CAT	380	19.14	1.53
H	His	CAC	118	5.94	0.47
I	Ile	ATA	511	25.74	0.91
I	Ile	ATT	843	42.47	1.50
I	Ile	ATC	335	16.88	0.60
K	Lys	AAG	270	13.6	0.55
K	Lys	AAA	715	36.02	1.45
L	Leu	TTG	431	21.71	1.20
L	Leu	TTA	618	31.13	1.72
L	Leu	CTG	140	7.05	0.39
L	Leu	CTA	329	16.57	0.92
L	Leu	CTT	479	24.13	1.33
L	Leu	CTC	158	7.96	0.44
M	Met	ATG	453	22.82	1.00
N	Asn	AAT	723	36.42	1.52

Table 4-1-6. Codon usage of *M. pubescens* cp genome from RSCU tools (continue)

Amino Acid	Symbol	Codon	Number	/1000	RSCU
N	Asn	AAC	230	11.59	0.48
P	Pro	CCG	120	6.05	0.59
P	Pro	CCA	230	11.59	1.13
P	Pro	CCT	296	14.91	1.46
P	Pro	CCC	165	8.31	0.81
Q	Gln	CAG	189	9.52	0.52
Q	Gln	CAA	540	27.2	1.48
R	Arg	AGG	136	6.85	0.67
R	Arg	AGA	345	17.38	1.71
R	Arg	CGG	99	4.99	0.49
R	Arg	CGA	303	15.26	1.50
R	Arg	CGT	250	12.59	1.24
R	Arg	CGC	81	4.08	0.40
S	Ser	AGT	284	14.31	1.07
S	Ser	AGC	95	4.79	0.36
S	Ser	TCG	170	8.56	0.64
S	Ser	TCA	320	16.12	1.21
S	Ser	TCT	455	22.92	1.72
S	Ser	TCC	267	13.45	1.01
T	Thr	ACG	130	6.55	0.53
T	Thr	ACA	296	14.91	1.20
T	Thr	ACT	365	18.39	1.48
T	Thr	ACC	193	9.72	0.78
V	Val	GTG	156	7.86	0.59
V	Val	GTA	400	20.15	1.50
V	Val	GTT	373	18.79	1.40
V	Val	GTC	136	6.85	0.51
W	Trp	TGG	336	16.93	1.00
Y	Tyr	TAT	570	28.72	1.63
Y	Tyr	TAC	128	6.45	0.37

4.1.3 Phylogenetic analysis

cp genomes are valuable sources of information for species identification and evolutionary analysis (Fan et al., 2021). They serve as organelle-based "barcodes" to distinguish species and reveal interspecies phylogenetic relationships (Yang et al., 2013). Furthermore, the progressive advancements in next-generation sequencing technology, specifically the implementation of second-generation technology, have facilitated the simplification of *cp genome* sequencing. Thus, an accumulating body of studies has employed complete *cp genome* sequences to examine phylogenetic relationships within angiosperms. The phylogenetic position of *M. pubescens* was analyzed by downloading 19 complete *cp* genomes from the GenBank database, all of which belonged to the *Gramineae* family. The genomes were aligned using the MAFFT (Kato et al., 2013), and the phylogenetic tree was constructed with the Mega-X v10.0.5 software (Kumar et al., 2016) employing the maximum likelihood method and 1000 bootstrap replicates (Figure 4-1-3). The observed *cp genome* sequences played a vital role in elucidating and comprehending the phylogenetic relationships among *Mussaenda* species.

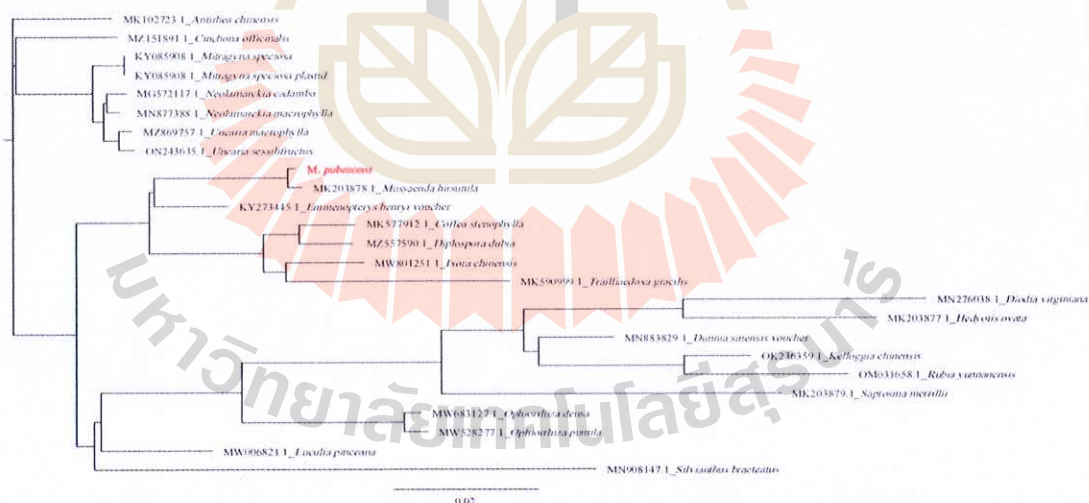


Figure 4-1-3. The phylogenetic tree of *M. pubescens*

The diversification of the species, *M. pubescens*, was attributed to the presence of a highly diverse set of genes, intermolecular recombination in the LSC region, and the co-occurrence of tandem repeats. The phylogenetic analyses yielded highly similar topologies across the complete *cp genomes*, LSC regions, and SSC regions (the complete

cp genome displayed complete consistency with the LSC region), and every node in the phylogenetic trees exhibited high bootstrap support, apart from *Antirhea chinensis* and *Cinchona officinalis* (Figure 4-1-3). *Rubiaceae* species, along with species in the same genus, showed a tendency to cluster together on a single large branch. The *Rubiaceae* branch was divided into two clades with *Antirhea*, *Cinchona*, *Mitragyna*, *Neolamarckia*, and *Uncaria* to other 20 genera. *Mussaenda* was found to be related to 19 other genera, and within these, it was determined that *M. pubescens* shared a close relationship with *M. hirsutula*, and five other genera (*Emmenopterys*, *Coffea*, *Diplospora*, *Lxora*, and *Trailliaedoxa*). The phylogenetic tree demonstrated that *Mussaenda* was polyphyletic and originated from the intercalation of branches from the genera *M. hirsutula*. Moreover, *M. pubescens* and *M. hirsutula* were found to be closely related genera. The findings support the identification and taxonomic study of *M. pubescens*, enabling resource collection, cultivation, study of pharmacological activities, and development of functional products.



4.2. Metabolomics reveals the importance of metabolites in *M. pubescens*

4.2.1 Metabolomic profiling of Mp leaves at different developmental stages

In this study, metabolomics analysis was carried out on samples collected at three stages: Mp bud, tender, and mature leaves (Figure 4-2-1). The primary classification of substances revealed that Mp leaves contained 957 metabolites, the most abundant of which were phenolic acids (185), lipids (155), and terpenoids (109). Furthermore, 85 organic acids, 81 flavonoids, 78 amino acids and their derivatives, 66 nucleotides and their derivatives, 33 lignans and coumarins, and 31 alkaloids were identified. The overlay analysis of the QC-TIC diagram and the sample multi-peak detection diagram revealed that the data collected in this study was both repeatable and reliable. Furthermore, the three biological replicates of each sample showed significantly higher correlation coefficients ranging from 0.89 to 0.99, indicating that the samples were homogeneous.



Figure 4-2-1. Phenotypes of the leaves surface and back of Mp at the different growth stages. From left to right are MpBud, MpTen and MpMat.

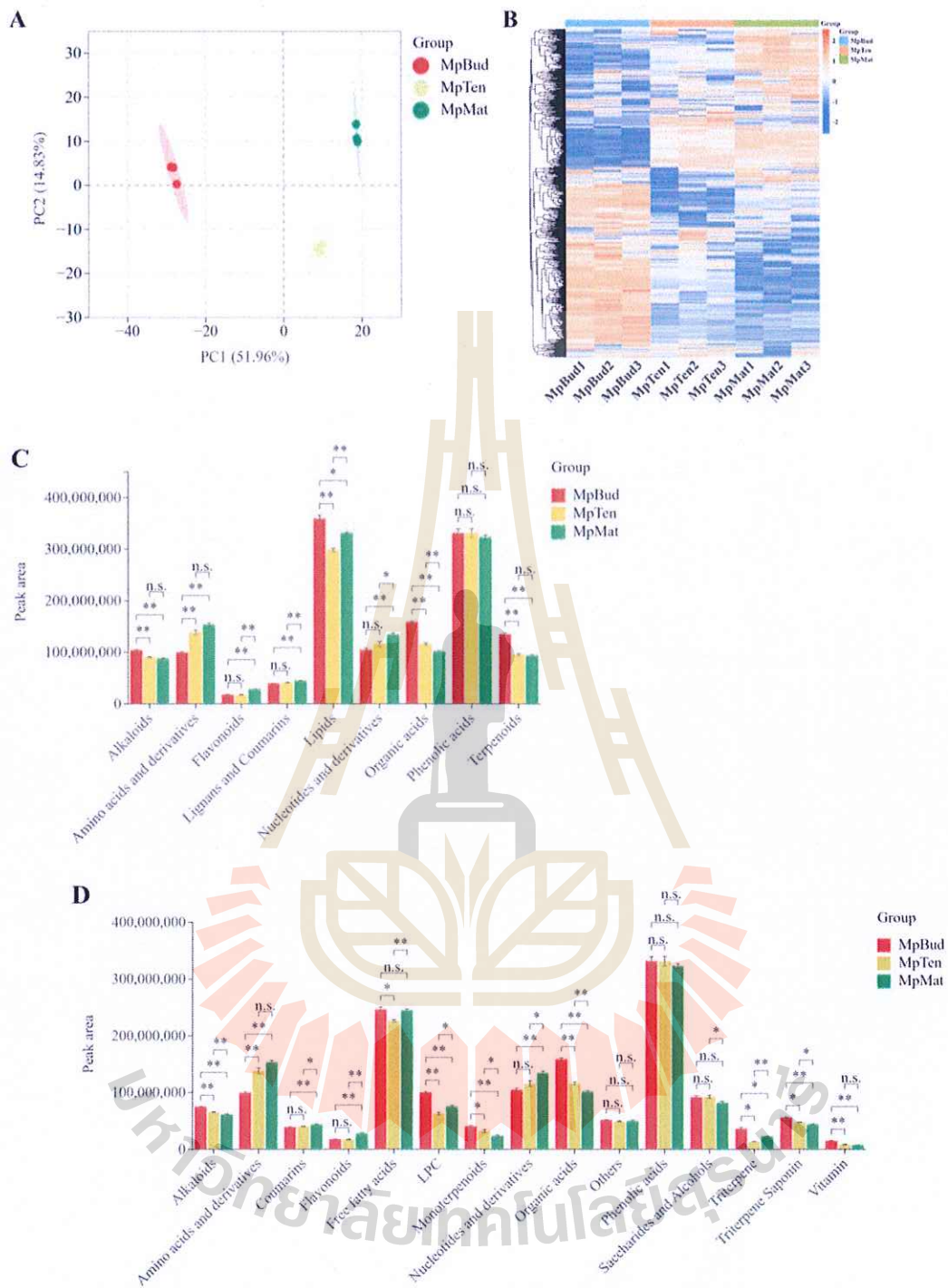


Figure 4-2-2. Abundance and differential expression of metabolites in the leaves of Mp. (A) PCA analysis of metabolites, (B) Clustering heatmap, (C) Abundance of the first-level classification of metabolites, (D) Abundance of the second-level classification of metabolites.

4.2.2 PCA and OPLS-DA for Mp

In the PCA plot, leaves at three distinct developmental stages were clearly separated. The three biological replicates of each group clustered closely, with PC1 and PC2 accounting for 51.96% and 14.84% of the variation, respectively (Figure 4-2-2A). These findings demonstrated the repeatability and reliability of the entire analysis, as well as significant differences between the three groups. A total of 957 substances were identified across the samples collected, as shown in the heatmap, which manifested the visible hierarchical clustering among the groups. The content of substances in the bud leaves varied significantly compared to that in the tender and mature leaves, with approximately half of the samples showing relatively higher levels, while the others had lower content (Figure 4-2-2B). The first-level classification of substances showed that lipids and phenolic acids were the main parts of Mp leaves. The levels of these substances were higher in the bud leaves compared to the tender and mature leaves (Figure 4-2-2C). The total amount of organic acids, terpenoids, and alkaloids was also relatively abundant in the bud leaves. However, the accumulation of nucleotides and derivatives, amino acids and derivatives, lignans and coumarins, and flavonoids significantly increased as the leaves matured (in the tender and mature leaves). Phenolic acids play pivotal physiological roles in the plant life cycle and are the primary group of plant secondary metabolites (Dursun et al., 2023). The increasing interest in the profile of phenolic acids is closely associated with their antioxidant activity and potential health benefits (Qiu et al., 2010). In the present study, phenolic acids were observed to be the predominant fraction in Mp leaves, which suggested that this plant might possess natural antioxidant properties and could be utilized as a medicinal plant for therapeutic purposes. According to the abundance of secondary classifications of substances, the buds and leaves contained the most phenolic acids, free fatty acids, and organic acids (Figure 4-2-2D). It was also discovered that tender leaves contained a greater number of phenolic acids, saccharides, alcohols, and other substances, whereas mature leaves contained more free fatty lipids, nucleotides and their derivatives, amino acids and their derivatives, coumarins, and flavonols. These findings indicated that the metabolite profiling of Mp leaves was significantly influenced by their growth and development at various stages.

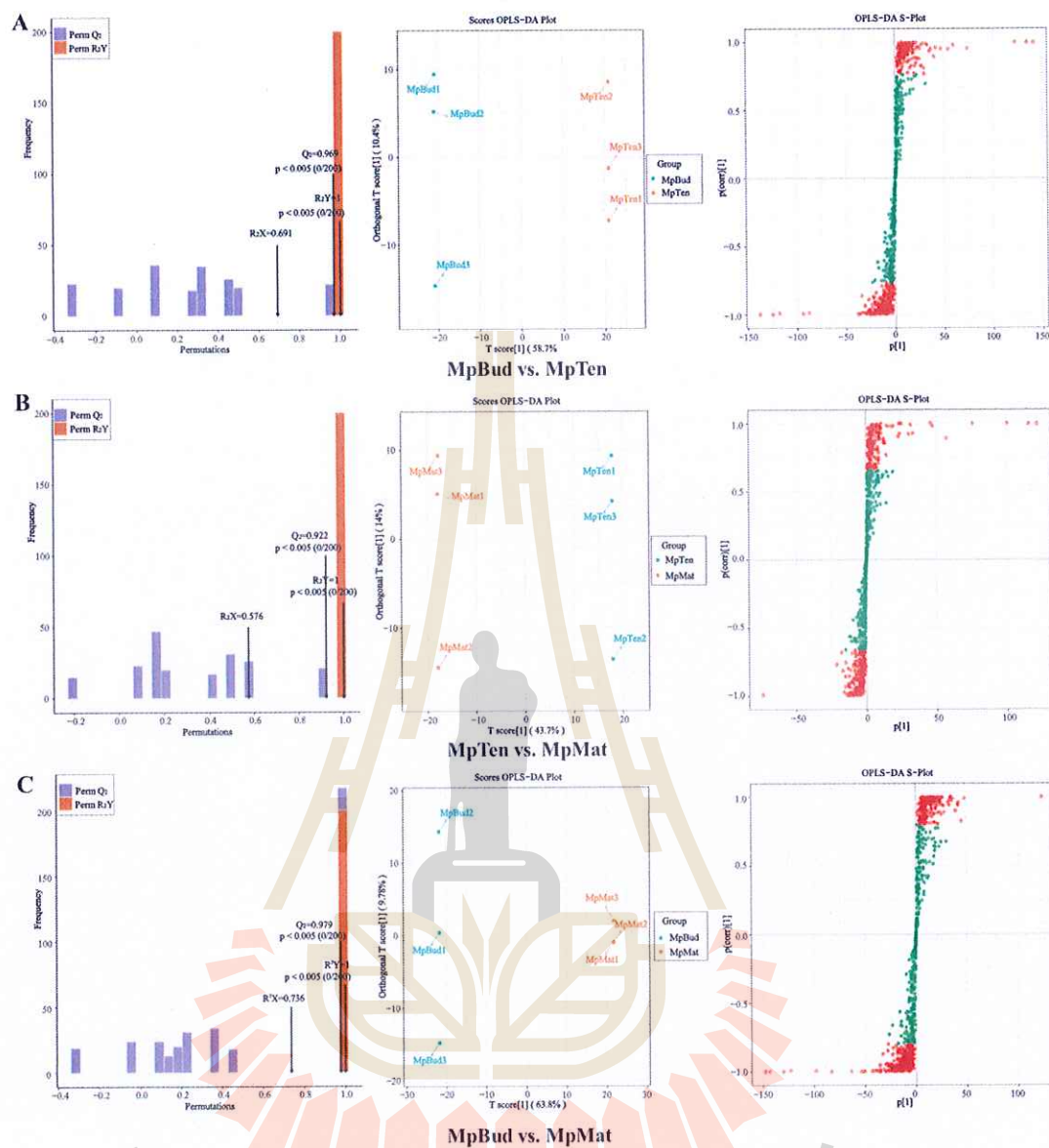


Figure 4-2-3. Orthogonal partial least squares-discriminant analysis (OPLS-DA) scores of Mp leaves. (A) MpBud vs. MpTen, (B) MpTen vs. MpMat, and (C) MpBud vs. MpMat. From left to right are permutation of OPLS-DA model, Scores of the OPLS-DA model, and OPLS-DA S-plot model. R^2Y scores and Q^2 values represent the interpretation rate of the model to the Y matrix and the prediction ability of the model, respectively. When $Q^2 > 0.5$, the model can be considered an effective model, and $Q^2 > 0.9$ is an excellent model.

Furthermore, OPLS-DA was used to identify the variables that explain the differences between these three groups. In the current study, the OPLS-DA model was used to compare the metabolites of the samples in the comparisons to evaluate the differences in MpBud vs. MpTen ($R^2X = 0.691$, $R^2Y = 1$, $Q^2 = 0.969$), MpTen vs. MpMat ($R^2X = 0.576$, $R^2Y = 1$, $Q^2 = 0.922$), and MpBud vs. MpMat ($R^2X = 0.736$, $R^2Y = 1$, $Q^2 = 0.979$) (Figure 4-2-3). The Q^2 values of all the comparisons were greater than 0.9, indicating that these models were stable and credible. The OPLS-DA score plots revealed a clear separation between the three stages, implying significant differences in the metabolic phenotypes of Mp leaves at different developmental stages. These results revealed that the mature stage was the primary process in the evolution of metabolites, followed by the bud stage, while the tender stage had the least impact.

4.2.3 Differentially accumulated metabolites screening, functional annotation, and enrichment analysis among the Mp leaves at different developmental stages

To determine the impact of each stage on the metabolites present at different developmental stages of Mp leaves, the critical differences between these processes were investigated. A total of 317 DAMs were screened, of which 202 DAMs were observed in MpBud vs. MpTen (Figure 4-2-4A, 74 up-regulation and 128 down-regulation), 54 DAMs were observed in MpTen vs. MpMat (Figure 4-2-4B, 27 up-regulation and 27 down-regulation), and 254 DAMs were observed in MpBud vs. MpMat (Figure 4-2-4C, 107 up-regulation and 147 down-regulation).

The Venn diagram exhibited the presence of both common and unique metabolites among the comparisons (Figure 4-2-4D). Specifically, MpBud vs. MpTen and MpTen vs. MpMat possessed 29 common substances that were simultaneously affected by the growth and development of Mp leaves. Additionally, 149 common metabolites were observed in MpBud vs. MpTen and MpBud vs. MpMat, which illustrated that these common metabolites accumulated more during the bud to tender stages, with particular emphasis on phenolic acids, flavonoids, and terpenoids. Furthermore, 27 common metabolites were identified in MpTen vs. MpMat and MpBud vs. MpMat, which were less affected by Mp leaf growth and development from tender to mature. Importantly, three comparisons (MpBud vs. MpTen, MpTen vs. MpMat, and MpBud vs. MpMat) shared only 12 common metabolites such as benzamide, 2-phenylethanol, pinocembrin-7-*O*-glucoside (pinocembroside), mussaenoside, and $1\beta,2\alpha,3\alpha,19\alpha$ -tetrahydroxyurs-12-en-28-

oic acid. These DAMs exhibited the highest metabolic activity during the growth of Mp leaves, which was consistent with a previous report suggesting a close correlation with alterations in leaf color, biochemical components, and functionality (Li et al., 2021). Meanwhile, 90 metabolites unique to MpBud vs. MpMat were only affected by the growth and development of the leaves. Among these, 36 metabolites (i.e., 24,30-dihydroxy-12(13)-enolupinol, $3\beta,19\alpha$ -dihydroxyolean-12-en-28-oic acid, and $2\alpha,3\beta,19\alpha$ -trihydroxyurs-12-en-23,28-dioic acid-28-O-glucoside) were only biosynthesized and accumulated during bud to tender stages. These components may have contributed to the leaf color change of Mp. Conversely, ten metabolites (i.e., 4-hydroxybenzoic acid, 5,6-dihydroxyindole-5-O- β -glucoside, and kaempferol-3-O-sophoroside) were only biosynthesized and accumulated during tender to mature stages (Figure 4-2-4D). We proposed that the DAMs found in MpBud vs. MpTen and MpTen vs. MpMat may contribute to the biosynthesis of functional and nutritional ingredients and the leaf color change in Mp. These findings indicated significant differences in the metabolites present in bud, tender, and mature leaves. As a result, the levels of various functional and nutritional ingredients varied at different stages of Mp leaf growth and development (tissues or cells), as these components were constantly synthesized and accumulated as the leaves grew. These results further confirmed the essential role of unique metabolites presented in mature leaves in driving the transformation of metabolites. Furthermore, mature leaves had higher levels of these metabolites than buds and tender leaves during Mp leaf growth and development, implying that leaf aging may stimulate hydrolysis, isomerization, oxidation, and other metabolic reactions.

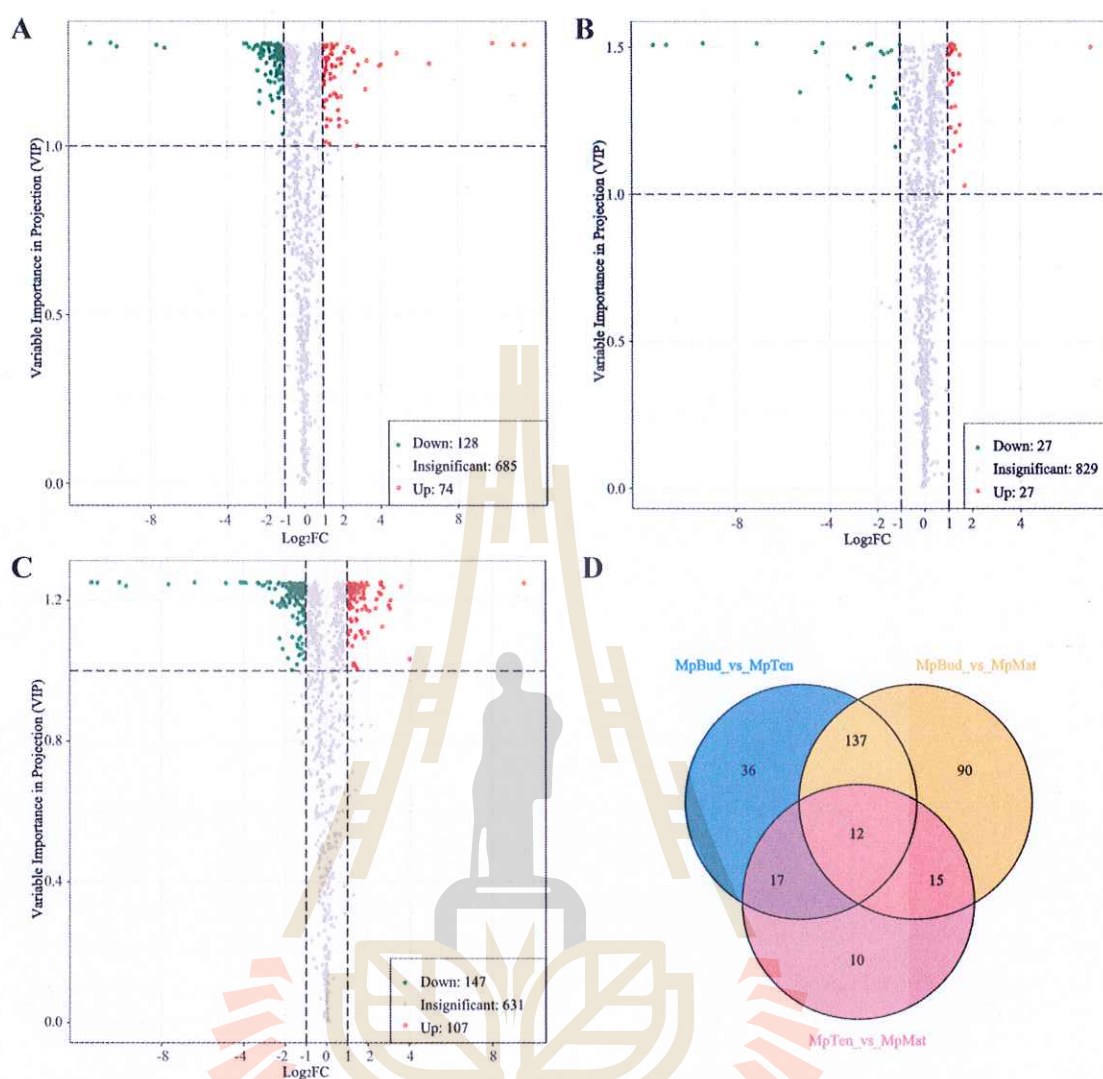


Figure 4-2-4. Differential metabolites present in Mp leaves. Volcano plot of the differential metabolites in three comparisons of (A) MpBud vs. MpTen, (B) MpTen vs. MpMat, and (C) MpBud vs. MpMat. (D) Venn diagram of the differential metabolites in multiple pairwise comparison of MpBud vs. MpTen, MpTen vs. MpMat, and MpBud vs. MpMat.

From K-means cluster analysis of metabolite abundance (Figure 4-2-5), the contents of metabolites in Sub Class 1, 4, 5, 7, and 9 were higher in the bud leaves, with a total of 176 metabolites, mainly including 2-isopropylmaleic acid, 2-phylllethylamine, lysoPC 18:1 (2n isomer), and *L*-lyclopentylglycine. Sub Class 3 and 6 contained 118 metabolites, the majority of which increased with leaf maturity, mainly including adenosine, *L*-isoleucine, and quercetin-3-*O*-galactoside (hyperin).

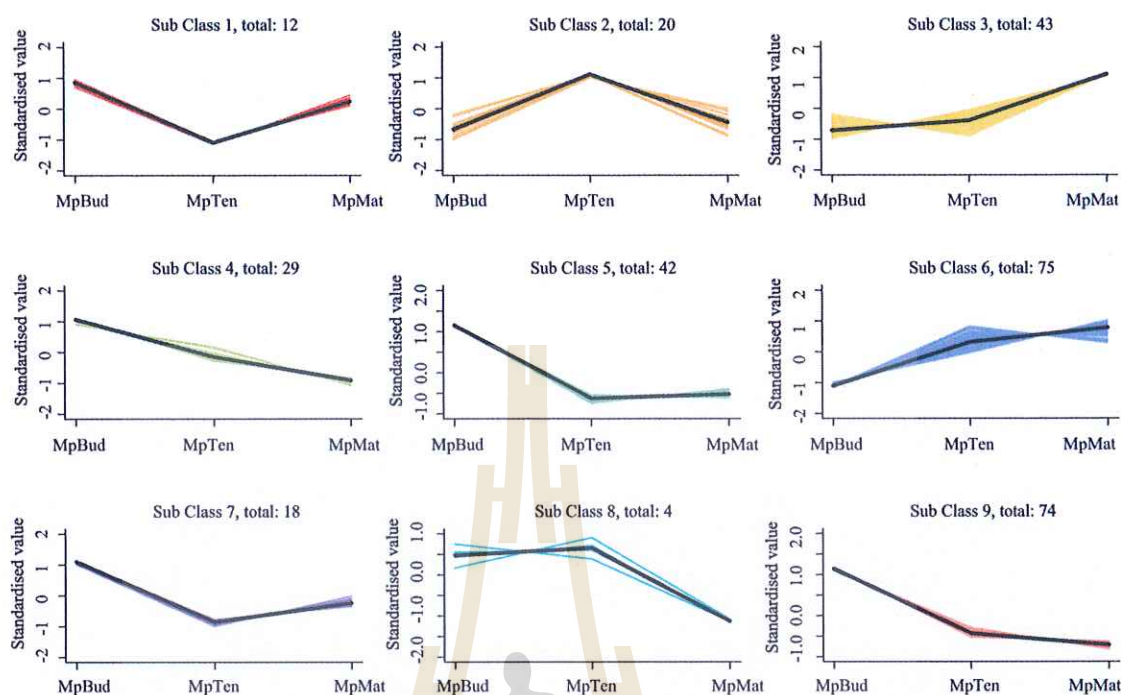
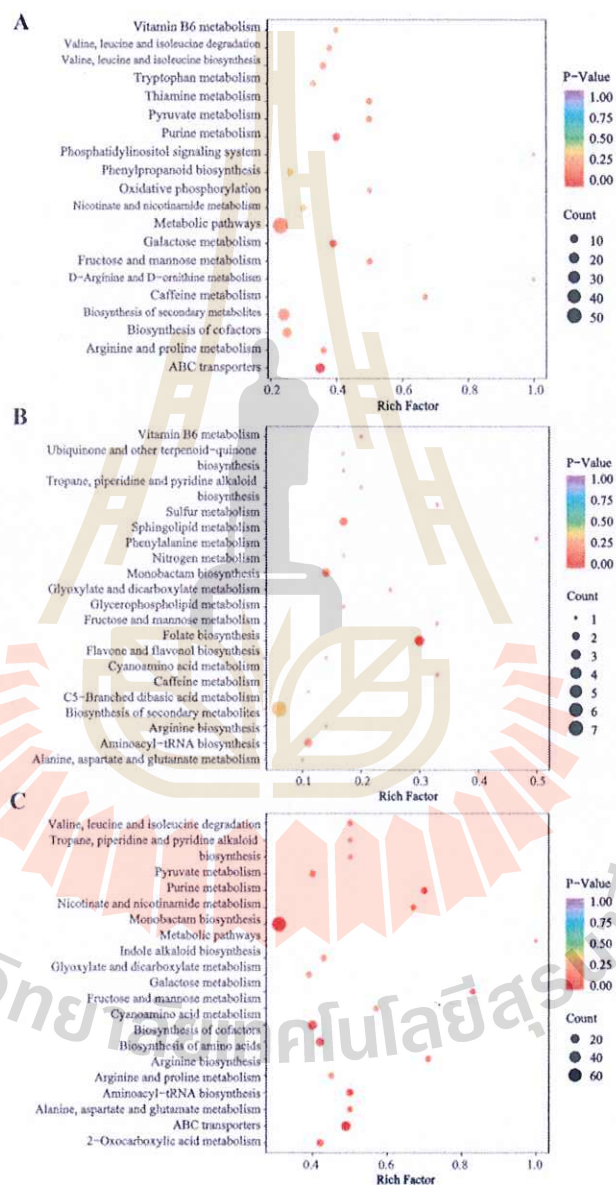


Figure 4-2-5. Trend analysis of differential metabolites during the development of Mp leaves.

In Sub Class 2, the content of 20 metabolites in tender leaf was significantly higher, such as caffeine, kaempferol-3-*O*-rutinoside-7-*O*-glucoside, quercetin-7-*O*-rutinoside-4'-*O*-glucoside, and mussaenoside. When compared to tender leaves, the amount of dehydrocastus lactone, which belongs to sesquiterpenoids, decreased to 48.2%; mussaenoside in the sesquiterpenoids increased by 2.3 times, whereas penstemonoside and deacetylasperosidic acid decreased to 49.1% and 35.8%, respectively. Triterpenoids showed a downward trend, with a decline range of 13.1%–46.0%, and the most significant decrease was observed in 1 β ,2 α ,3 α ,9 α -tetrahydroxurs-12-en-28-oic acid and the least in 23-hydroxybetulinic acid. In flavonoids, the glycoside of kaempferol increased, while that of quercetin decreased. Specifically, kaempferol-3-*O*-rutinoside-7-*O*-glucoside increased by 15.5 times, whereas quercetin-3-*O*- (6''-*O*-acetyl) glucoside decreased to 17.8%. Compared with mature leaves, the isohyperoside and quercetin-3-*O*-glucoside (isoquercitrin) of flavonols and scopoletin-7-*O*-glucoside (scopolin) of coumarin increased by 2.1–2.3 times in tender leaves. The content of 2-phenylethylamine, which belongs to alkaloids, has decreased significantly, with mature

leaves accounting for only 20.7% of the content in tender leaves. However, the mussaenoside of sesterpenes and the kaempferol-3-*O*-rutinoside-7-*O*-glucoside of flavonols in mature leaves were only 13.1% and 2% of the tender leaves, respectively. In addition, the triterpene 2,3-dihydroxy-12-ursen-28-oic acid increased by 2.1 times.



Note: (A) MpBud vs. MpTen, (B) MpTen vs. MpMat, and (C) MpBud vs. MpMat. Each bubble in the plot represents a metabolic pathway whose abscissa and bubble size jointly indicate the magnitude of the impact factors of the pathway. A larger bubble size indicates a larger impact factor. The bubble colors represent the *p*-values of the enrichment analysis, with darker colors showing a higher degree of enrichment.

The differential metabolites for MpBud vs. MpTen, MpTen vs. MpMat, and MpBud vs. MpMat were involved in 66, 37, and 75 pathways, respectively (Figure 4-2-6A-C). Most noteworthy, the top ten metabolic pathways, including "ABC transporters", "purine metabolism", and "galactose metabolism" were significantly up-regulated (*p*-value < 0.05) in MpBud vs. MpTen (Figure 4-2-6A).

Similarly, the top ten metabolic pathways, including "flavone and flavonol biosynthesis", "nitrogen metabolism", "phenylalanine metabolism", "folate biosynthesis", and "sphingolipid metabolism" were enriched in the comparison of MpTen vs. MpMat (Figure 4-2-6B). Whereas "ABC transporters", "nicotinate and nicotinamide metabolism", "fructose and mannose metabolism", "metabolic pathways", "arginine biosynthesis", "biosynthesis of cofactors", "biosynthesis of amino acids", "aminoacyl-tRNA biosynthesis", "monobactam biosynthesis", and "indole alkaloid biosynthesis" showed a *p*-value < 0.05 in the enrichment analysis of MpBud vs. MpMat (Figure 4-2-6C).

4.2.4 Evaluation of the different metabolites during the growth and development of Mp leaves

During the growth and development of Mp leaves, 317 different metabolites were identified, including 150 primary metabolites (33 amino acids and derivatives, 21 organic acids, 16 lipids, 31 nucleotides and derivatives, and 49 others) and 167 secondary metabolites (48 phenolic acids, 35 flavonoids, 54 terpenoids, 14 lignans and coumarins, and 16 alkaloids) (Figure 4-2-7A). Among them, 36 DAMs were unique to MpBud vs. MpTen, accounting for 11.4% of the total metabolites (Figure 4-2-7B), and 90 DAMs were unique to MpBud vs. MpMat, accounting for 28.4% of the total substances (Figure 4-2-7C).

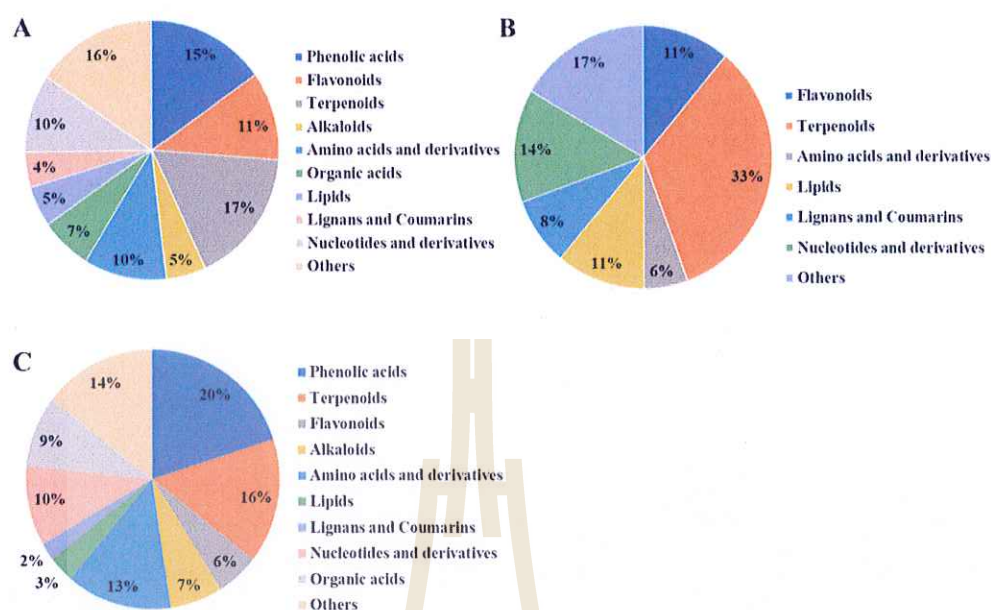


Figure 4-2-7. Pie chart of the number of different types in Mp leaves

Note: (A) all metabolites, (B) specific metabolites of MpBud vs. MpTen, and (C) specific metabolites of MpBud vs. MpMat.

4.2.4.1 Secondary metabolites

Secondary metabolites, which include flavonoids, terpenoids, phenolics, and alkaloids, are small organic compounds derived from primary metabolites, particularly carbohydrates. These secondary metabolites do not play a direct role in plant cell and organ growth and development. However, they serve as vital health-promoting phytochemicals for functional foods or medicines, and they also interact with the bioenvironment to establish defense mechanisms (Heike & Dietrich, 1995). Flavonoids, which comprise the majority of described phenolic secondary metabolites, are found in diverse plant species and fall into six distinct categories: flavonols, flavanones, flavones, isoflavones, anthocyanidins, and flavonols (Montoro et al., 2005). Among the 35 different flavonoids examined herein, 21 DAMs significantly altered were involved in ten up-regulated differences (e.g., quercetin-3-*O*-galactoside (hyperin) and kaempferol-4'-*O*-glucoside) and 11 down-regulated differences (e.g., quercetin-3-*O*-sambubioside-5-*O*-glucoside and kaempferol-3-*O*-rutinoside-7-*O*-rhamnoside) across all three growth stages of Mp leaves (MpBud vs. MpMat). Additionally, a total of 25 metabolites significantly accumulated with 14 differences of apigenin-6,8-di-*C*-glucoside (vicenin-2) and epicatechin or decreased with 11 differences of luteolin-7-*O*-sophoroside-

5-*O*-arabinoside as the buds grew into the tender leaves (MpBud vs. MpTen). While 15 significantly changed with many of the down-regulated substances such as kaempferol-3-*O*-rutinoside-7-*O*-glucoside and quercetin-7-*O*-rutinoside-4'-*O*-glucoside in the maturation stage of leaves (MpTen vs. MpMat). What's more, it was found that five compounds were unique to all three growth stages, with the example of kaempferol-3-*O*-glucoside (astragalin) and quercetin-4'-*O*-glucoside (spiraeoside). Several compounds with high accumulation have been proven to have beneficial bioactivities, such as kaempferol, quercetin, naringenin, and their glycosides (Li et al., 2021). For instance, naringenin and kaempferol-3-*O*-glucoside are both types of flavonoids, specifically flavanones and flavonols, respectively, and they exhibit various bioactivities such as antioxidant, anticancer, and anti-inflammatory properties (Dharambir et al., 2017; Nyane et al., 2017). These highly accumulated flavonoid metabolites, as mentioned above, were observed in the bud leaves, confirming a positive association with antioxidant activity.

Phenolic acids possess various important medicinal compounds such as hydroxybenzoic acid, hydroxycinnamic acid, and their derivatives in tea plants (Wu et al., 2018). In this research, a total of 48 phenolic acid compounds were detected. Among these, 46 exhibited significant alteration across three different stages, with 21 up-regulated (e.g., 1-*O*-caffeoyl- β -*D*-glucose*) and 25 down-regulated (e.g., trans-4-hydroxycinnamic acid) DAMs. Among 26 different substances, nine significantly accumulated metabolites were observed for the example of 2-naphtho, and 11 remarkably decreased metabolites were obtained such as benzoylmalic acid (MpBud vs. MpMat). However, only seven substances involved in five up-regulated (e.g., ethylparaben) and two down-regulated (e.g., benzamide) differences were found in the maturation stage (MpTen vs. MpMat). Furthermore, 18 DAMs were unique to the entire growth stage of leaves (MpBud vs. MpMat), with eight significantly up-regulated metabolites such as homogentisic acid, and ten remarkably down-regulated metabolites such as 2-hydroxybenzaldehyde (salicylaldehyde). The high accumulation of these phenolic acid metabolites, especially trans-4-hydroxycinnamic acid methyl ester, in the bud leaves were consistent with the results reported by Liu et al (2020) who found that phenolic acids were higher than those of the old leaves.

The various terpenoid metabolites were obtained, including monoterpenoids, sesquiterpenoids, triterpene, and triterpene saponin. The analysis of 54 terpenoid

substances revealed that many metabolites presented a declining trend, with the most significant down-regulation observed during the growth stage of Mp leaves (MpBud vs. MpTen), including ursolic acid and morolic acid. In contrast, these samples contained eight metabolites, including an increase in dehydrovomifoliol and a decrease in mussaenoside during the maturation stage. In addition, 11 DAMs with the example substances of dehydrovomifoliol and asiatic increased significantly, and 27 down-regulated metabolites were observed for mussaenosidic acid and mussaenoside in three different stages of Mp leaves (MpBud vs. MpMat). Additionally, almost all five triterpenes (e.g., asiatic acid), triterpene saponin (cadambagenic acid), and monoterpenoid (sweroside) were remarkably up-regulated, as were seven monoterpenoids, with the example metabolites including geniposidic acid and mussaenosidic acid that were unique to this stage (MpBud vs. MpMat). The concentration of terpenoids, particularly mussaenosidic acid and mussaenoside, was higher in the bud leaves than in the tender and mature leaves, indicating that the abundant terpenoid compounds had antibacterial, anti-inflammatory, and antioxidant properties (Islam et al., 2015; Shylaja et al., 2017).

Alkaloids are considered the primary bioactive components in plant chemicals, which possess various bioactivities because of their properties (Kuang et al., 2021). Among the 16 alkaloids substances examined herein, 14 differences exhibited remarkable up-regulation (e.g., 3-indoleacrylic acid) or down-regulation (e.g., betaine) during leaf development (MpBud vs. MpMat). Nine DAMs involved in the three accumulated metabolites (e.g., caffeine and *N*-acetyl-5-hydroxytryptamine) and six decreased substances (e.g., 2-phenylethylamine and indole-3-cyano-2-*O*-glucoside) were observed in the growth stage of Mp leaves (MpBud vs. MpTen). In addition, three down-regulated metabolites such as caffeine, 2-phenylethylamine, and *N*-oleoylethanolamine were found in the maturation stage (MpTen vs. MpMat). Almost all six substances (for example, 3-indoleacrylic acid and 2-glucosyl-glucosyloxy-2-phenylacetic acid amide) found in all three stages were up-regulated. Caffeine, which is abundant in the tea plant, contributes significantly to its health benefits. However, the quantities of caffeine in the bud and tender leaves were slightly higher than that in the mature leaves, which was consistent with a study reported by Bhandari et al. (Bhandari et al., 2019) who showed that the caffeine content of black tea processed by fresh and tender buds or leaves in spring was higher than that of mature leaves in monsoon and autumn seasons.

As for lignans and coumarins, 14 different substances were detected herein. Among these, eight metabolites showed significant changes, with five up-regulated differences (e.g., daphnin) and three down-regulated differences (e.g., 6,7-dihydroxy-4-methylcoumarin) observed across three different stages of Mp leaves (MpBud vs. MpMat). Five significantly increased metabolites (e.g., daphnin and lariciresinol-4'-O-glucoside) and seven significantly decreased substances (e.g., scopoletin (7-hydroxy-6-methoxycoumarin) and 6,7-dihydroxy-4-methylcoumarin) were found in MpBud vs. MpTen. In addition, five DAMs were significantly up-regulated (e.g., lariciresinol-4'-O-glucoside) or down-regulated (e.g., epipinoresinol*) during the maturation stage (MpTen vs. MpMat). Two up-regulated substances, esculin (6,7-dihydroxycoumarin-6-glucoside) and syringaresinol-4'-O-(6"-acetyl) glucoside, were discovered to be unique to all stages of Mp leaf.

4.2.4.2 Primary metabolites

Primary metabolites such as amino acids, organic acids, lipids, and sugars are necessary for cell survival and serve as an important energy source, as well as some small molecular compounds for secondary metabolism (Hounsome et al., 2008). Free amino acids not only bring fresh and brisk tastes to Mp tea infusion by participating in the formation of aroma substances, but also contribute to its nutritional and functional properties (Saeed et al., 2017). Among the 33 amino acids and their derivatives examined herein, 30 DAMs showed significant changes across all growth and development stages of Mp leaves. Fifteen DAMs were significantly up-regulated as the buds grew into tender leaves, with *L*-arginine and *S*-sulfo-*L*-cysteine being the most notably affected by the growth and development of Mp leaves. While, only six metabolites were significantly up-regulated or down-regulated in the mature stage of leaves, such as *L*-serine, *L*-glutamine, and *N*-alpha-acetyl-*L*-asparagine. In addition, 12 DAMs were unique during the mature period, including nine up-regulated metabolites (e.g., ophan and γ -glutamyl-*L*-valine) and three down-regulated metabolites (e.g., 5-oxoproline). Many up-regulated metabolites during the growth stage might contribute to the formation of taste and aroma substances.

Organic acids serve as important intermediate products of carbohydrate catabolism, which contribute to the vinegar taste and fruity flavor of Mp tea while restraining bitterness and sourness (Chen et al., 2023). A total of 21 organic acids were examined herein, of which 19 substances showed significant changes as buds grew into

mature leaves, with the majority showing down-regulation. A total of 11 metabolites exhibited remarkable alteration, with nine substances being down-regulated (e.g., shikimic acid, triethyl citrate, and 2-picolinic acid) and two compounds up-regulated (e.g., α -ketoglutaric acid). Whereas, only two metabolites were significantly up-regulated (citraconic acid) or down-regulated (*L*-pipecolic acid) as the tender leaves matured. Many of the down-regulated metabolites detected in our research were consistent with the study by Chen et al. (Chen et al., 2023) who reported that the content of organic acids in fresh leaves was obviously higher than that in mature leaves. In addition, eight DAMs involved in three up-regulated (e.g., γ -aminobutyric acid) and five down-regulated metabolites (e.g., tartronate semialdehyde*) were unique organic acid substances during the process of maturation. These compounds played a crucial role in reconciling the taste of the Mp tea and enhancing its functional and nutritional components.

Lipids in fresh tea leaves were responsible for the production of flavor and aroma substances (Feng et al., 2019; Ravichandran, 2002). A total of 16 lipids were examined herein, among which 11 substances were significantly up-regulated (e.g., 13-methylmyristic acid and palmitoleic acid) or down-regulated (e.g., lysoPC 16:1 and lysoPC 18:1). Twelve metabolites exhibited remarkable alterations, with the most down-regulated differences observed during the growth stage of Mp leaves (MpBud vs. MpTen), such as methyl linolenate, hydroxy ricinoleic acid, and lysoPC 18:4. However, only two metabolites, lysoPE 20:3 and lysoPC 18:4, were detected, both of which showed a decreasing trend. In addition, only three up-regulated or down-regulated compounds involved in (5*S*,8*R*,9*Z*,12*Z*)-5,8-dihydroxyoctadeca-9,12-dienoate and 1-stearidonoyl-glycerol were unique to the mature stage of Mp leaves (MpBud vs. MpMat). The significant accumulation of majority LPC compounds, such as lysoPC 15:0, lysoPC 16:1 and lysoPC 18:1, were observed in buds and tender leaves. This finding was consistent with a study reported by Liu et al. (2017) who demonstrated higher levels of PC compounds in new shoots compared to mature leaves, suggesting that the abundant lipid metabolites contribute to the formation of tea aroma.

4.2.5 Total phenolics, flavonoids, terpenoids, anthocyanins, and antioxidant activity

Total phenolics, flavonoids, terpenoids, anthocyanin, DPPH radical scavenging activities, radical cation ABTS+ scavenging activities, and ferric reducing antioxidant power (FRAP) were displayed in Figure 4-2-8. Total phenolics, flavonoids, anthocyanin,

DPPH, ABTS, and FRAP ranged from 4.27 to 6.24 mg/g, 3.66 to 5.94 mg/g, 0.82 to 24.7 µg/g, 9.93 to 23.59%, 108.32 to 150.87 µmol Trolox/g, and 87.05 to 140.16 µmol Trolox/g, respectively. The contents or activities of bud leaves was significantly higher than those of the other two samples, with tender leaves being the lowest and no significant difference from mature leaves. However, terpenoids in the three samples ranged from 0.59 to 0.91 mg/g. The content of terpenoids in mature leaves was significantly higher than that in the other two samples, with bud leaves being the lowest.

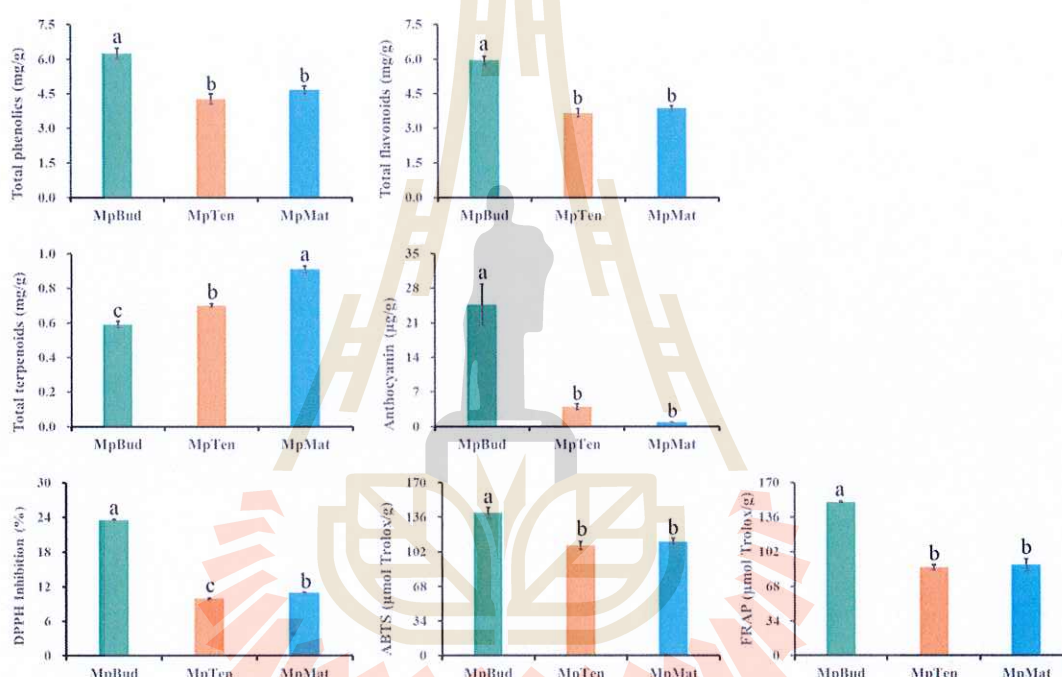


Figure 4-2-8. The content of total phenolics, flavonoids, terpenoids, anthocyanin, and antioxidant activities of DPPH, ABTS and FRAP assays during three different stages of Mp leaves.

These findings revealed that the concentrations of total phenolics, flavonoids, and anthocyanin gradually decreased as Mp leaves grew and developed, while terpenoids increased significantly. This suggested that these components played a role in enhancing the functional and nutritional properties of Mp leaves. Phenolic compounds involved in phenolics, flavonoids, and anthocyanin are considered the primary antioxidant components of diverse plants, with higher levels found in bud leaves compared to mature leaves (Damiano et al., 2017). The relatively abundant contents of

these three components were observed in the buds, as confirmed in this study. Meanwhile, a high accumulation of anthocyanin was found in the bud leaves with the purple-red color, which was believed to be associated with the formation of leaf color (Li et al., 2021). Like a study reported by Wang et al. (Wang et al., 2023), who demonstrated that higher levels of flavonoids and anthocyanin were responsible for the purple leaves. The DPPH, ABTS, and FRAP values of these three samples revealed significant differences in antioxidant activity among Mp leaves, with bud leaves in Mp having higher antioxidant activities than mature leaves. This finding was positively associated with changes in the contents of total flavonoids, phenolics, and anthocyanin, indicating that high levels of total phenolic compounds may contribute to antioxidant activity (Lou et al., 2015).

4.2.6 Correlation analysis between DAMs and antioxidant activity

A comprehensive analysis of Mp leaves revealed the presence of 371 different DAMs, encompassing a diverse range of chemical classes. These include 16 alkaloids, 33 amino acids, 35 flavonoids, 16 lipids, 31 nucleotides, 21 organic acids, 48 phenolic acids, 54 terpenoids, 14 lignans and coumarins, and 49 other compounds. Among these, flavonoids, terpenoids, and phenolics are well known for their potent antioxidant properties with various pharmacological activities such as anti-cancer and anti-inflammatory effects (Bhadwal et al., 2023; Xiong et al., 2024; Yan et al., 2023). The secondary metabolites, including monoterpenoids, phenolic acids, sesquiterpenoids, triterpenes, and chalcones, exhibited a positive correlation with antioxidant activity, as determined by ABTS, DPPH, and FRAP assays. In contrast, triterpene saponins showed a negative correlation with ABTS activity (Figure 4-2-9A). Most notably, the top 20 metabolites associated with antioxidants were shown in Figure 4-2-9B. Among these, madasiatic acid, $2\alpha,3\alpha,23$ -trihydroxyolean-12-en-28-oic acid, trihydroxycinnamoylquinic acid, and 2-hydroxyoleanolic acid were significantly positively correlated with ABTS. In addition to the four metabolites mentioned above, alphitolic acid also exhibited a significant positive correlation with DPPH. Besides that, madasiatic acid, $2\alpha,3\alpha,23$ -trihydroxyolean-12-en-28-oic acid, trihydroxycinnamoylquinic acid, mussaenosidic acid, diisobutyl phthalate, butyl isobutyl phthalate, trans-4-hydroxycinnamic acid methyl ester, p-coumaric acid methyl ester, 2-hydroxyoleanolic acid, and 4-methoxycinnamic acid exhibited a positive correlation with FRAP, whereas 1-*O*-glucosyl sinapate and 6-*O*-feruloyl-*D*-glucose showed a significant negative correlation.

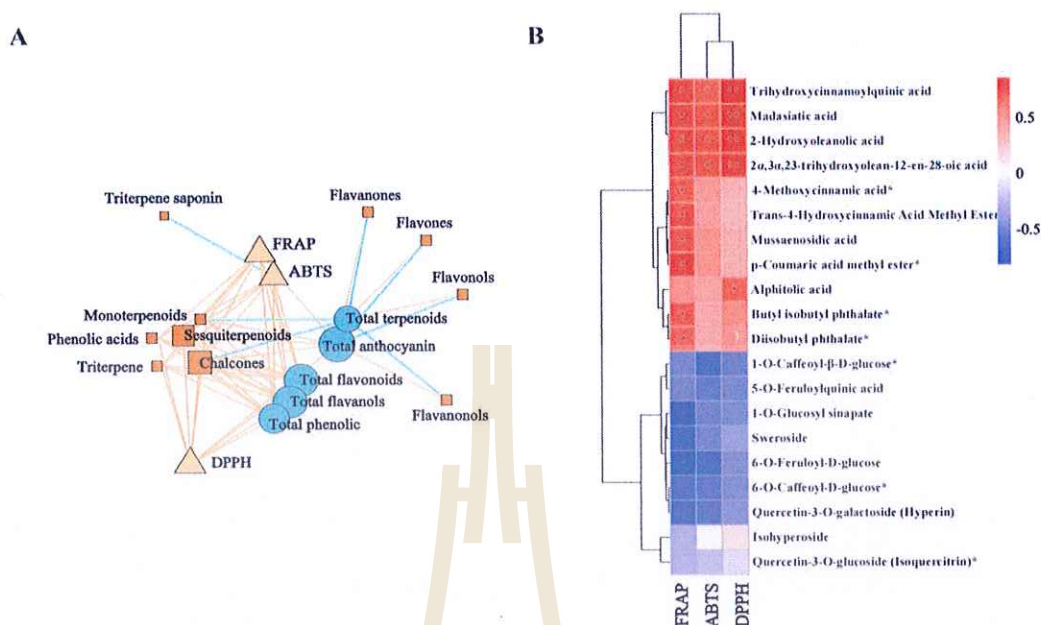


Figure 4-2-9. Correlation analysis between DAMs and antioxidant activity.

Note: (A) Total antioxidant substances correlated with antioxidant activity. Light blue circles represent total content of metabolites, orange squares represent metabolites of secondary classification, and yellow triangles represent antioxidant activity. (B) Top 20 antioxidant metabolites correlated with antioxidant activity. Squares colored in “red” and “blue” represent positive and negative correlations, respectively.

4.3. Metabolomic and Transcriptomic Profiling Reveals the Flavonoid Components and Discoloration Mechanism of *M. pubescens* Leaves

4.3.1 Differences in biological phenotypes, pigment and functional components

The bud (MpBud), tender (MpTen) and mature leaves (MpMat) were collected to clarify the phenotypes and physiological characteristics during the color change of Mp at the different developmental stage. The color differences were clear between the MpBud, MpTen and MpMat (Figure 4-3-1A, B). More specifically, MpBud leaves were predominantly purple red in color, while MpTen leaves only had purple petioles, and MpMat leaves were entirely green.

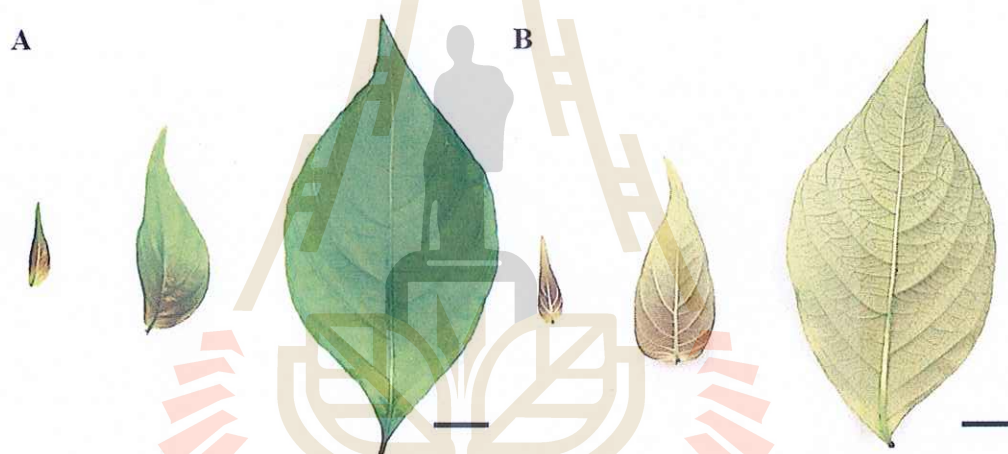


Figure 4-3-1 Phenotypes and colour of the leaves surface (A) and back (B) of MP at the different growth stages. From left to right are MpBud, MpTen and MpMat. Scale bar = 2 cm.

Leaves serve as the primary photosynthetic organs and are also involved in both biotic and abiotic stress responses (Aude et al., 2018). The color of the leaves was strongly influenced by the types and proportions of pigments present in purple-leaf plants (Li et al., 2021). However, the coloration of plant tissues arises from three primary pigments: flavonoids, carotenoids, and chlorophylls (Lightbourn et al., 2008; Shen et al., 2018). Leaf coloration is mainly dependent on flavonoids/anthocyanins, which are responsible for the red, blue, and purple pigments in leaves (Winkel-Shirley, 2001), when their concentrations are high enough to overshadow the green color of chlorophylls

(Panagiota & Manetas, 2006). The results showed that total flavonoid, anthocyanin, and flavanols during the developmental process of Mp leaves ranged from 3.66 mg/g to 5.94 mg/g, 0.82 $\mu\text{g/g}$ to 24.7 $\mu\text{g/g}$, and 0.06 mg/g to 0.1 mg/g, respectively (Figure 4-3-2). The content of these three biochemical components in bud leaves was significantly higher than that in the other two samples, with the lowest content in tender leaves and no significant difference from the content in mature leaves. Similarly, the carotenoids content presented the same trend as the three functional components mentioned above, with higher values in bud leaves (70.63 $\mu\text{g/g}$) and lower in tender leaves (67.58 $\mu\text{g/g}$). Conversely, the levels of total chlorophylls, chl a, and chl b in the three samples displayed a completely different pattern of change, with the highest content in mature leaves and bud leaves being the lowest (Figure 4-3-2). These results demonstrated a gradual decrease in the content of total flavonoids, anthocyanins, flavanols, and carotenoids during the growth and development of Mp leaves, while the content of chl a, and chl b showed a significant increase, indicating that the variation in pigment content seems to be responsible for the distinct colors observed in the Mp leaves, while other components play a role in amplifying the functional and nutritional properties.

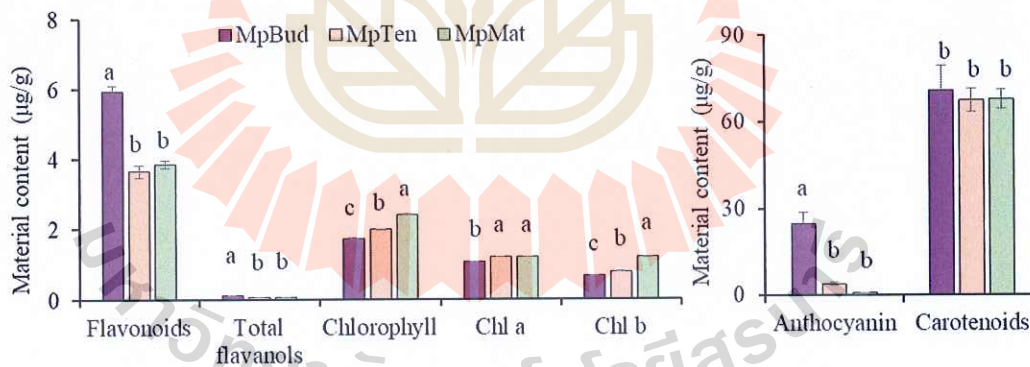


Figure 4-3-2 Difference of color and functional components in different leaves of Mp. Different letters above the bars indicate significant difference between each other ($p < 0.05$).

4.3.2 Metabonomic analysis

4.3.2.1 Quantitative analysis of flavonoids metabolite components in the Mp leaves

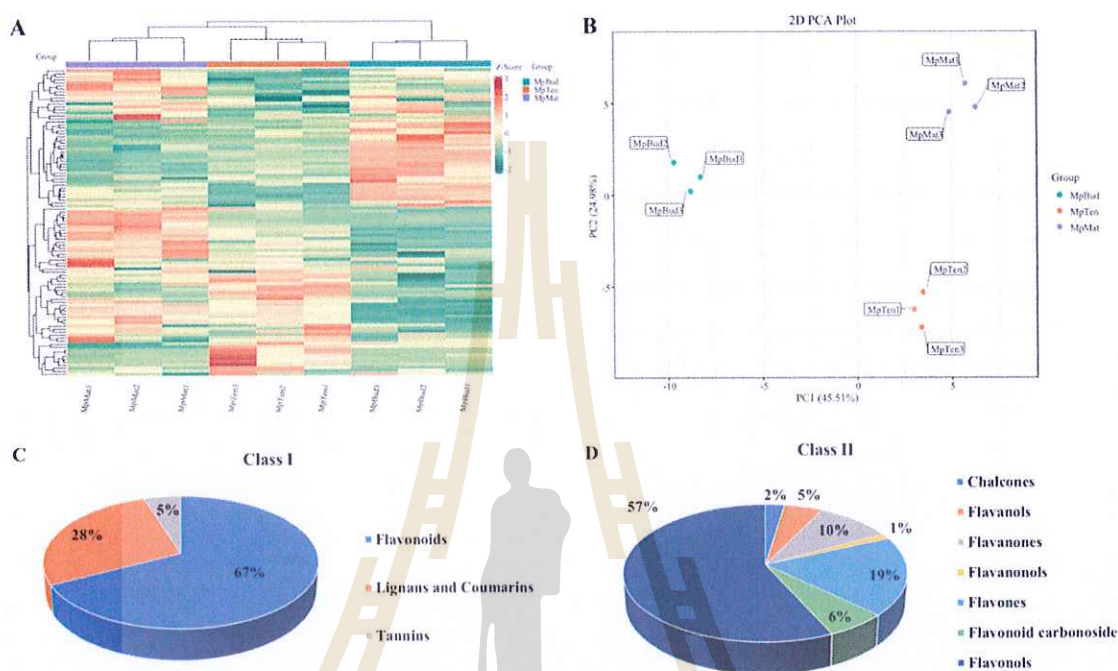


Figure 4-3-3 Quantitative analysis of metabolite components in Mp leaves.

Note: (A) Heatmap of the quantified metabolites. (B) PCA plot of different growth stages and QC samples. (C) First-level classification of the flavonoids in all samples. (D) Second-level classification of the flavonoids in all samples.

UPLC-MS/MS analysis was performed on samples collected from the different growth stages of Mp leaves (MpBud, MpTen and MpMat) to obtain the related secondary metabolites. A total of 81 flavonoids metabolites were identified from the nine samples, exhibiting the obvious hierarchical clustering among the treatments with the heatmap (Figure 4-3-3A). PCA plot showed that QC samples separated from other samples and three biological replicates within the group were significantly clustered together, which demonstrated that the whole analysis was of stabilization and repeatability (Figure 4-3-3B). Correlation analysis showed a remarkable correlation between the two samples within the group with R coefficient greater than 0.8. Additionally, OPLS-DA plot and

model validation were used to filter out the differential variables and predict the excellence of the model by removing irrelevant differences. Detailly, samples were significantly separated in pairs among the three comparisons in the OPLS-DA plot. In the OPLS-DA model validation, R^2X , R^2Y and Q^2 values were all higher than 0.778, 1.0 and 0.993 in MpBud vs MpTen, MpTen vs MpMat and MpBud vs MpMat, respectively.

Furthermore, the obtained flavonoids metabolites were divided into seven categories at the second level classification involved in Chalcones (2), Flavanols (4), Flavanones (8), Flavanonols (1), Flavones (15), Flavonols (46), and Flavonoid carbonoside (5) (Figure 4-3-3C-D).

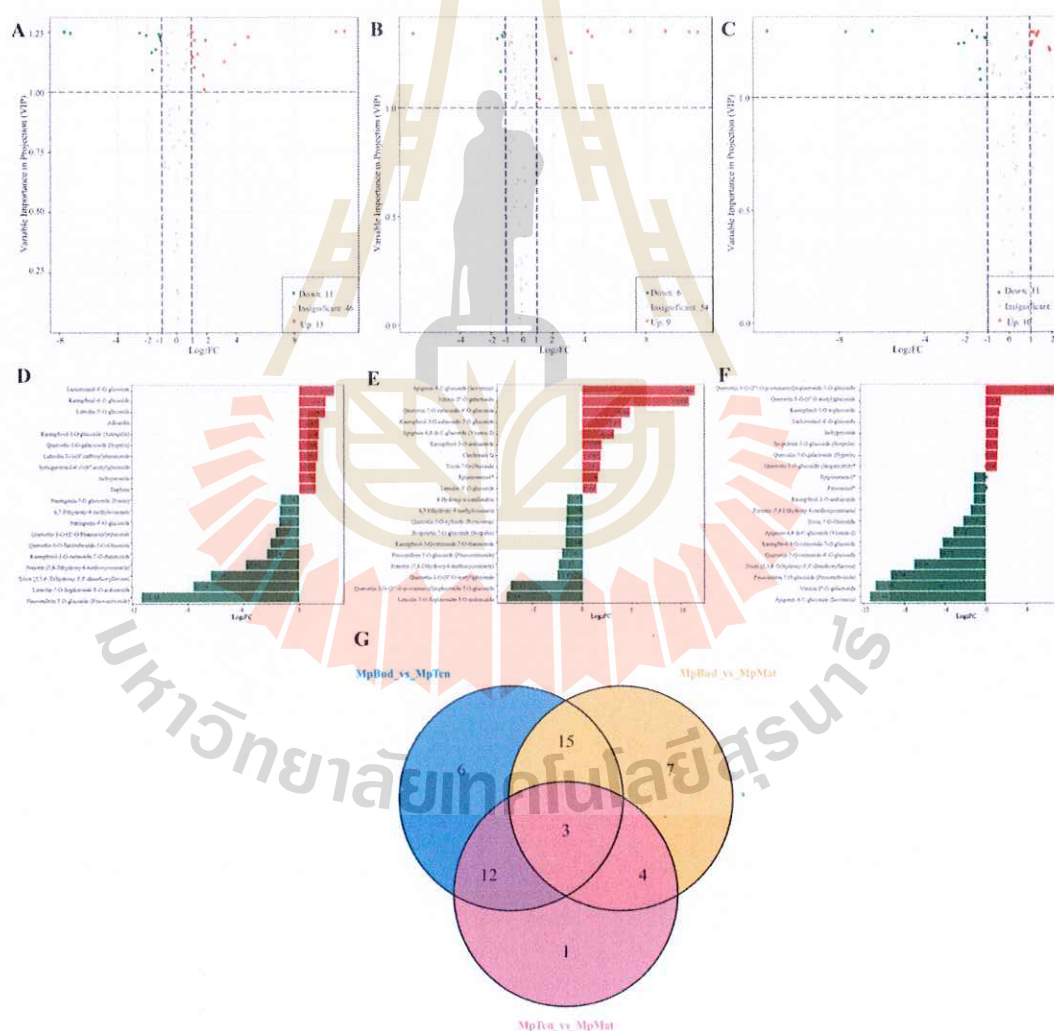


Figure 4-3-4 Differential accumulated flavonoids metabolites in Mp leaves.

Note: Volcano plot of the DAMs in (A) MpBud vs MpTen, (B) MpTen vs MpMat, and (C) MpBud vs MpMat. Red solid circles indicate up-regulated DAMs, whereas down-regulated DAMs are shown in green. Top ten up-regulated and down-regulated DAMs in (D) MpBud vs MpTen, (E) MpTen vs MpMat, and (F) MpBud vs MpMat. Red bars represent up-regulated DAMs, and green bars represent down-regulated DAMs. First-level classification of the identified metabolites in all samples. (G) Venn diagram of DAMs in a multiple pairwise comparison.

4.3.2.2 Accumulation of flavonoids Metabolites in the Mp leaves

The acquired metabolites were screened by the criterion of VIP and fold change ≥ 2 or fold change ≤ 0.5 . A total of 61 flavonoids metabolites were obtained, of which 25 flavonoids (14 up-regulation and 11 down-regulation, Figure 4-3-4A), 15 flavonoids (6 up-regulation and 9 down-regulation, Figure 4-3-4B) and 21 flavonoids (10 up-regulation and 11 down-regulation, Figure 4-3-4C) were identified from the comparisons of MpBud vs MpTen, MpTen vs MpMat and MpBud vs MpMat, respectively. In addition, the difference multiple diagrams showed the metabolites in the top 20 (up-regulation and down-regulation) of the different multiples at the three growth stages, indicating that the up-regulation and down-regulation ranges of different multiples in differential metabolites were the largest in MpBud vs MpTen, MpTen vs MpMat and MpBud vs MpMat, respectively (Figure 4-3-4D, E, F). Particularly, Apigenin-6-C-glucoside (Isovitexin) and Luteolin-7-O-Sophoroside-5-O-arabinoside had the largest multiple differences with $\text{Log}_2\text{FC} \geq 11.44$ or $\text{Log}_2\text{FC} \leq -7.16$ as the bud leaves grew into the tender leaves (MpBud vs MpTen) (Figure 4-3-4D); while, the most up-regulated and down-regulated metabolites were Quercetin-3-O-(2''-O-p-coumaroyl)sophoroside-7-O-glucoside with $\text{Log}_2\text{FC} \geq 7.01$ and Apigenin-6-C-glucoside (Isovitexin) with $\text{Log}_2\text{FC} \leq -11.44$ as the tender leaves grew into the mature leaves (MpTen vs MpMat) (Figure 4-3-4E); for the whole growth cycle of leaves (MpBud vs MpMat), Pinocembrin-7-O-glucoside (Pinocembroside) had the largest down-regulated multiple with $\text{Log}_2\text{FC} \leq -11.38$ (Figure 4-3-4F).

Furthermore, Venn diagram exhibited the common and unique differential metabolites in all pairwise comparisons (Figure 4-3-4G). Whereas 29 differential metabolites (15 up-regulation and 14 down-regulation) were only found in MpBud vs MpMat. One metabolite was unique to MpTen vs MpMat, and most of them exhibited the down-regulated trend. However, MpBud vs MpTen possessed the most specific metabolites (18 up-regulation and 18 down-regulation), with the most abundant substances.

4.3.2.3 KEGG functional annotation and enrichment analysis of flavonoids metabolites in the Mp leaves

KEGG pathway analysis showed that six differential metabolites obtained from the comparison of MpBud vs MpTen were enriched in five pathways involved in “biosynthesis of various plant secondary metabolites”, “biosynthesis of secondary metabolites”, “metabolic pathways”, “flavonoid biosynthesis” and “flavone and flavonol biosynthesis”, of which the most enriched metabolites were “biosynthesis of various plant secondary metabolites” and “biosynthesis of secondary metabolites” with a proportion of 66.67%. whereas, only six substances identified from MpTen vs MpMat were enriched in four pathways including “biosynthesis of various plant secondary metabolites”, “biosynthesis of secondary metabolites”, “metabolic pathways” and “flavone and flavonol biosynthesis”, of which the most abundant pathways of metabolites were “biosynthesis of secondary metabolites” with a percentage of 83.33%. In addition, five components observed between MpBud and MpMat were enriched in five pathways such as “biosynthesis of various plant secondary metabolites”, “biosynthesis of secondary metabolites”, “flavonoid biosynthesis”, “metabolic pathways” and “flavone and flavonol biosynthesis”, of which “biosynthesis of secondary metabolites” were the pathways with the most abundant metabolites (four DAMs with a proportion of 80%).

Additionally, KEGG enrichment pathway revealed that “biosynthesis of various plant secondary metabolites” (ko00999) and “biosynthesis of secondary metabolites” (ko01110) were significantly altered in MpBud vs MpTen, and the metabolites enriched in this pathway were remarkably up-regulated (Apigenin-6,8-di-C-glucoside (Vicenin-2)) or down-regulated (Kaempferol-3-O-rutinoside-7-O-rhamnoside). Whereas, “biosynthesis of secondary metabolites” (ko01110) occupied the top enriched pathway in MpTen vs MpMat, and the differences enriched in this pathway included Quercetin-3-O-(2"-O-p-coumaroyl)sophoroside-7-O-glucoside up-regulated and Apigenin-6,8-di-C-glucoside (Vicenin-2) down-regulated. Furthermore, “biosynthesis of secondary metabolites” (ko01110) was significantly changed in MpBud vs MpMat, of which the substances enriched in the former pathway were up-regulated daphnin and down-regulated 6,7-Dihydroxy-4-methylcoumarin.

4.3.3 Transcriptomic analysis

The gene expression of Mp leaves at different stages was further analyzed by

transcriptome sequencing, with three biological replicates for each sample, totaling nine samples. The average high-quality reads obtained for MpBud, MpTen, and MpMat were 6.4, 6.6, and 6.5 G, respectively, with the proportion of bases for clean data exceeding 40 among these three samples averaging 43.51%, 43.50%, and 43.55%, respectively. Using the TRINITY assembly software, after filtering the low expression transcripts, a total of 95481 unigenes were assembled with an N50 length of 2256 bp.

PCA on the gene expression levels of Mp leaves indicated that PC1 and PC2 contributed 77.61% and 9.03%, respectively, to the samples (Figure 4-3-5A). Meantime, the samples in MpMat group were closely clustered with those in MpTen group and significantly separated from those in MpBud. A total of 95481 genes were assembled and annotated in this transcriptome, with each sample possessing a Q30 base percentage exceeding 93.74%.

A total of 11021 DEGs were identified, and the expression of these DEGs showed significant differences among the comparisons of MpBud, MpTen and MpMat (Figure 4-3-5B), which was consistent with the accumulation of DAMs. The statistics of DEGs indicated that MpBud vs MpTen and MpBud vs MpMat exhibited the highest number of DEGs, consisting of 40 upregulated and 58 downregulated genes. The comparison of MpTen vs MpMat had the least DEGs, with 2 upregulated and 4 downregulated genes (Figure 4-3-5C). In addition, only 4 DEGs were common to these three comparisons; while 22, 2 and 20 DEGs were unique to MpBud vs MpTen, MpTen vs MpMat and MpBud vs MpMat, respectively (Figure 4-3-5D).

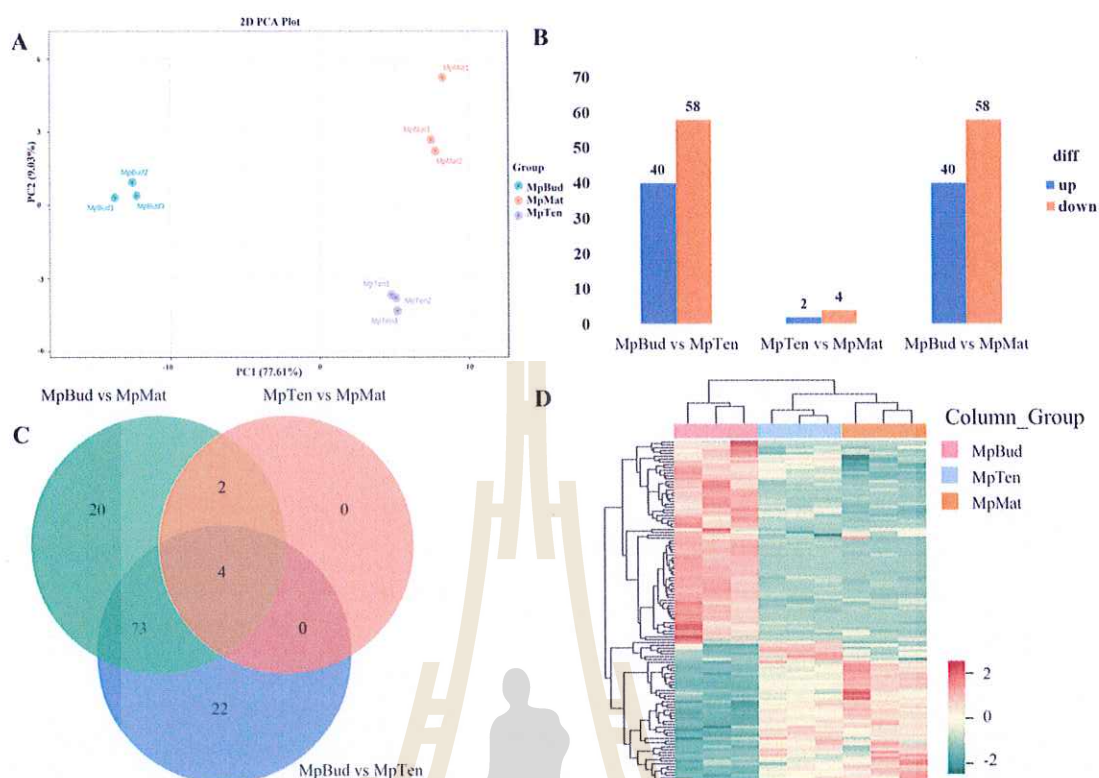


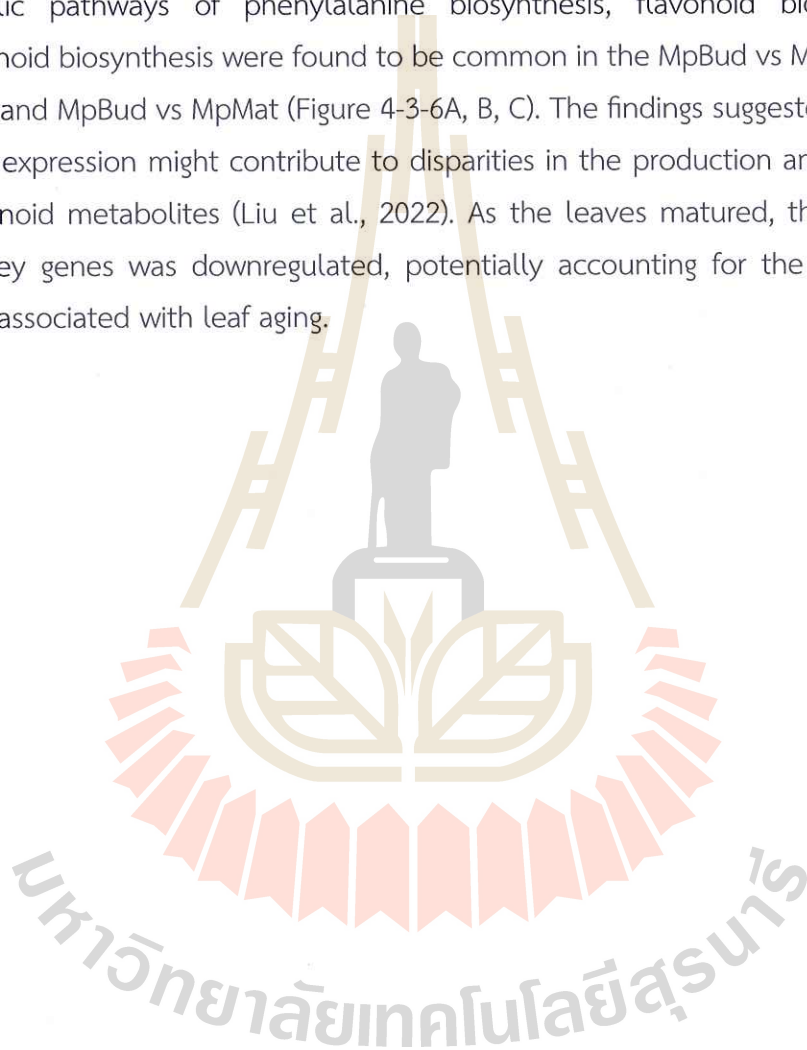
Figure 4-3-5 Overview of transcriptome analysis of Mp leaves.

Note: (A) PCA analysis of the expression of unigenes for MpBud, MpTen and MpMat. (B) Bar graph of up and downregulated genes from pairwise comparisons. (C) Venn diagram showing the mutual overlaps of DEGs in MpBud, MpTen and MpMat. (D) Heatmap of DEGs expression in MpBud, MpTen and MpMat.

In GO annotation analysis, MpBud vs MpTen, MpTen vs MpMat and MpBud vs MpMat were annotated with a total of 99, 6, and 99 DEGs, respectively, into the categories of biological processes, molecular functions, and cellular components. In the biological process category, the GO terms involved in metabolic process (43, 65, 65) and cellular process (24, 24, 24) were most common. In the cellular component category, most DEGs were assigned to the cell (29, 28, 28) and cell part (29, 28, 28). For the molecular function category, the majority of DEGs were annotated into binding (43, 41, 41) and catalytic function (90, 92, 92).

Additionally, the top GO analysis further revealed that the terms of molecular functions involved in binding (GO: 0005488) and catalytic activity (GO: 0003824), the terms of biological process such as metabolic process (GO: 0008152) and cellular process (GO: 0009987), and the terms of cellular component including cell (GO: 0005623) and cellular part (GO: 0044464) were the most enriched terms.

The KEGG enrichment analysis of differential genes revealed that “MAPK signaling pathway-plant”, “Plant hormone signal transduction”, “Biosynthesis of secondary metabolites”, and “Sesquiterpenoid and triterpenoid biosynthesis” were the most enriched across the three growth stages of Mp leaves. Top KEGG analysis further suggested that the highest representation of DEGs were identified based on the difference in the significant values of genes enriched in each pathway (Figure 4-3-6). The metabolic pathways of phenylalanine biosynthesis, flavonoid biosynthesis, and isoflavonoid biosynthesis were found to be common in the MpBud vs MpTen, MpTen vs MpMat, and MpBud vs MpMat (Figure 4-3-6A, B, C). The findings suggested that variation in gene expression might contribute to disparities in the production and accumulation of flavonoid metabolites (Liu et al., 2022). As the leaves matured, the expression of these key genes was downregulated, potentially accounting for the observed color change associated with leaf aging.



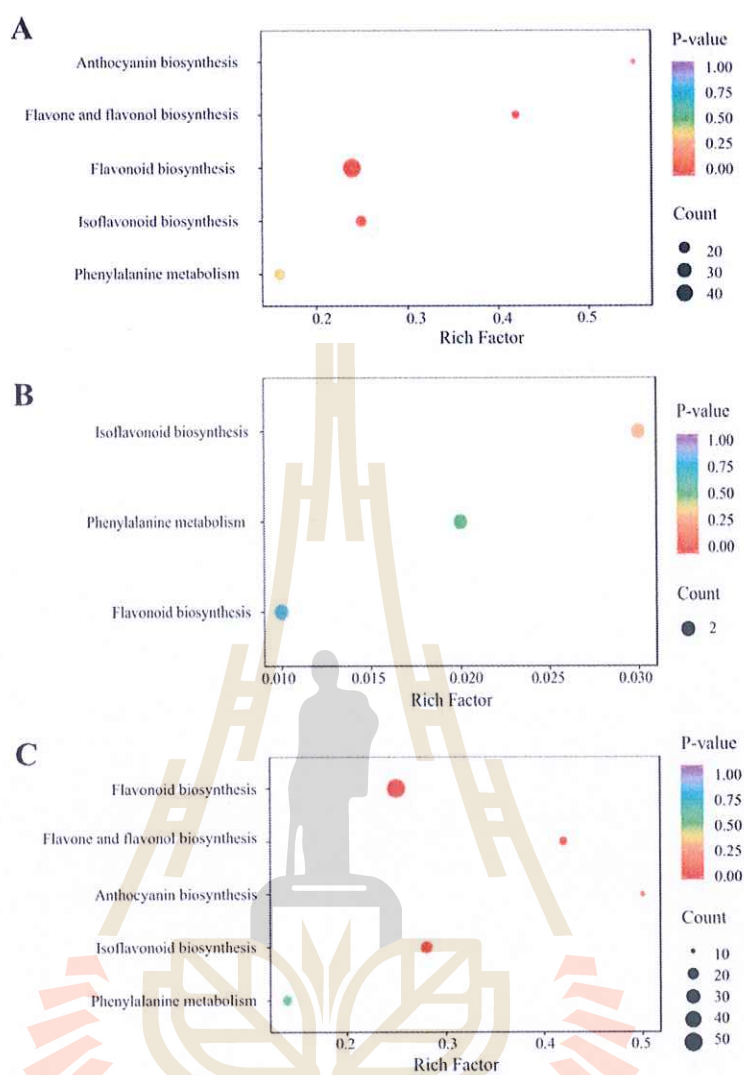


Figure 4-3-6 KEGG enrichment analyses of DEGs in Mp leaves.

Note: (A) MpBud vs MpTen, (B) MpTen vs MpMat, and (C) MpBud vs MpMat. The size and color of the solid circles represent the number of transcripts involved in the certain pathway and the significant value (p -value) of the rich factor, respectively.

4.3.4 Correlation analysis of transcriptome and metabolome

Nine-quadrant maps were created to depict the relationship between genes and metabolites associated with the flavonoid metabolic pathway (Figure 4-3-7A). The majority of DEGs (21749 in MpBud vs MpTen, 17934 in MpTen vs MpMat, and 20836 in MpBud vs MpMat) and DAMs (102 in MpBud vs MpTen, 101 in MpTen vs MpMat, and 100 in MpBud vs MpMat) were assigned to quadrant 2, 4, 6, and 8, which was no observed correspondence between the analyzed genes and metabolites. Remarkably, DAMs and

DEGs in quadrants 3 and 7 exhibited a positive correlation. For MpBud vs MpTen, 23 DAMs and 4564 DEGs located in quadrant 3 were upregulated, and 19 DAMs and 4571 DEGs located in quadrant 7 were downregulated (Figure 4-3-7B). For MpTen vs MpMat, 8 DAMs and 674 DEGs were up-regulated in quadrant 3, and 13 DAMs and 1438 DEGs were down-regulated in quadrant 7 (Figure 4-3-7C). For MpBud vs MpMat, 19 DAMs and 4248 DEGs located in quadrant 3 exhibited up-regulated trend, and 14 DAMs and 3578 DEGs located in quadrant 7 showed down-regulated trend (Figure 4-3-7D). In addition, KEGG enrichment analysis was performed on DEGs, and DAMs located in quadrants 3 and 7. Three flavonoid metabolite biosynthesis pathways involved in flavonoid biosynthesis (ko00941), isoflavonoid biosynthesis (ko00943), flavone and flavonol biosynthesis (ko00944) were identified. It was observed that many of the DAMs were associated with the flavonoid biosynthesis pathway (Figure 4-3-7E).

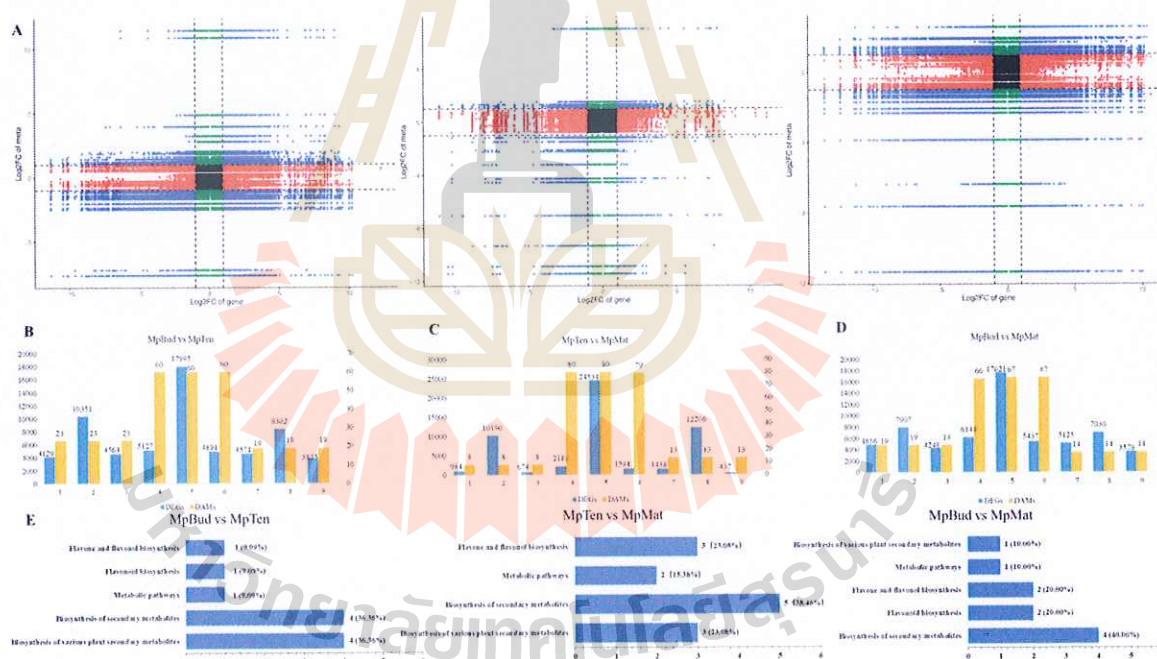


Figure 4-3-7 Integrated analysis of DAMs and DEGs.

Note: (A) Nine-quadrant map of genes and flavonoid metabolites. The number of DAMs and DEGs for MpBud vs MpTen (B), MpTen vs MpMat (C), and MpBud vs MpMat (D) in each quadrant. (E) KEGG analysis of differential flavonoid metabolites.

In view of the combined analysis of transcriptome and metabolome, we concluded that flavonoid metabolism, especially flavonoid biosynthesis, possessed a

significant impact in Mp leaves. Thereby, this study presented a flavonoid biosynthesis pathway, which included relevant metabolites and genes, by combining the KEGG database. The pathway comprised a total of 34 metabolites and 5664 structural genes.

For MpBud vs MpTen, one of the 36 identified DAMs was found to have high accumulation levels, and the expression of fourteen structural genes was up-regulated in the pathway of flavonoid biosynthesis. In the one down-regulated DAM, the \log_2FC of a flavanone including Naringenin-7-*O*-glucoside (Prunin) was -1.05 times those in control. The expression of structural genes, including seven shikimate *O*-hydroxycinnamoyltransferase (HCT, Cluster-11344.0, Cluster-11994.0, Cluster-13228.0, Cluster-13510.0, Cluster-16830.0, Cluster-17328.0, Cluster-25908.6), one chalcone reductase (CHS, Cluster-12145.0), three chalcone isomerase (E5.5.1.6, Cluster-23680.2, Cluster-23680.4, Cluster-23680.7) and three phlorizin synthase (PGT1, Cluster-24462.2, Cluster-24462.7, Cluster-24462.8) were up-regulated, whereas twenty-one genes encoding seven HCT (Cluster-11003.0, Cluster-17897.1, Cluster-17897.3, Cluster-21222.0, Cluster-5667.0, Cluster-6478.0, Cluster-8431.0), one E5.5.1.6 (Cluster-11205.0), six flavanone 7-*O*-glucoside 2''-*O*-beta-*L*-rhamnosyltransferase (C12RT1, Cluster-12803.0, Cluster-21367.1, Cluster-21367.2, Cluster-30963.0, Cluster-30963.1, Cluster-8544.0), one anthocyanidin synthase (ANS, Cluster-13920.0), one naringenin 3-dioxygenase (F3H, Cluster-15366.0), two CHS (Cluster-24201.1, Cluster-4543.0), one bifunctional dihydroflavonol 4-reductase/flavanone 4-reductase (DFR, Cluster-5332.0), one flavonoid 3'-monooxygenase (CYP75B1, Cluster-6742.0) and one PGT1 (Cluster-8618.0) were down-regulated (Figure 4-3-8).

For MpTen vs MpMat, there were no significantly enriched DAMs. The expression of structural genes involved in one PGT1 (Cluster-24462.8) and one CYP75B1 (Cluster-6742.0) was significantly down-regulated (Figure 4-3-8).

For MpBud vs MpMat, two of the 29 obtained DAMs, along with their corresponding DEGs, were found to be significantly down-regulated. Among them, the \log_2FC of Naringenin-7-*O*-glucoside (Prunin) and Phloretin-2'-*O*-glucoside (Phlorizin) were -1.34, and -1.12 times lower than those in control, respectively, and consistently, twelve genes encoding seven HCT (Cluster-11344.0, Cluster-11994.0, Cluster-13228.0, Cluster-13510.0, Cluster-16830.0, Cluster-17328.0, Cluster-25908.6), one chalcone synthase CHS (, Cluster-12145.0), two chalcone isomerase (CHI, Cluster-23680.4, Cluster-23680.7) and two PGT1 (Cluster-24462.1, Cluster-24462.7) were up-regulated, whereas nineteen genes encoding six HCT (Cluster-17897.1, Cluster-17897.3, Cluster-21222.0, Cluster-22915.0,

Cluster-5667.0, Cluster-8431.0), one CHS (Cluster-4543.0), one CHI (Cluster-11205.0), one PGT1 (Cluster-8618.0), one ANS (Cluster-13920.0), one F3H (Cluster-15366.0), six C12RT1 (Cluster-12803.0, Cluster-21367.1, Cluster-21367.2, Cluster-30963.0, Cluster-30963.1, Cluster-8544.0), one CHI (Cluster-11205.0), and one DFR (Cluster-5332.0) were down-regulated (Figure 4-3-8).

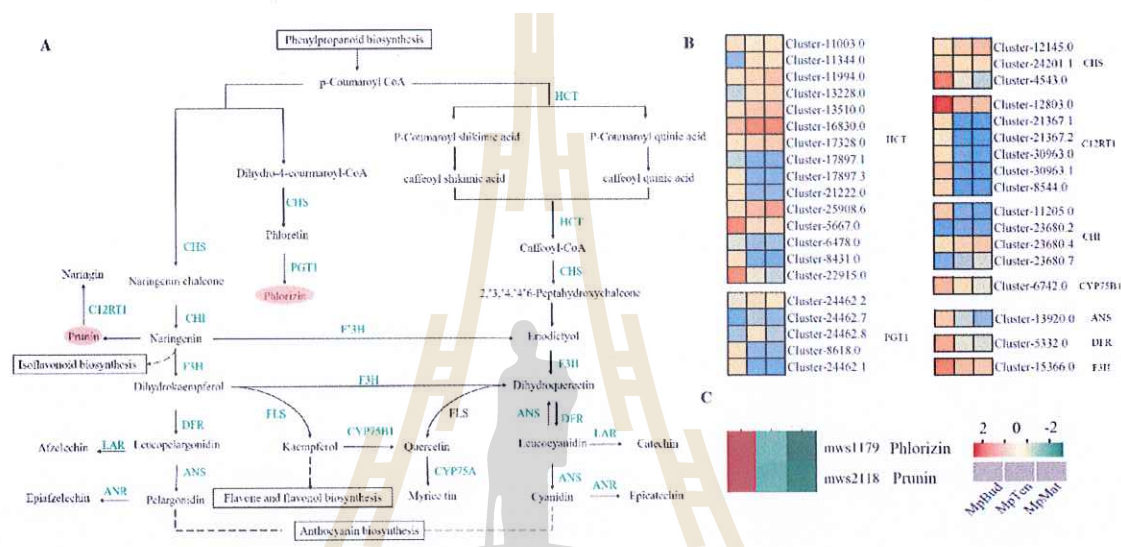


Figure 4-3-8 Transcript profiling of genes in the phenylpropanoid and flavonoid biosynthetic pathways in MpBud, MpTea, and MpMat.

Note: (A) Flavonoid biosynthetic pathway. Proposed pathway of biosynthesis derived from the literature, (Wei et al., 2018) (B) Heat map representation of the expression patterns of flavonoid-related genes. Gene expression is displayed as heat map depicting the log₂ (FPKM) values. Red and green fonts indicate up- and down-regulated genes, respectively.

Collectively, the accumulation of flavonoids in MpBud vs MpTen and MpBud vs MpMat was primarily due to the up-regulation of seven HCT (Cluster-11344.0, Cluster-11994.0, Cluster-13228.0, Cluster-13510.0, Cluster-16830.0, Cluster-17328.0, Cluster-25908.6), one CHS (Cluster-12145.0), three CHI (Cluster-23680.2, Cluster-23680.4, Cluster-23680.7) and four PGT1 (Cluster-24462.1, Cluster-24462.2, Cluster-24462.7, Cluster-24462.8), and the decrease of flavonoids were primarily due to the down-regulation of eight HCT (Cluster-11003.0, Cluster-17897.1, Cluster-17897.3, Cluster-21222.0, Cluster-5667.0, Cluster-6478.0, Cluster-8431.0, Cluster-22915.0), CHS (Cluster-12145.0), two

chalcone synthase (CHS, Cluster-24201.1, Cluster-4543.0), one CHI (Cluster-11205.0), one ANS (Cluster-13920.0), six C12RT1 (Cluster-12803.0, Cluster-21367.1, Cluster-21367.2, Cluster-30963.0, Cluster-30963.1, Cluster-8544.0), F3H (Cluster-15366.0), one DFR (Cluster-5332.0), one CYP75B1 (Cluster-6742.0) and two PGT1 (Cluster-8618.0, Cluster-24462.8) (Figure 4-3-8).

The integration of various omics techniques can aid in exploring the mechanisms of plant development (Xie et al., 2022) and responses to abiotic stresses (Asakura et al., 2021; Li et al., 2022), as well as contribute to the expression of leaf color (Yan et al., 2022) and the synthesis of plant metabolites (Chen et al., 2020). In our study, the integrated analysis of the transcriptome and metabolome revealed that the biosynthesis pathways of flavonoid metabolites, such as flavonoid, isoflavonoid, flavone, and flavonol, were significantly enriched during leaf development in *M. pubescens*. Specifically, the isoflavonoid biosynthesis pathway showed the most pronounced enrichment. Previous studies have suggested that specific structural genes within the flavonoid pathways play a crucial role in regulating coloration (Song et al., 2017; Zhou et al., 2020). For instance, structure genes involved in C4H, DFR and FLS, as well as regulatory genes, such as MYB and WRKY, acted as important roles in these pathways (Mei et al., 2021; Mei, et al., 2019). Whereas, the regulation of flavonoid biosynthesis involves multiple structural genes, and the product of flavonoid synthesis originates from phenylalanine. Meanwhile, several DEGs, including CHS, CHI (E5.5.1.6), DFR, F3H, FLS, LAR, ANS, and PGT, were identified during the developmental stage of MpBud, MpTen, and MpMat.

4.3.5 TFs related to metabolomic biosynthesis

Transcription factors are vital for regulating plant growth and development. For example, the main TFs associated with stress regulation include the AP2/ERF, bZIP, and C2H2 transcription factor families, zinc finger, and SBP. Importantly, MYB families are crucial regulators in the biosynthesis of isoflavonoids in plants. NAC proteins play a crucial role in regulating the growth and development of various plants, which functions encompass a wide range of processes, such as secondary wall formation (Sun et al., 2020), leaf senescence (Guo & Gan, 2006), as well as the regulation of hormones like auxin, cytokinin, ethylene, and gibberellin (He et al., 2005). bHLH, as an important family of TFs, regulates the growth and development processes in diverse plant species, which is involved in various functions such as seed germination, flowering time control, cell

fate determination, the JA signaling pathway (Hao et al., 2021), and plant isoflavonoid biosynthesis (Rai et al., 2016). What's more, WRKY is a type of TFs that plays a crucial role in plant defense against pathogens and stresses (Jiang et al., 2017).

TFs were identified by hmmscan alignment using iTAK software combined with PlnTFDB and PlantTFDB databases. A total of 2754 differentially expressed TFs were identified in the three comparisons of MpBud vs. MpTen, MpTen vs. MpMat and MpBud vs. MpMat, which were annotated as bHLH (4.83%), MYB-related (4.83%), AP2/ERF-ERF (4.43%), SET (3.81%), C2H2 (3.77%), WRKY (3.63%), C3H (3.56%), NAC (2.87%), bZIP (2.83%) and other family factors (60.98%). R2R3-MYB genes, such as the flavonol regulator AtMYB12/AtMYB111 and the anthocyanin regulator AtMYB12, as well as R2R3-MYB repressors with a truncated R2 domain, have been demonstrated to function as regulators of anthocyanin biosynthesis in plants (Deluc et al., 2020; Ma et al., 2018). ZmWRKY79 was reported to positively regulate drought tolerance through elevating ABA biosynthesis (Gulzar et al., 2021) and abiotic stress (Banerjee & Roychoudhury, 2015). Dihydrokaempferol (DHK) serves as a precursor for anthocyanin synthesis and acts as a metabolic intermediate for flavonols, while the enzyme F3H catalyzes the hydroxylation of the substrate naringenin, leading to the DHK formation (Falcone et al., 2012). Meanwhile, F3'H catalyzes the hydroxylation of the intermediate substrate DHK at the 3'-position of the B-ring, resulting in the formation of dihydromyricetin (DHM) which serves as the precursor to produce cyaniding (Seitz et al., 2007). Additionally, CHS play a crucial role in the overall accumulation of anthocyanins (Peng et al., 2019).

In total, 493 TFs (159 upregulation and 334 downregulation) were obtained from MpBud vs. MpTen, out of which 38 WRKY (36 upregulation and 2 downregulation involved in WRKY 12 and WRKY 13) and 35 bHLH (10 upregulation such as bHLH 25 and bHLH 35, and 25 downregulation including bHLH 30, bHLH 37, bHLH 96 and bHLH 120) TF families were the most abundant. While a number of 37 TFs (5 upregulation and 32 downregulated) and 345 TFs (92 upregulated and 253 downregulated) were identified from the comparisons of MpTen vs. MpMat and MpBud vs. MpMat, respectively, indicating that the majority of the downregulated differentially expressed TFs were uncorrelated with growth and color change of Mp leaves. Among these TF families, AP2/ERF (almost all eight TFs were downregulated such as DRE1B and DRE1D) and bHLH (twenty-six TFs downregulated involved in bHLH 35 and bHLH 92) were observed to be the highest expression in MpTen vs. MpMat and MpBud vs. MpMat, respectively.

4.3.6 qRT-PCR validation of DEGs in transcriptome sequencing

To validate the accuracy of transcriptome data, nine candidate genes (two up-regulation and seven down-regulation) associated with phenylpropanoid, flavonoid and anthocyanidin biosynthesis were selected for qRT-PCR analysis in MpBud, MpTen and MpMat elucidated that the relative expression levels of nine genes identified from the whole growth stage of Mp leaves were performed by RNA-Seq and qRT-PCR analyses (Figure 4-3-9).

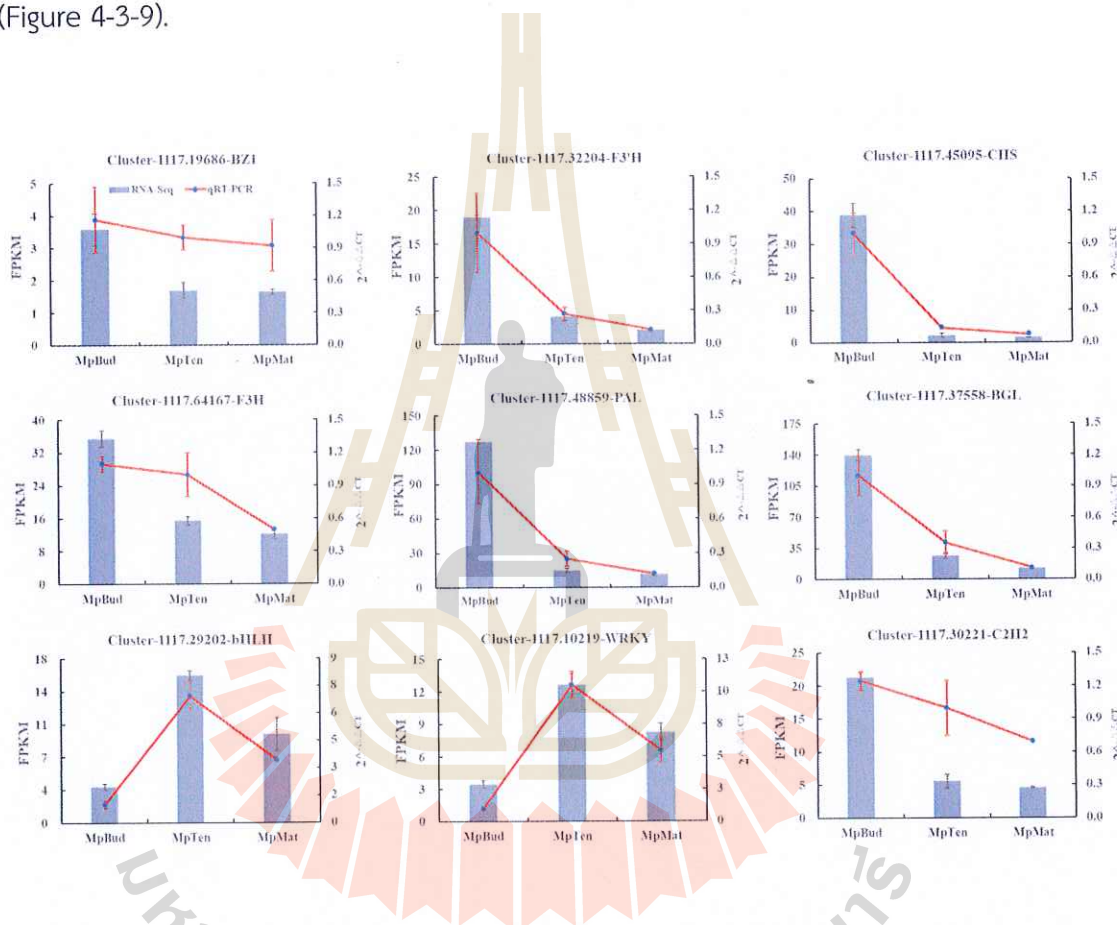
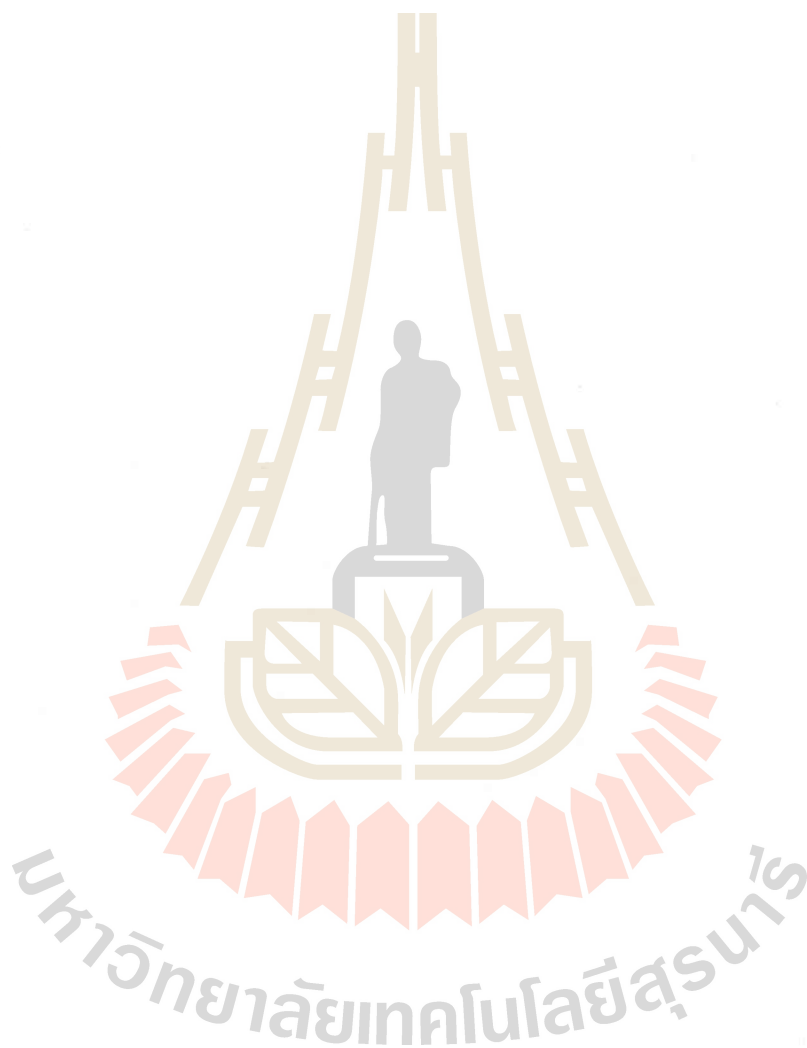


Figure 4-3-9 qRT-PCR validation of candidate genes associated with phenylpropanoid, flavonoid and anthocyanidin biosynthesis in Mp leaves.

Note: Nine genes include BZ1, F3'H, CHS, F3H, PAL, BGL, bHLH, WRKY, and C2H2. The abscissa represents samples at different growth stages of leaves (MpBud, MpTen, and MpMat). The right vertical coordinates represent the relative gene expression level ($2^{-\Delta\Delta C_t}$) by qRT PCR analysis.

In general, the expression levels of these candidate genes detected by qRT-PCR analysis were in accordance with relevant FPKM values obtained from RNA-Seq results.

In addition, the expression levels of seven down-regulated genes involved in BZ1, F3'H, CHS, F3H, PAL, BGL and C2H2 gradually decreased as the leaves grew into maturity, while the expression levels of two up-regulated genes including WRKY and C2H2 exhibited a trend of rising first and then falling across the whole growth cycle. These results showed that numerous genes had similar expression profiles detected with these two methods, indicating that the obtained transcription data was reliable.



4.4. The Acute Toxicity Assessment and Protective Effects of *M. pubescens*

4.4.1 Sensory evaluation and components analysis of MpBT

The quality characteristics of five aspects involved in the shape, infusion color, aroma, flavor and leaf base were subjected to sensory evaluation in accordance with the national standards for tea (GB/T 23776-2018). The shape of MpBT was relatively complete with approach tight cable (Figure 4-4-1B). Tea infusion was characterized by orange-red and blight color, sweet fragrance, and a fresh and mellow taste, with red blight and soft leaf base (Figure 4-4-1C). In addition, a total of 957 metabolites were identified from MpBT, such as 185 phenolic acids, 109 terpenoids, and 81 flavonoids.



Figure 4-4-1. *Mussaenda pubescens* black tea (MpBT).

Note: (A) Phenotypic characteristics of *Mussaenda pubescens* (Mp), (B) Shape of Mp black tea (MpBT), and (C) Infusion of MpBT.

4.4.2 Acute toxicity assessment of MpBT

The MpBT-related developmental toxicity was assessed by treating *zebrafish* with a dose-dependent manner of MpBT (Table 4-4-1). After 48 h exposure, low concentrations of MpBT did not have a significant effect on the mortality of *zebrafish* compared with control treatment ($P > 0.05$); while high concentrations of MpBT treated with 4, 8, 10, 20, and 50 mg/mL significantly increased the mortality of *zebrafish* embryos ($P < 0.05$). Additionally, LC_{50} values for 24 h and 48 h were 3.54 mg/mL and 3.47 mg/mL, respectively.

Table 4-4-1 Acute toxicity assessment of MpbT^a

Density mg/mL	Cumulative mortality/%		Body length/ μ m	Eye length/ μ m	Heart rate/min	SV-BA/ μ m
	24 hpf	48 hpf				
0	0.00 \pm 0.00b	0.00 \pm 0.00b	3839.13 \pm 39.36a	325.87 \pm 2.75a	161.00 \pm 4.24a	226.97 \pm 1.80a
0.2	0.00 \pm 0.00b	0.00 \pm 0.00b	3847.37 \pm 40.11a	320.50 \pm 2.72a	155.90 \pm 6.58a	213.30 \pm 3.31ab
0.4	0.00 \pm 0.00b	0.00 \pm 0.00b	3857.57 \pm 36.20a	321.40 \pm 2.70a	154.60 \pm 4.13a	201.23 \pm 2.62ab
0.8	0.00 \pm 0.00b	0.00 \pm 0.00b	3862.43 \pm 33.51a	322.77 \pm 2.25a	162.10 \pm 2.42a	208.93 \pm 2.25ab
1	0.00 \pm 0.00b	0.00 \pm 0.00b	3835.70 \pm 33.84a	321.33 \pm 2.94a	166.40 \pm 2.22a	202.93 \pm 3.26ab
2	3.33 \pm 3.33b	3.33 \pm 3.33b	3741.90 \pm 131.87a	311.60 \pm 10.96a	163.40 \pm 6.37a	185.33 \pm 10.0b
4	73.33 \pm 16.67a	73.33 \pm 16.67a	1001.97 \pm 308.81b	84.43 \pm 26.01b	48.40 \pm 14.98b	52.77 \pm 16.29c
8	93.33 \pm 3.33a	93.33 \pm 3.33a	249.67 \pm 173.62c	10.30 \pm 10.30c	5.90 \pm 5.90c	6.80 \pm 6.80d
10	96.67 \pm 3.33a	100.0 \pm 0.00a	0.00 \pm 0.00c	0.00 \pm 0.00c	0.00 \pm 0.00c	0.00 \pm 0.00d
20	100.0 \pm 0.00a	100.0 \pm 0.00a	0.00 \pm 0.00c	0.00 \pm 0.00c	0.00 \pm 0.00c	0.00 \pm 0.00d
50	100.0 \pm 0.00a	100.0 \pm 0.00a	0.00 \pm 0.00c	0.00 \pm 0.00c	0.00 \pm 0.00c	0.00 \pm 0.00d

Note: ^a All data are expressed as mean \pm SE (n=3), and different lowercase letters represent statistically significant differences among the treatments ($P < 0.05$).

Similarly, low concentrations of MpBT treated with 0.2, 0.4, 0.8, 1.0, and 2.0 mg/mL exhibited no remarkable impact on the morphology and development of *zebrafish* embryos involved in body length, eye length, SV-BA and heart rate compared with control treatment ($P > 0.05$); however, high concentrations of MpBT treatment obviously inhibited the morphology and development of *zebrafish* ($P < 0.05$).

4.4.3 Morphological and developmental effects of *zebrafish* embryos exposure to MpBT

The *zebrafish* trials were applied to evaluate whether and how MpBT affects the development of the embryos. In the current study, the survival rates of embryos exposed to MpBT at 24-144 hpf were exhibited in Figure 4-4-2A. The survival rates of *zebrafish* embryos were observed to be significantly different after 48 hpf in all treatments, especially at 144 hpf. More specifically, the survival rate of *zebrafish* embryos exposure to CuSO_4 remarkably decreased to 30.1% compared with control group ($p < 0.05$). Whereas co-treatment with CuSO_4 + MpBT of 0.5, 1.0, and 1.5 mg/mL significantly raised the survival rates of embryos to 82.22%, 84.4%, and 80.0%, respectively, in comparison with CuSO_4 treatment ($p < 0.05$). These findings suggested that MpBT had the ability to improve CuSO_4 -induced damage and survival rate of *zebrafish* embryos.

Hatching is a crucial developmental process in the life cycle in which embryos are digested by the chorion from the egg through chlorolytic enzymes (Li et al., 2022). In this study, the hatching rates of *zebrafish* embryos were determined at 24-144 hpf (Figure 4-4-2B). The hatching rates were observed for 68.9% at 96 hpf and 97.8% at 120 hpf in a control group, but only for 28.9% and 55.6% in CuSO_4 treatment, indicating that the hatching of *zebrafish* embryos was remarkably postponed by CuSO_4 ($p < 0.05$). The postponement in hatchability of *zebrafish* embryos exposed to CuSO_4 might be due to the interference of hatching enzymes digested by chorionic membrane or the delay of embryonic development induced by hypoxia (Nipun et al., 2021). However, the hatching rates of *zebrafish* embryos exposure to co-treatment with CuSO_4 + MpBT of 0.5, 1.0 and 1.5 mg/mL were recorded for 55.6%, 57.8%, 62.2% at 96 hpf, and 82.1%, 84.9%, 87.3% at 120 hpf, respectively. These results suggested that MpBT treatment was capable of ameliorating CuSO_4 -induced hatchability postponement in the development of *zebrafish* embryos.

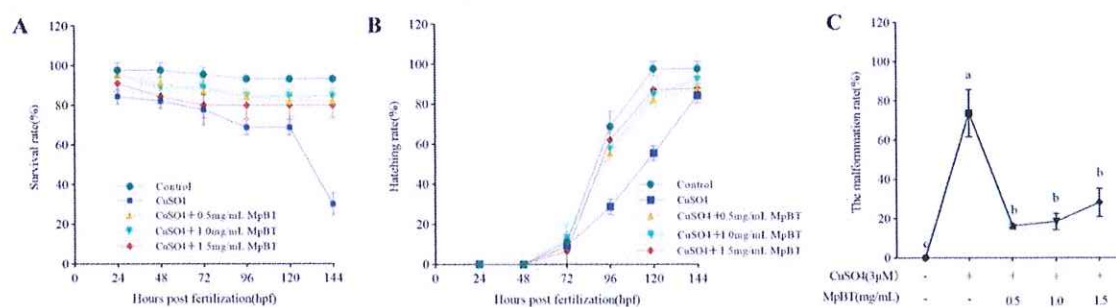


Figure 4-4-2. Effects of MpBT on CuSO₄-induced developmental damage in *zebrafish* embryos at 24-144 hpf.

Note: (A) Survival rate; (B) Hatching rate; (C) The malformation rate. All data are expressed as mean \pm SE (n=3), and different lowercase letters represent statistically significant differences among the treatments ($p < 0.05$)

The toxicity of MpBT was also examined by evaluating the malformations of *zebrafish* embryos at 144 hpf (Figure 4-4-2C). No difference in malformations was observed in the control. In contrast, that of embryos exposed to CuSO₄ increased to 73.6%. However, total malformation rate ranging from 16.3% to 28.2% co-treated with CuSO₄ + MpBT of 0.5, 1.0, and 1.5mg/mL were remarkably reduced in *zebrafish* embryos in comparison with CuSO₄ treatment ($p < 0.05$). These results indicated that *zebrafish* embryos exposure to copper sulfate caused a significant increase in the incidence of spinal curvature, tail deformity, and pericardial edema. At the same time, the supplement with MpBT was able to alleviate teratogenic effects on *zebrafish* embryos, showing the defense against CuSO₄-induced malformation.

To further investigate the effects of the co-treatment (CuSO₄ + MpBT) and CuSO₄ along with the growth and development of *zebrafish*, the body length, eye length, the distance of SV-BA, and heart rate were measured at 144 hpf. The *zebrafish* embryos exposed to CuSO₄ exhibited obvious abnormalities in morphological features compared to the control and co-treatment (Figure 4-4-3).

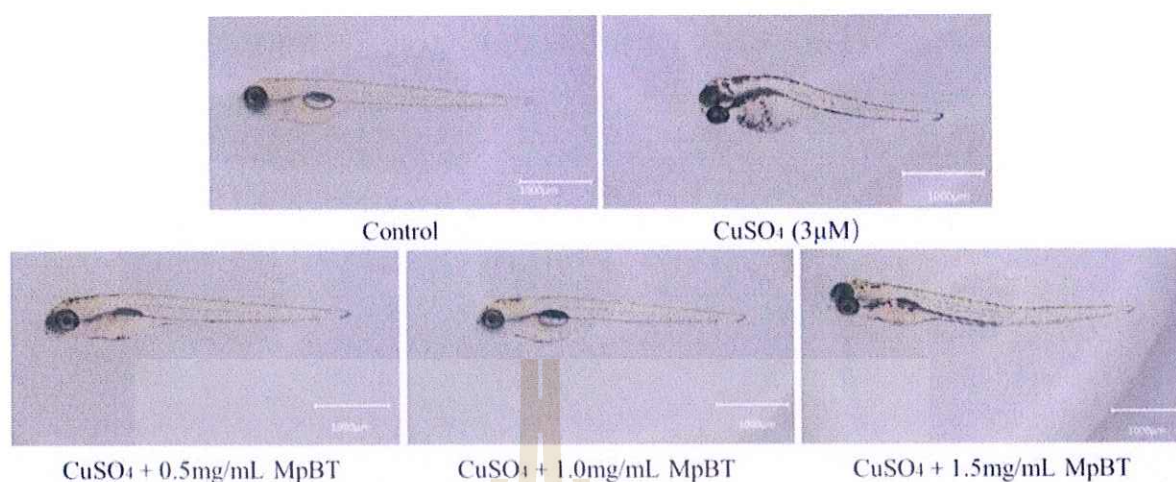


Figure 4-4-3. The morphological features of *zebrafish* embryos exposed to CuSO_4 .

Table 4-4-2 Significance analysis of *zebrafish* morphological index of MpBT at different concentrations

Concentration	Morphological Development Index			
	Body length/ μm	Eye length/ μm	SV-BV/ μm	Heart rate/min
Control	4185 \pm 39.80a	358 \pm 3.52a	187 \pm 2.23a	147 \pm 1.15a
CuSO_4 + 0.5 mg/mL MpBT	4035 \pm 48.17b	346 \pm 3.71b	161 \pm 1.67b	145 \pm 1.72a
CuSO_4 + 1.0 mg/mL MpBT	3947 \pm 54.84b	341 \pm 3.10b	155 \pm 3.09b	139 \pm 0.95b
CuSO_4 + 1.5 mg/mL MpBT	3937 \pm 53.56b	339 \pm 1.93b	154 \pm 1.92b	136 \pm 1.33b
CuSO_4	3607 \pm 22.92c	320 \pm 3.30c	127 \pm 3.20c	121 \pm 1.27c

Note: All data are expressed as mean \pm SE (n=3), and different lowercase letters represent statistically significant differences among the treatments ($p < 0.05$).

The body length, eye length, the distance of SV-BV, and the heart rate of embryos exposure to CuSO_4 markedly decreased compared to the control group ($p < 0.05$), while co-treatment with CuSO_4 + MpBT of 0.5, 1.0, and 1.5 mg/mL significantly improved the morphology of *zebrafish* compared with CuSO_4 alone treatment ($p < 0.05$) (Table 4-4-2). Collectively, the induction of CuSO_4 inhibited the development of *zebrafish* larvae, whereas the development of embryos exposed to co-treatment with CuSO_4 + MpBT was slower than that of the control group but faster than that of *zebrafish* treated with CuSO_4 alone. For this study, the co-treatment of CuSO_4 and MpBT significantly renovated the heart rate of larvae in the CuSO_4 alone treatment in

comparison with the control group, indicating that MpBT possessed an excellent protective action on CuSO₄-induced embryonic damage.

4.4.4 Analysis of oxidative-stress-related biochemical indicators

CuSO₄-induced oxidative damage caused cellular injuries and excessive production of free radicals as well as many health problems (Park et al., 2016). However, frequent consumption of antioxidants contributed to the prevention of such oxidative stress-associated diseases (Lanzarin et al., 2021; Rajiv et al., 2021). Therefore, the levels of antioxidant enzymes involved in ROS, MDA, SOD, and CAT were examined to investigate the effect of MpBT on CuSO₄-induced oxidative damage in larvae at 120 hpf.

The overproduction of ROS might cause endothelial dysfunction and tissue damage, leading to inflammatory response and oxidative stress (Bhagat et al., 2021; Gong et al., 2020). MDA is a lipid peroxidation product caused by ROS attacking polyunsaturated fatty acids in biomembrane, which is a common biomarker for identifying oxidative damage in organisms (Wang et al., 2021). The contents of ROS and MDA in *zebrafish* embryos exposed to CuSO₄ alone were significantly increased by 173.2% and 33.8% compared with the control group (Figure 4-4-4A-B), respectively. However, CuSO₄ induces toxicity by producing reactive oxygen species in cells. The co-treatment of CuSO₄ and MpBT of 0.5, 1.0, and 1.5 mg/mL remarkably reduced the contents of ROS and MDA compared with the CuSO₄ treatment alone (Figure 4-4-4A-B), decreasing by 29.7%-36.2% for ROS and 11.9%-31.4% for MDA ($p < 0.05$), respectively. These results indicated that the alleviation of CuSO₄-induced oxidative lipid damage by MpBT was possibly relative to the free radical scavenging activity of MpBT and the activation of *zebrafish* embryonic antioxidant defense system.

The endogenous antioxidant defense prevents ROS-induced damage (Hahn et al., 2015). SOD is one of the crucial endogenous antioxidant enzymes, which can directly prevent ROS from converting O₂⁻ into O₂ and hydrogen peroxide (H₂O₂), whereas CAT catalyzes the transformation from H₂O₂ into O₂ and H₂O (Pessina et al., 2021; Velayutham et al., 2021). As shown in Figure 4C and D, SOD and CAT activities of embryos exposure to CuSO₄ alone significantly decreased by 56.5% and 23.1%, respectively, compared with those in the control group ($p < 0.05$). However, enzyme activities of *zebrafish* embryos exposed to the co-treatment of CuSO₄ and MpBT of 0.5, 1.0, and 1.5 mg/mL were improved by 35.6%, 83.8%, 191.7% for SOD, and 71.9%, 120.9%, 157.3% for CAT, respectively, compared to CuSO₄ treatment alone. SOD and CAT enzymes act as crucial

roles in antioxidant defense system, and antioxidant system could alleviate oxidative stress by increasing the expressions of antioxidant enzymes (Wang et al., 2021). Therefore, these results indicated that MpBT could improve the antioxidant activity of these two enzymes induced by CuSO_4 in *zebrafish* embryos to enhance antioxidant defense system.

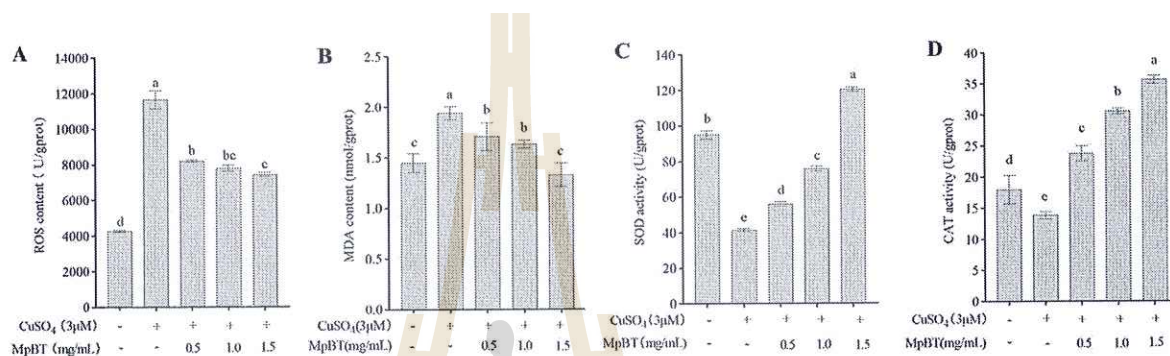


Figure 4-4-4. Effects of on CuSO_4 -induced oxidative damage in *zebrafish* embryos at 120 hpf.

Note: (A) ROS content; (B) MDA content; (C) SOD activity; (D) CAT activity. All data are expressed as mean \pm SE (n=3), and different lowercase letters represent statistically significant differences among the treatments ($p < 0.05$).

4.4.5 Protein expression levels

In the process of cellular stress response, HSP70 is a crucial protein that protects cells from the adverse influence of oxidative damage and is essential for resisting copper toxicity (Nguyen et al., 2020). Bax and Bcl-2 are intracellular apoptotic protein and anti-apoptotic protein, respectively (Wang et al., 2021). To evaluate the effects of MpBT on the apoptosis of *zebrafish* embryos treated with CuSO_4 at the protein levels, the expression levels of the relevant proteins involved in HSP70, Bax, and Bcl-2 were determined after treatment with MpBT at 120 hpf (Figure 4-4-5A-C). The results indicated that CuSO_4 treatment of *zebrafish* larvae was observed to significantly increase the contents of HSP70 and Bax, and remarkably decrease Bcl-2 content in comparison with the control group ($p < 0.05$), while the co-treatment with CuSO_4 and MpBT of 0.5, 1.0, and 1.5mg/mL caused a significant decrease in HSP70 and Bax, and increase in Bcl-2 protein content. Therefore, MpBT was speculated to possess a potential protective effect on cell apoptotic damage.

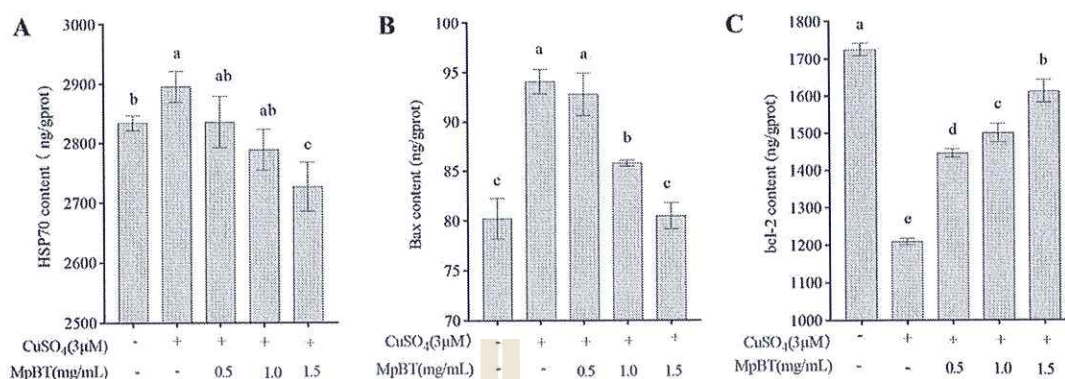


Figure 4-4-5. Effects of MpBT on CuSO₄-induced protein expression level in *zebrafish* embryos at 120 hpf.

Note: (A) HSP70 content; (B) Bax content; (C) bcl-2 content. All data are expressed as mean \pm SE (n=3), and different lowercase letters represent statistically significant differences among the treatments ($p < 0.05$).

4.4.6 Effects on antioxidant, inflammation, and apoptosis related gene expression

To explore the function of MpBT defense against CuSO₄-induced oxidative damage and inflammation in embryos at 120 hpf, the expression levels of antioxidant-associated genes (Mn-sod, Cat and Gpx1 α) and anti-inflammation genes (TNF- α , 1L-1 β and TNF- γ) were determined.

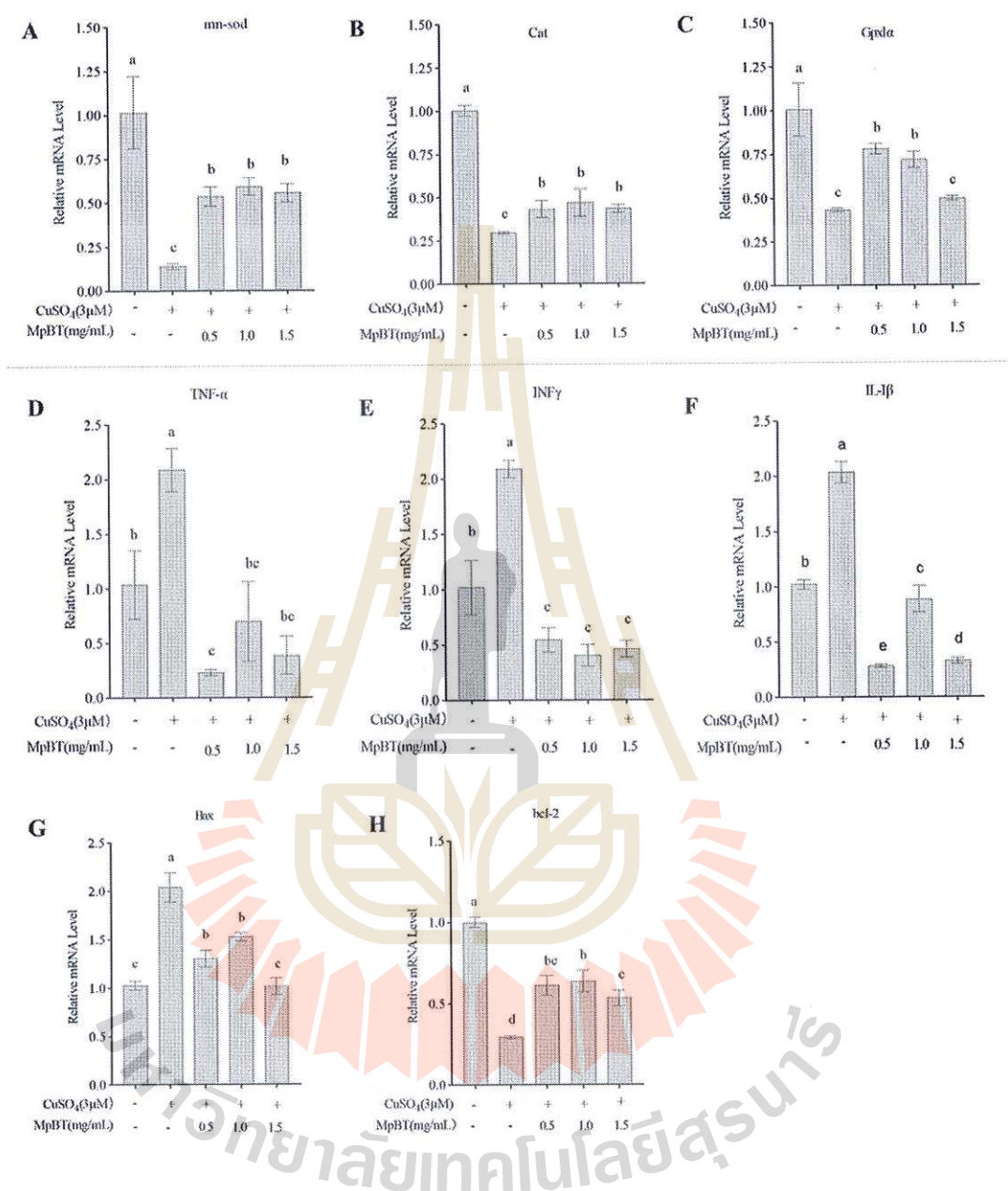
4.4.6.1 Effects of MpBT on CuSO₄-induced antioxidant in *zebrafish* larvae

Figure 4-4-6. Effects of MpBT on CuSO₄-induced antioxidant-, inflammation- and apoptosis-related gene expression in *zebrafish* embryos at 120 hpf.

Note: (A) mn-sod mRNA level; (B) Cat mRNA; (C) Gpx1α level; (D) TNF-α mRNA level; (E) INFγ mRNA level; (F) IL-1β level; (G) Bax mRNA level; (H) bcl-2 mRNA level. All data are expressed as mean ± SE (n=3), and different lowercase letters represent statistically significant differences among the treatments (p < 0.05).

The expression and induction of antioxidant defense that can reduce oxidative damage are critical factors influencing susceptibility to oxidative stress (Hahn et al., 2015). Excessive free radicals can induce oxidative damage of biomacromolecules in cells to break the balance between oxidation and antioxidant defense system as well as induce oxidative stress (Nipun et al., 2021; Zhao et al., 2016; Zhao et al., 2013). In the current study, CuSO₄ treatment alone significantly decreased the mRNA expression levels of oxidative stress-related genes involved in Mn-sod, Cat, and Gpx1 α in comparison of the control group ($p < 0.05$) (Figure 4-4-6A-C), indicating that CuSO₄ induced oxidative damage. However, the co-treatment of CuSO₄ with MpBT of 0.5, 1.0, and 1.5 mg/mL remarkably improved these three expression levels of *zebrafish* embryos compared with CuSO₄ treatment alone, increasing by 285.7%-321.4% for Mn-sod, 25%-29.2% for Cat, and 46.5%-81.4% for Gpx1 α (Figure 4-4-6A-C). These findings were consistent with a report described by (Vidyalakshmi et al., 2008) who showed that Mp exhibited antioxidant property was attributed to the presence of flavonoids and phenolic compounds. Taken together, these results indicated that MpBT could upgrade expression levels of antioxidant-related genes and reduce the severe oxidative damage with CuSO₄-induced *zebrafish* larvae, which provided a potential protection against oxidative damage.

4.4.6.2 Effects of MpBT on CuSO₄-induced anti-inflammatory in *zebrafish* larvae

The inflammatory response is a defense response that is a common pathological phenomenon during severe disturbances to the homeostasis, which eliminates the harmful stimuli by killing microbes and removing stimulator (Gong et al., 2020; Wang et al., 2019; Zhou et al., 2020). Oxidative stress can stimulate the generation of pro-inflammatory cytokines and induce inflammatory response (Gong et al., 2020; Nipun et al., 2021; Wang et al., 2021). Tumor necrosis factor- α (TNF- α), interleukin-1 β (IL-1 β), and IFN- γ are the crucial pro-inflammatory cytokines, which are commonly served as biomarkers of activated inflammatory response. In this study, the expression levels of pro-inflammatory cytokines such as TNF- α , IFN- γ , and IL-1 β in *zebrafish* embryos treated with CuSO₄ alone were dramatically up-regulated by 140%, 100%, and 100%, respectively, compared with the control group ($p < 0.05$) (Figure 4-4-6D-F), which suggested that CuSO₄ promoted the release of pro-inflammatory cytokines to induce inflammation response. While the expression levels of these three genes in *zebrafish*

larvae exposed to co-treatment of CuSO₄ with MpBT of 0.5, 1.0, and 1.5 mg/mL significantly down-regulated by 62.3%-86.3% for IL-1 β , 58.4%-96.1% for TNF- α , and 73.5%-80.4% for IFN- γ in comparison with CuSO₄ treatment alone, and even lower than those of the control group ($p < 0.05$). These findings suggested that MpBT might exert probable anti-inflammatory activity by inhibiting the up-regulation of pro-inflammatory cytokines in *zebrafish* embryos induced by CuSO₄, which was consistent with the research reported by (Vidyalakshmi et al., 2008) who exhibited that the anti-inflammatory activity of Mp was associated with some important biochemicals such as flavonoids and phenolic compounds.

4.4.6.3 Effects of MpBT on CuSO₄-induced apoptosis in *zebrafish* larvae

Apoptosis is an evolutionarily conserved form of programmed cell death (PCD), which is essential for animal development and tissue homeostasis (D'Arcy, 2019). Oxidative stress and inflammation are the crucial factors in inducing apoptosis (Wang et al., 2022). The expression levels of apoptosis-associated genes such as Bax of *zebrafish* embryos exposure to CuSO₄ treatment alone was significantly increased, and Bcl-2 gene was remarkably decreased compared with the control group ($p < 0.05$) (Figure 4-4-6G and H). The significant up-regulation and down-regulation of apoptosis-related factors indicated that CuSO₄ treatment promoted the apoptosis damage of *zebrafish* embryos. However, the mRNA expression in the co-treatment of CuSO₄ and MpBT of 0.5, 1.0, and 1.5 mg/mL significantly improved by 34.8%-35.8% for Bcl-2 gene and decreased by 76.7%-113.3% for Bax gene in comparison with the CuSO₄ treatment alone (Figure 4-4-6G and H). Quercetin, an important natural flavonoid derived from various crop plants such as vegetables, fruits, and herbs (Wach et al., 2005), was reported to regulate the expression levels of apoptosis-associated genes (Bax, Bcl-2) in *zebrafish* induced by TAA, indicating that quercetin was able to possess an anti-apoptosis effect (Wang et al., 2021). Whereas our study showed that MpBT significantly improved the expression levels of CuSO₄-induced apoptosis-related genes in *zebrafish* and provided a potential protective effect on *zebrafish* embryonic apoptosis treated with CuSO₄, which might be attributed to the fact that many flavonoid compounds involved in quercetin of MpBT could alleviate CuSO₄-induced oxidative damage and inflammation response in *zebrafish* embryos (Vidyalakshmi et al., 2008).

CHAPTER V

CONCLUSION

5.1. The complete *cp genome* of *M. pubescens* and phylogenetic analysis

M. pubescens was compared with the specimens of Chinese *Mussaenda*, indicating that *M. pubescens* was closely related to *M. hirsutula*. However, *M. pubescens* was distinguished by its gyro-shaped corolla tubes measuring 3-4 mm in length, ovate oblong or ovate lanceolate leaves, and oblong lanceolate corolla lobes. Furthermore, this study determined the complete *cp genomes* of *M. pubescens* for the first time and revealed their basic structures, conservation, and variability. The complete *cp genomes*, including their LSC and SSC regions, were employed to investigate the robust phylogenetic relationships within and between genera. Additionally, the availability of this information would offer useful references for subsequent studies on taxonomic identification, phylogenetics, population structure, and biodiversity within the genus *Mussaenda*. Furthermore, the comparative analysis of *cp genomics* in the genus *Mussaenda* contributed to our comprehension of *cp genome* dynamics, complexity, and evolution within the *Rubiaceae* family. In conclusion, this study served as a valuable reference for future research on species identification, evolutionary relationships, and the development of genetic resources within the *Rubiaceae* family.

5.2. Metabolite profiles of *M. pubescens*

In summary, a UPLC-MS/MS-based metabolome was performed to evaluate the differences in metabolites among Mp leaves at different developmental stages. The maturation period of Mp leaves had the greatest impact on the evolution of metabolites. A total of 957 metabolites were identified, among which 317 DAMs were most clearly affected by the growth and development of Mp leaves. Additionally, 202, 54, and 254 DAMs were found in MpBud vs. MpTen, MpTen vs. MpMat, and MpBud vs. MpMat, respectively. Metabolic pathway analysis showed significant enrichment of “flavone and flavonol biosynthesis”, “phenylalanine metabolism”, “ABC transporters”, “folate biosynthesis”, “fructose and mannose metabolism”, “arginine biosynthesis”, and “biosynthesis of amino acids”. Comparisons of functional components (including total phenolics, flavonoids, terpenoids, and anthocyanin) and antioxidant activities among the

Mp leaves showed that these compounds were the main factors for the difference in antioxidant activity among bud, tender, and mature leaves, and they had a strong correlation. Further analysis expounded the evolutionary processes of the terpenoids, phenolic acids, flavonoids, alkaloids, amino acids and derivatives, organic acids, lipids, lignans and coumarins, and nucleotides and derivatives, wherein the up-regulation of these DAMs were the key factor driving the function and quality of the Mp tea.

The findings of this research not only contribute to a better understanding of the metabolites and functional ingredients that possess antioxidant activities in Mp, but they also provide new insights into the mechanism by which metabolites are formed in Mp leaves. In addition, they have the potential to provide researchers with assistance in the comparative evaluation of targeted leaves that possess particular functional properties and quality traits, thereby providing a new theoretical foundation for the development of Mp tea.

5.3. Metabolomic and Transcriptomic Profiling Reveals the Flavonoid Components and Discoloration Mechanism of *M. pubescens* Leaves

In the current study, the molecular mechanisms of leaf color change and functional components alteration in the whole growth stages of Mp leaves were performed by combining metabolome and transcriptome analyses. The biosynthesis and accumulation of pigments during the leaf color formation were mainly associated with the key metabolites and structural genes of flavonoid biosynthesis. The two DAMs, Naringenin-7-*O*-glucoside (Prunin) and Phloretin-2'-*O*-glucoside (Phlorizin), were the primary factors influencing the changes in leaf color. Furthermore, the expression of flavonoid biosynthesis genes (HCT, CHS, E5.5.1.6 and PGT1) were up-regulated, as well as the majority of their transcription factors significantly down-regulated in the tender leaves. Additionally, the expression of genes involved in CYP75B1, ANS, F3H, DFR, and C12RT1 exhibited a highly correlative relationship with metabolites such as phloretin-2'-*O*-glucoside (phlorizin) and naringenin-7-*O*-glucoside (prunin) in the flavonoid biosynthesis across the whole growth cycle of Mp leaves. These findings may enhance our understanding of the molecular regulatory mechanism involved in leaf color alteration and provide valuable guidance for the development of Mp leaves as functional food.

5.4. The Acute Toxicity Assessment and Protective Effects of *M. pubescens*

In summary, MpBT reduced CuSO₄-induced adverse damage involved in postponed hatching, malformation, mortality, and overall morphological characteristics

in *zebrafish* embryos. Additionally, MpBT activated the antioxidative defense system by reducing the generation of ROS, restoring the activities of antioxidant enzymes (MDA, SOD, and CAT) and increasing the expression levels of oxidative stress-associated genes such as Mn-sod, Cat, and GPx1 α . Furthermore, MpBT inhibited the up-regulated expression of pro-inflammatory cytokine genes involved in TNF- α , IL-1 β , and IFN γ induced by CuSO₄ to alleviate inflammatory response and improved regulations of apoptosis-associated genes (Bax, Bcl-2) in *zebrafish* embryos. Therefore, MpBT could serve as protective effects on CuSO₄-induced *zebrafish* embryonic developmental damage, oxidative stress, inflammation, and apoptosis, which provided a potential value as a source of novel drugs for the development and utilization of MpBT.



REFERENCES

- Abd Rashid, N. A., Lau, B. F., & Kue, C. S. (2022). Differential toxicity and teratogenic effects of the hot water and cold-water extracts of *Lignosus rhinoceros* (Cooke) Ryvarden sclerotium on zebrafish (*Danio rerio*) embryos. *JOURNAL OF ETHNOPHARMACOLOGY*, 285, 114787.
- Abdullah, Mehmood, F., Shahzadi, I., Waseem, S., Mirza, B., Ahmed, I., & Waheed, M. T. (2020). Chloroplast genome of *Hibiscus rosa-sinensis* (Malvaceae): Comparative analyses and identification of mutational hotspots. *GENOMICS*, 112(1), 581-591.
- Afonso, S., Oliveira, I. V., Meyer, A. S., Aires, A., Saavedra, M. J., & Berta, G. (2020). Phenolic Profile and Bioactive Potential of Stems and Seed Kernels of Sweet Cherry Fruit. *ANTIOXIDANTS*, 9(12), 1295.
- Afridi, R., Khan, A. U., Khalid, S., Shal, B., Rasheed, H., Ullah, M. Z., Shehzad, O., Kim, Y. S., & Khan, S. (2019). Anti-hyperalgesic properties of a flavanone derivative Poncirin in acute and chronic inflammatory pain models in mice. *BMC PHARMACOLOGY & TOXICOLOGY*, 20(1), 57.
- Ai, F., Huang, X., Wu, Y., Ji, C., Gao, Y., Yu, T., & Yan, F. (2023). Alleviative effects of a novel strain *Bacillus coagulans* XY2 on copper-induced toxicity in zebrafish larvae. *JOURNAL OF ENVIRONMENTAL SCIENCES*, 125, 750-760.
- Ajuru, M. G., Ajuru, G., Nmom, F. W., Worlu, C. W., & Igoma, P. G. (2019). Acute Toxicity Study and Determination of Median Lethal Dose of *Catharanthus roseus* in Wistar Albino Rats. *JOURNAL OF APPLIED SCIENCES*, 19(3), 217-222.
- Alejandro, G. D., Razafimandimbison, S. G., & Schumann, S. L. (2005). Polyphyly of *Mussaenda* inferred from ITS and trnT-F data and its implication for generic limits in *Mussaendeae* (Rubiaceae). *AMERICAN JOURNAL OF BOTANY*, 92(3), 544-557.
- Arceci, R. J., King, A. A., Simon, M. C., Orkin, S. H., & Wilson, D. B. (1993). Mouse GATA-4: a retinoic acid-inducible GATA-binding transcription factor expressed in endodermally derived tissues and heart. *MOLECULAR AND CELLULAR BIOLOGY*, 13(4), 2235-2246.
- Asaf, S., Khan, A. L., & Khan, A. R. (2016). Complete Chloroplast Genome of *Nicotiana glauca* and its Comparison with Related Species. *FRONTIERS IN PLANT SCIENCE*, 7(447), 843.
- Asakura, H., Yamakawa, T., Tamura, T., Ueda, R., Taira, S., Saito, Y., Abe, K., & Asakura, T. (2021). Transcriptomic and Metabolomic Analyses Provide Insights into the

- Upregulation of Fatty Acid and Phospholipid Metabolism in Tomato Fruit under Drought Stress. *JOURNAL OF AGRICULTURAL AND FOOD CHEMISTRY*, 69(9), 2894-2905.
- Aude, M., & Laufs, P. (2018). Getting leaves into shape: a molecular, cellular, environmental and evolutionary view. *DEVELOPMENT*, 145(13), 161646.
- Ayabe, H., & Aoshima, S. (2007). Prevention of the deterioration of polyphenol-rich beverages. *FOOD CHEMISTRY*, 100(1), 350-355.
- Banerjee, A., & Roychoudhury, A. (2015). WRKY Proteins: Signaling and Regulation of Expression during Abiotic Stress Responses. *THE SCIENTIFIC WORLD JOURNAL*, 2015, 807560.
- Bankevich, A. A., Nurk, S. A., Antipov, D. A., Gurevich, A. A. A., Dvorkin, M. A., Kulikov, A. S. A. B., Lesin, V. M. A., Nikolenko, S. I. A. B., Pham, S. C., Pribelski, A. D. A., Pyshkin, A. V. A., Sirotkin, A. V. A., Vyahhi, N. A., Tesler, G. D., Alekseyev, M. A. A. E., & Pevzner, P. A. A. C. (2012). SPAdes: A new genome assembly algorithm and its applications to single-cell sequencing. *JOURNAL OF COMPUTATIONAL BIOLOGY*, 19(5), 455-477.
- Bedrní, E., Jirotková, D., Kadlec, J., Laknerová, I., Vrchotová, N. D., Triska, J., Samková, E., & Smetana, P. (2020). Thermal stability and bioavailability of bioactive compounds after baking of bread enriched with different onion by-products. *FOOD CHEMISTRY*, 319, 923.
- Bhadwal, S., Sharma, S., & SinghDhanwinder (2023). Interactive effects of selenium and arsenic on phenolic constituents and antioxidant activity in rice (*Oryza sativa* L.). *CHEMOSPHERE*, 350(0), 141071.
- Bhagat, J., Zang, L., & Nakayama, H. (2021). Effects of nanoplastic on toxicity of azole fungicides (ketoconazole and fluconazole) in zebrafish embryos. *The Science of the Total Environment*, 800, 149463.
- Bhandari, K., De, B., & Goswami, T. K. (2019). Evidence based seasonal variances in catechin and caffeine content of tea. *SN Applied Sciences*, 1(12), 1-6.
- Bhattacharyya, J., & de Almeida, M. Z. (1985). Isolation of the Constituents of the Rootbark of *Guettarda platypoda*. *JOURNAL OF NATURAL PRODUCTS*, 48(1), 148-149.
- Biswas, S. K. (2016). Does the interdependence between oxidative stress and inflammation explain the antioxidant paradox. *Oxidative Medicine and Cellular Longevity*, 2016, 5698931.
- Chen, H., Yu, F., & Kang, J. (2023). Quality Chemistry, Physiological Functions, and Health Benefits of Organic Acids from Tea (*Camellia sinensis*). *MOLECULES (BASEL, SWITZERLAND)*, 28(5), 2339.

- Chen, Q., Zhu, Y., Liu, Y., Liu, Y., Dong, C., Lin, Z., & Teng, J. (2022). Black tea aroma formation during the fermentation period. *FOOD CHEMISTRY*, *374*, 574.
- Chen, S., Chen, S., Luo, Z., Luo, Z., Zhang, D., & Zhang, D. (2013). Self-pollination in buds and homostyly in *Mussaenda shikokiana* (Rubiaceae), a monomorphic species in a distylous clade. *JOURNAL OF SYSTEMATICS AND EVOLUTION*, *51*(6), 731-742.
- Chen, S., Luo, Z., & Zhang, D. (2014). Pre- and post-zygotic reproductive isolation between co-occurring *Mussaenda pubescens* var. *alba* and *M. shikokiana* (Rubiaceae). *JOURNAL OF INTEGRATIVE PLANT BIOLOGY*, *56*(4), 411-419.
- Chen, W., Yu, K., Bin, L., Lan, Y., Sun, R., Li, Q., He, F., Pan, Q., Duan, C., & Wang, J. (2017). Comparison of transcriptional expression patterns of carotenoid metabolism in 'Cabernet Sauvignon' grapes from two regions with distinct climate. *JOURNAL OF PLANT PHYSIOLOGY*, *213*, 75-86.
- Chen, X., Cai, W., Xia, J., Yu, H., Wang, Q., Pang, F., & Zhao, M. (2020). Metabolomic and Transcriptomic Analyses Reveal that Blue Light Promotes Chlorogenic Acid Synthesis in Strawberry. *JOURNAL OF AGRICULTURAL AND FOOD CHEMISTRY*, *68*(44), 12485-12492.
- Chen, X., Li, M., Ni, J., Hou, J., Shu, X., Zhao, W., Su, P., Wang, D., Shah, F. A., Huang, S., Liu, Z., & Wu, L. (2021). The R2R3-MYB transcription factor SsMYB1 positively regulates anthocyanin biosynthesis and determines leaf color in Chinese tallow (*Sapium sebiferum* Roxb.). *INDUSTRIAL CROPS & PRODUCTS*, *164*, 113335.
- Cheng, J., Liao, L., Zhou, H., Gu, C., Wang, L., & Han, Y. (2015). A small indel mutation in an anthocyanin transporter causes variegated colouration of peach flowers. *JOURNAL OF EXPERIMENTAL BOTANY*, *66*(22), 7227-7239.
- Choi, K. S., & Park, S. (2015). The complete *chloroplast genome* sequence of *Aster spathulifolius* (Asteraceae); genomic features and relationship with Asteraceae. *GENE*, *572*(2), 214-221.
- Chu, C., Du, Y., Yu, X., Shi, J., Yuan, X., Liu, X., Liu, Y., Zhang, H., Zhang, Z., & Yan, N. (2020). Dynamics of antioxidant activities, metabolites, phenolic acids, flavonoids, and phenolic biosynthetic genes in germinating Chinese wild rice (*Zizania latifolia*). *FOOD CHEMISTRY*, *318*, 126483.
- Cui, H., Yu, J., Xia, S., Duhoranimana, E., Huang, Q., & Zhang, X. (2019). Improved controlled flavor formation during heat-treatment with a stable Maillard reaction intermediate derived from xylose-phenylalanine. *FOOD CHEMISTRY*, *271*, 47-53.
- Damiano, S., Forino, M., De, A., Vitali, L. A., Lupidi, G., & Tagliatela-Scafati, O. (2017). Antioxidant and antibiofilm activities of secondary metabolites from *Ziziphus jujuba* leaves used for infusion preparation. *FOOD CHEMISTRY*, *230*, 24-29.
- Daniell, H., Lin, C., Yu, M., & Chang, W. (2016). *Chloroplast genomes*: Diversity, evolution,

- and applications in genetic engineering. *GENOME BIOLOGY*, 17(1), 1-29.
- D'Arcy, M. S. (2019). Cell death: a review of the major forms of apoptosis, necrosis and autophagy. *CELL BIOLOGY INTERNATIONAL*, 43(6), 582-592.
- Das, P. R., Kim, Y., Hong, S., & Eun, J. (2019). Profiling of volatile and non-phenolic metabolites – Amino acids, organic acids, and sugars of green tea extracts obtained by different extraction techniques. *FOOD CHEMISTRY*, 296.
- Deluc, L., Bogs, J., Walker, A. R., Ferrier, T., Decendit, A., Merillon, J., Robinson, S. P., & Barrieu, F. (2020). The Transcription Factor VvMYB5b Contributes to the Regulation of Anthocyanin and Proanthocyanidin Biosynthesis in Developing Grape Berries. *PLANT PHYSIOLOGY*, 147(4), 204-2053.
- Deng, X. D. X., & Zhang, D. Z. D. (2006). Three new synonyms in *Mussaenda* (Rubiaceae) from China. *ACTA PHYTOTAXONOMICA SINICA*(No.5), 608-611.
- Deng, X., & Zhang, D. (2006). Three new synonyms in *Mussaenda* (Rubiaceae) from China. *JOURNAL OF SYSTEMATICS AND EVOLUTION*, 44(5), 608-611.
- Devi, A. M., Devi, K. K., Devi, P. P., Devi, M. L., & Das, S. (2023). Metabolic engineering of plant secondary metabolites: prospects and its technological challenges. *FRONTIERS IN PLANT SCIENCE*, 14, 1171154.
- Dharambir, K., Ajay, S., Hardeep, S. T., Katrin, S., Sandeep, P., & Tapan, K. M. (2017). Kaempferol – A dietary anticancer molecule with multiple mechanisms of action: Recent trends and advancements. *Journal of Functional Foods*, 30, 203-219.
- Dobrogojski, J. D., Adamiec, M. G., & Ski, R. L. (2020). The *chloroplast genome*: a review. *ACTA PHYSIOLOGIAE PLANTARUM*, 42(6), 1-13.
- Dong, H., Li, M., Jin, L., Xie, X., Li, M., & Wei, J. (2022). Cool Temperature Enhances Growth, Ferulic Acid and Flavonoid Biosynthesis While Inhibiting Polysaccharide Biosynthesis in *Angelica sinensis*. *MOLECULES*, 27(1), 320.
- Duan, H., Guo, J., Xuan, L., Wang, Z., Li, M., Yin, Y., & Yang, Y. (2020). Comparative chloroplast genomics of the genus *Taxodium*. *BMC GENOMICS*, 21(1), 1-14.
- Duan, H., Zhang, Q., Wang, C., Li, F., Tian, F., Lu, Y., Hu, Y., Yang, H., & Cui, G. (2021). Analysis of codon usage patterns of the *chloroplast genome* in *Delphinium grandiflorum* L. reveals a preference for AT-ending codons as a result of major selection constraints. *PeerJ*, 9(1), e10787.
- Duan, R., Huang, M., Yang, L., & Liu, Z. (2017). Characterization of the complete *chloroplast genome* of *Emmenopterys henryi* (Gentianales: Rubiaceae), an endangered relict tree species endemic to China. *Conservation Genetics Resources*, 9(3), 459-461.
- Duan, T., Deng, X., Chen, S., Luo, Z., Zhao, Z., Tu, T., Khang, N. S., Razafimandimbison, S. G., & Zhang, D. (2018). Evolution of sexual systems and growth habit in

- Mussaenda* (Rubiaceae): Insights into the evolutionary pathways of dioecy. *MOLECULAR PHYLOGENETICS AND EVOLUTION*, 123, 113-122.
- Duan, T., Gong, W., & Zhang, D. (2012). Development of microsatellite markers from *Mussaenda pubescens* (Rubiaceae). *AMERICAN JOURNAL OF BOTANY*, 99(11), e437-e439.
- DUAN, T., & ZHANG, D. (2016). Fourteen additional microsatellite markers for *Mussaenda pubescens* and cross-species amplification. *JOURNAL OF GENETICS*, 94(1), e44-7.
- Dursun, K., Yusuf, C., & Rizvan, O. (2023). Accumulation of phenolic compounds and expression of phenylpropanoid biosynthesis-related genes in leaves of basil transformed with *A. rhizogenes* strains. *PHYSIOLOGY AND MOLECULAR BIOLOGY OF PLANTS*, 29(5), 629-640.
- Dutt, V., Thakur, S., Dhar, V. J., & Sharma, A. (2010). The genus *Gelsemium*: An update. *Pharmacognosy Reviews*, 4(8), 185-194.
- Falcone Ferreyra, M. L., Rius, S. P., & Casati, P. (2012). Flavonoids: biosynthesis, biological functions, and biotechnological applications. *FRONTIERS IN PLANT SCIENCE*, 3, 222.
- Fan, R., Ma, W., Liu, S., & Huang, Q. (2021). Integrated analysis of three newly sequenced fern *chloroplast genomes*: Genome structure and comparative analysis. *ECOLOGY AND EVOLUTION*, 11(9), 4550-4563.
- Félix, L. M., Luzio, A., Santos, A., Antunes, L. M., Coimbra, A. M., & Valentim, A. M. (2020). MS-222 induces biochemical and transcriptional changes related to oxidative stress, cell proliferation and apoptosis in *zebrafish* embryos. *COMPARATIVE BIOCHEMISTRY AND PHYSIOLOGY*, 237, 108834.
- Fen, W., Yuanfang, Z., Shanyu, F., Shuya, L., & Sisun, L. (2018). Effect of lanthanum chloride on tumor growth and apoptosis in human ovarian cancer cells and xenograft animal models. *Experimental and Therapeutic Medicine*, 16(2), 1143-1148.
- Feng, Z., Li, Y., Li, M., Wang, Y., Zhang, L., Wan, X., & Yang, X. (2019). Tea aroma formation from six model manufacturing processes. *FOOD CHEMISTRY*, 285(0), 347-354.
- Fidan, O., Ren, J., & Zhan, J. (2022). Engineered production of bioactive natural products from medicinal plants. *WORLD JOURNAL OF TRADITIONAL CHINESE MEDICINE*, 8(1), 59-76.
- Gao, J., Ren, R., Wei, Y., Jin, J., Ahmad, S., Lu, C., Wu, J., Zheng, C., Yang, F., & Zhu, G. (2020). Comparative Metabolomic Analysis Reveals Distinct Flavonoid Biosynthesis Regulation for Leaf Color Development of *Cymbidium sinense* 'Red Sun'. *INTERNATIONAL JOURNAL OF MOLECULAR SCIENCES*, 21(5), 1869.
- Gao, M., Huo, X., Lu, L., Liu, M., & Zhang, G. (2023). Analysis of codon usage patterns in

- Bupleurum falcatum chloroplast genome. *CHINESE HERBAL MEDICINES*, 15(2), 284-290.
- Gerber, D. E. (2008). Targeted Therapies: A New Generation of Cancer Treatments. *AMERICAN FAMILY PHYSICIAN*, 77(3), 311-319.
- Gong, L., Yu, L., Gong, X., Wang, C., Hu, N., Dai, X., Peng, C., & Li, Y. (2020). Exploration of anti-inflammatory mechanism of forsythiaside A and forsythiaside B in CuSO₄-induced inflammation in *zebrafish* by metabolomic and proteomic analyses. *JOURNAL OF NEUROINFLAMMATION*, 17(1), 173.
- Grecebio, J. D. A., Ulrich, M., & Sigrid, L. (2016). A Taxonomic Revision of Philippine *Mussaenda* (Rubiaceae, Mussaendeae). *ANNALS OF THE MISSOURI BOTANICAL GARDEN*, 101(3), 457-524.
- Gulzar, F., Fu, J., Zhu, C., Yan, J., Li, X., Meraj, T., Shen, Q., Hassan, B., & Wang, Q. (2021). Maize WRKY Transcription Factor ZmWRKY79 Positively Regulates Drought Tolerance through Elevating ABA Biosynthesis. *INTERNATIONAL JOURNAL OF MOLECULAR SCIENCES*, 22(18), 10080.
- Gunasekaran, S., Sathivelu, M., & Sathivelu, A. (2017). In vitro antioxidant and antibacterial activity of endophytic fungi isolated from *Mussaenda luteola*. *JOURNAL OF APPLIED PHARMACEUTICAL SCIENCE*, 7(8), 197-209.
- Guo, Y., & Gan, S. (2006). AtNAP, a NAC family transcription factor, has an important role in leaf senescence. *THE PLANT JOURNAL*, 46(4), 601-612.
- Hahn, M. E., Timme-Laragy, A. R., Karchner, S. I., & Stegeman, J. J. (2015). Nrf2 and Nrf2-related proteins in development and developmental toxicity: Insights from studies in *zebrafish* (*Danio rerio*). *FREE RADICAL BIOLOGY AND MEDICINE*, 88(Pt B), 275-289.
- Han, H., Qiu, R., Liu, Y., Zhou, X., Gao, C., Pang, Y., & Zhao, Y. (2022). Analysis of Chloroplast Genomes Provides Insights into the Evolution of Agropyron. *FRONTIERS IN GENETICS*, 13, 832809.
- Hao, Y., Zong, X., Ren, P., Qian, Y., & Fu, A. (2021). Basic Helix-Loop-Helix (bHLH) Transcription Factors Regulate a Wide Range of Functions in Arabidopsis. *INTERNATIONAL JOURNAL OF MOLECULAR SCIENCES*, 22(13), 7152.
- He, X. J., Mu, R. L., Cao, W. H., Zhang, Z. G., Zhang, J. S., & Chen, S. Y. (2005). AtNAC2, a transcription factor downstream of ethylene and auxin signaling pathways, is involved in salt stress response and lateral root development. *THE PLANT JOURNAL*, 44(6), 903-916.
- HE, Y., XU, X., & LI, X. (2016). Study on Species and Behaviors of Flower-visiting Insects on *Mussaenda pubescens*. *AGRICULTURAL SCIENCE & TECHNOLOGY*, 17(5), 1200-1203.

- Heike, D., & Dietrich, K. (1995). Strategies for the improvement of secondary metabolite production in plant cell cultures. *ENZYME AND MICROBIAL TECHNOLOGY*, *17*(8), 674-684.
- Hounsome, N., Hounsome, B., Tomos, D., & Edwards-Jones, G. (2008). Plant metabolites and nutritional quality of vegetables. *JOURNAL OF FOOD SCIENCE*, *73*(4), R48-R65.
- House, M. L. (2013). Evaluation of extracts used in traditional Chinese medicine for antiviral potential against herpes simplex virus type 1. (p. 6947948): MIDDLE TENNESSEE STATE UNIVERSITY.
- Hu, D., Sun, C., Ma, Q., You, C., Cheng, L., & Hao, Y. (2016). MdMYB1 Regulates Anthocyanin and Malate Accumulation by Directly Facilitating Their Transport into Vacuoles in Apples. *PLANT PHYSIOLOGY*, *170*(3), 1315-1330.
- Hu, X. Y., Hou, P. F., Li, T. T., Quan, H. Y., Li, M. L., Lin, T., Liu, J. J., Bai, J., & Zheng, J. N. (2018). The roles of Wnt/ β -catenin signaling pathway related lncRNAs in cancer. *INTERNATIONAL JOURNAL OF BIOLOGICAL SCIENCES*, *14*(14), 2003-2011.
- Hu, Y., Chen, X., Feng, X., Woeste, K., & Zhao, P. (2016). Characterization of the complete *chloroplast genome* of the endangered species *Carya sinensis* (Juglandaceae). *CONSERVATION GENETICS RESOURCES*, *8*(4), 467-470.
- Hu, Y., Wang, Q., & Han, F. (2011). Toxicity evaluation of biodegradable chitosan nanoparticles using a *zebrafish* embryo model. *INTERNATIONAL JOURNAL OF NANOMEDICINE*, *6*, 3351.
- Huang, D., Shang, X., Wang, Y., Xiao, L., Ming, R., Zeng, W., Cao, S., Lu, L., Wu, Z., & Yan, H. (2021). Identification of nutritional ingredients and medicinal components of *pueraria lobata* and its varieties using uplc-ms/ms-based metabolomics. *MOLECULES*, *26*(21), 6587.
- Huang, H., Shi, C., Liu, Y., Mao, S., & Gao, L. (2014). Thirteen *Camellia chloroplast genome* sequences determined by high-throughput sequencing: genome structure and phylogenetic relationships. *BMC EVOLUTIONARY BIOLOGY*, *14*(1), 151.
- Huang, Y., Wu, Q., Wang, S., Shi, J., Dong, Q., Yao, P., Shi, G., Xu, S., Deng, R., & Li, C. (2019). FtMYB8 from Tartary buckwheat inhibits both anthocyanin/Proanthocyanidin accumulation and marginal Trichome initiation. *BMC PLANT BIOLOGY*, *19*(1), 1-16.
- Huo, Z., Xu, W., Guo, H., Yang, P., Zhang, Q., Lu, X., & Wang, L. (2022). The complete *chloroplast genome* of *Persicaria perfoliata* and comparative analysis with Four Medicinal Plants of Polygonaceae. *GENOME*, *65*(7), 377-389.
- Huong, L. T., Thao, T. P., Trang, D. T., Lee, J., Tai, B. H., Van Kiem, P., Nhiem, N. X., & Dang, N. H. (2021). Anti-osteoclastogenic cycloartane saponins from *Mussaenda pubescens*. *NATURAL PRODUCT RESEARCH*, *36*(8), 1-8.

- Hyunju Kang, B. K. (2023). Bioactive Compounds as Inhibitors of Inflammation, Oxidative Stress and Metabolic Dysfunctions via Regulation of Cellular Redox Balance and Histone Acetylation State. *FOODS*, 12(5), 925.
- Isao, T., Hidemi, F., Shinichiro, M., Hiroyo, K., Fumiko, N., & Akihiko, I. (2009). Thermal preconditioning prevents fiber type transformation of the unloading induced-atrophied muscle in rats. *JOURNAL OF MUSCLE RESEARCH AND CELL MOTILITY*, 30(3-4), 145-152.
- Islam, F., Raihan, O., Chowdhury, D., Khatun, M., Zuberi, N., Khatun, L., Brishti, A., & Bahar, E. (2015). Apoptotic and antioxidant activities of methanol extract of *Mussaenda roxburghii* leaves. *PAKISTAN JOURNAL OF PHARMACEUTICAL SCIENCES*, 28(6), 2027-2034.
- Jakobek, L., & Blesso, C. (2023). Beneficial effects of phenolic compounds: native phenolic compounds vs metabolites and catabolites. *CRITICAL REVIEWS IN FOOD SCIENCE AND NUTRITION*, 63(10), 1-19.
- James, A., Yao, T., Ma, G., Gu, Z., Cai, Q., & Wang, Y. (2022). Effect of hypobaric storage on Northland blueberry bioactive compounds and antioxidant capacity. *SCIENTIA HORTICULTURAE*, 291, 110609.
- Jansen, R. K., Raubeson, L. A., Boore, J. L., DePamphilis, C. W., Chumley, T. W., Haberle, R. C., Wyman, S. K., Alverson, A. J., Peery, R., Herman, S. J., Fourcade, H. M., Kuehl, J. V., McNeal, J. R., Leebens-Mack, J., & Cui, L. (2005). Methods for obtaining and analyzing whole *chloroplast genome* sequences. *METHODS IN ENZYMOLOGY*, 359, 348-384.
- Jiang, J., Ma, S., Ye, N., Jiang, M., Cao, J., & Zhang, J. (2017). WRKY Transcription Factors in Plant Responses to Stresses. *JOURNAL OF INTEGRATIVE PLANT BIOLOGY*, 59(2), 86-101.
- Jiang, N., Hou, S., & Liu, Y. (2023). Combined LC-MS-based metabolomics and GC-IMS analysis reveal changes in chemical components and aroma components of Jujube leaf tea during processing. *FRONTIERS IN PLANT SCIENCE*, 14, 1179553.
- Jiao, F., Zhao, L., Wu, X., Song, Z., & Li, Y. (2020). Metabolome and transcriptome analyses of the molecular mechanisms of flower color mutation in tobacco. *BMC GENOMICS*, 21(1), 1-10.
- Jiao, Y., Chen, D., Fan, M., & Quek, S. (2019). UPLC-QqQ-MS/MS-based phenolic quantification and antioxidant activity assessment for thinned young kiwifruits. *FOOD CHEMISTRY*, 281, 97-105.
- Judkevich, M. D., Salas, R. M., & Gonzalez, A. M. (2022). Embryology of some flowers of the Gardenieae complex (Rubiaceae). *PROTOPLASMA*, 1-22.

- Kashyap, D., Sharma, A., Tuli, H. S., Sak, K., Punia, S., & Mukherjee, T. K. (2017). Kaempferol - A dietary anticancer molecule with multiple mechanisms of action: Recent trends and advancements. *JOURNAL OF FUNCTIONAL FOODS*, *30*, 203-219.
- Katoh, K., & Standley, D. (2013). MAFFT Multiple Sequence Alignment Software Version 7: Improvements in Performance and Usability. *MOLECULAR BIOLOGY AND EVOLUTION*, *30*(4), 772-780.
- Kexin, W., Yunyun, D., June, Z., Bo, C., Yong, H., Yunlong, M., Keyuan, Z., Guanghua, X., Jing, G., Yi, L., & Huiqiang, L. (2021). Toxicity of thioacetamide and protective effects of quercetin in *zebrafish* (*Danio rerio*) larvae. *ENVIRONMENTAL TOXICOLOGY*, *36*(10), 2062-2072.
- Khan, A., Asaf, S., Khan, A. L., Ahmed, A., Omar, A., AbdulKareem, N. M., Khan, A., Shehzad, T., Alsaady, N., Al-Lawati, A., Al-Rawahi, A., & Shinwari, Z. K. (2019). First complete chloroplast genomics and comparative phylogenetic analysis of *Commiphora gileadensis* and *C. foliacea*: Myrrh producing trees. *PLOS ONE*, *14*(1), e208511.
- Khan, A., Asaf, S., Khan, A. L., Al-Harrasi, A., Al-Sudairy, O., AbdulKareem, N. M., Khan, A., Shehzad, T., Alsaady, N., Al-Lawati, A., Al-Rawahi, A., & Shinwari, Z. K. (2019). First complete chloroplast genomics and comparative phylogenetic analysis of *Commiphora gileadensis* and *C. foliacea*: Myrrh producing trees. *PLOS ONE*, *14*(1), e208511.
- Kim, M. H., Park, K. H., Oh, M. H., Kim, H. H., Choe, K. I., Park, S. H., & Lee, M. W. (2012). Two new hemiterpene glycosides from the leaves of *Ilex rotunda*. *ARCHIVES OF PHARMACAL RESEARCH*, *35*(10), 1779-1784.
- Kuang, G., Wang, L., Yang, L., Zhang, Y., Luo, D., Zhou, Y., Chen, N., Wu, Z., Wang, G., & Li, Y. (2021). One new sesquiterpene pyridine alkaloid from the stems and leaves of *Euonymus fortunei*. *JOURNAL OF ASIAN NATURAL PRODUCTS RESEARCH*, *23*(4), 399-406.
- Kumar, S., Stecher, G., & Tamura, K. (2016). MEGA7: Molecular Evolutionary Genetics Analysis Version 7.0 for Bigger Datasets. *MOLECULAR BIOLOGY & EVOLUTION*, *33*(7), 1870-1874.
- Lai, C., & Chan, Y. (2009). Confirmation of gelsemium poisoning by targeted analysis of toxic gelsemium alkaloids in urine. *JOURNAL OF ANALYTICAL TOXICOLOGY*, *33*(1), 56-61.
- Lanzarin, G., Ven Ncio, C., Félix, L. M., & Monteiro, S. (2021). Inflammatory, Oxidative Stress, and Apoptosis Effects in *Zebrafish* Larvae after Rapid Exposure to a Commercial Glyphosate Formulation. *BIOMEDICINES*, *9*(12), 1784.
- Lanzarin, G., Venâncio, C., Félix, L. M., & Monteiro, S. (2021). Inflammatory, oxidative

- stress, and apoptosis effects in *zebrafish* larvae after rapid exposure to a commercial glyphosate formulation. *BIOMEDICINES*, 9(12), 1784.
- Lee, S. G., Vance, T. M., Nam, T., Kim, D., Koo, S. I., & Chun, O. K. (2016). Evaluation of pH differential and HPLC methods expressed as cyanidin-3-glucoside equivalent for measuring the total anthocyanin contents of berries. *JOURNAL OF FOOD MEASUREMENT AND CHARACTERIZATION*, 10(3), 562-568.
- Leonardo, P. D. S., Karolina, G., Yariv, B., Tohge, T., & Alisdair, F. (2020). The Acetate Pathway Supports Flavonoid and Lipid Biosynthesis in Arabidopsis. *PLANT PHYSIOLOGY*, 182(2), 857-869.
- Li, A., Wu, X., Zhang, D., & Barrett, S. C. H. (2010). Cryptic dioecy in *Mussaenda pubescens* (Rubiaceae): a species with stigma-height dimorphism. *ANNALS OF BOTANY*, 106(4), 521-531.
- Li, C., Xu, Y., Ma, J., Jin, J., Huang, D., Yao, M., Ma, C., & Chen, L. (2016). Biochemical and transcriptomic analyses reveal different metabolite biosynthesis profiles among three color and developmental stages in 'Anji Baicha' (*Camellia sinensis*). *BMC PLANT BIOLOGY*, 16(1), 195.
- Li, C., Xu, Y., Ma, J., Jin, J., Huang, D., Yao, M., Ma, C., & Chen, L. (2016). Biochemical and transcriptomic analyses reveal different metabolite biosynthesis profiles among three color and developmental stages in 'Anji Baicha' (*Camellia sinensis*). *BMC PLANT BIOLOGY*, 16(1), 195.
- Li, C., Zhou, L., Nie, J., Wu, S., Li, W., Liu, Y., & Liu, Y. (2023). Codon usage bias and genetic diversity in *chloroplast genomes* of *Elaeagnus* species (Myrtiflorae: Elaeagnaceae). *PHYSIOLOGY AND MOLECULAR BIOLOGY OF PLANTS*, 29(2), 239-251.
- Li, D., Zhao, C., & Liu, X. (2019). Complete *Chloroplast Genome* Sequences of *Kaempferia Galanga* and *Kaempferia Elegans*: Molecular Structures and Comparative Analysis. *MOLECULES*, 24(3), 474.
- Li, D., Zhao, C., & Liu, X. (2019). Complete *Chloroplast Genome* Sequences of *Kaempferia Galanga* and *Kaempferia Elegans*: Molecular Structures and Comparative Analysis. *MOLECULES*, 24(3), 474.
- Li, D., Zheng, X., Duan, L., Deng, S., Ye, W., Wang, A., & Xing, F. (2017). Ethnobotanical survey of herbal tea plants from the traditional markets in Chaoshan, China. *JOURNAL OF ETHNOPHARMACOLOGY*, 205, 195-206.
- Li, H., Liu, L., Xing, D., & Chen, W. R. (2010). Inhibition of the JNK/Bim pathway by Hsp70 prevents Bax activation in UV-induced apoptosis. *FEBS LETTERS*, 584(22), 4672-4678.
- Li, H., Tiwari, M., Tang, Y., Wang, L., Yang, S., Long, H., Guo, J., Wang, Y., Wang, H., Yang,

- Q., Jagadish, S. V. K., & Shao, R. (2022). Metabolomic and transcriptomic analyses reveal that sucrose synthase regulates maize pollen viability under heat and drought stress. *ECOTOXICOLOGY AND ENVIRONMENTAL SAFETY*, *246*, 114191.
- Li, M., Luo, X., Ho, C., Li, D., Guo, H., & Xie, Z. (2022). A new strategy for grading of Lu'an guapian green tea by combination of differentiated metabolites and hypoglycaemia effect. *FOOD RESEARCH INTERNATIONAL*, *159*, 111639.
- Li, S., Deng, B., Tian, S., Guo, M., CA, H. L., & CA, X. Z. (2021). Metabolic and transcriptomic analyses reveal different metabolite biosynthesis profiles between leaf buds and mature leaves in *Ziziphus jujuba* mill. *FOOD CHEMISTRY*, *347*, 129005.
- Li, W., Luo, F., Wu, X., Fan, B., Yang, M., Zhong, W., Guan, D., Wang, F., & Wang, Q. (2022). Anti-Inflammatory Effects and Mechanisms of Dandelion in RAW264.7 Macrophages and *Zebrafish* Larvae. *Frontiers in Pharmacology*, *13*, 906927.
- Li, W., Wen, L., Chen, Z., Zhang, Z., Pang, X., Deng, Z., Liu, T., & Guo, Y. (2021). Study on metabolic variation in whole grains of four proso millet varieties reveals metabolites important for antioxidant properties and quality traits. *FOOD CHEMISTRY*, *357*, 129791.
- Li, X., Li, Y., Zhao, M., Hu, Y., Meng, F., Song, X., Tigabu, M., Chiang, V. L., Sederoff, R., Ma, W., & Zhao, X. (2021). Molecular and Metabolic Insights into Anthocyanin Biosynthesis for Leaf Color Change in Chokecherry (*Padus virginiana*). *INTERNATIONAL JOURNAL OF MOLECULAR SCIENCES*, *22*(19), 10697.
- Li, X., Li, Y., Zhao, M., Hu, Y., Meng, F., Song, X., Tigabu, M., Chiang, V. L., Sederoff, R., Ma, W., & Zhao, X. (2021). Molecular and metabolic insights into anthocyanin biosynthesis for leaf color change in chokecherry (*Padus virginiana*). *INTERNATIONAL JOURNAL OF MOLECULAR SCIENCES*, *22*(19), 10697.
- Li, X., Li, Y., Zhao, M., Hu, Y., Meng, F., Song, X., Tigabu, M., Chiang, V., Sederoff, R., Ma, W., & Zhao, X. (2021). Molecular and Metabolic Insights into Anthocyanin Biosynthesis for Leaf Color Change in Chokecherry (*Padus virginiana*). *INTERNATIONAL JOURNAL OF MOLECULAR SCIENCES*, *22*(19), 10697.
- Li, Y., Ooi, L. S. M., Wang, H., But, P. P. H., & Ooi, V. E. C. (2004). Antiviral activities of medicinal herbs traditionally used in southern mainland China. *PHYTOTHERAPY RESEARCH*, *18*(9), 718-722.
- Li, Y., Wang, R., Li, Y., Sun, G., & Mo, H. (2022). Protective effects of tree peony seed protein hydrolysate on Cd-induced oxidative damage, inflammation and apoptosis in *zebrafish* embryos. *FISH AND SHELLFISH IMMUNOLOGY*, *126*, 292-302.
- Li, Y., Yang, K., & Long, X. (2022). Toxicity assessment of gelsenicine and the search for effective antidotes. *HUMAN & EXPERIMENTAL TOXICOLOGY*, *41*, 1177.

- Li, Z., Yu, J., Peng, Y., & Huang, B. (2017). Metabolic pathways regulated by abscisic acid, salicylic acid and γ -aminobutyric acid in association with improved drought tolerance in creeping bentgrass (*Agrostis stolonifera*). *PHYSIOLOGIA PLANTARUM*, *159*(1), 42-58.
- Liang, D., Wang, H., Zhang, J., Zhao, Y., & Wu, F. (2022). Complete *Chloroplast Genome* Sequence of *Fagus longipetiolata* Seemen (Fagaceae): Genome Structure, Adaptive Evolution, and Phylogenetic Relationships. *LIFE*, *12*(1), 2022.
- LICHTENTHALER, H. K., & WELLBURN, A. R. (1983). Determinations of total carotenoids and chlorophylls a and b of leaf extracts in different solvents. *BIOCHEMICAL SOCIETY TRANSACTIONS*, *11*(Part 5), 591-592.
- Lightbourn, G. J., Griesbach, R. J., Novotny, J. A., Clevidence, B., Rao, D. D., & Stommel, J. R. (2008). Effects of anthocyanin and carotenoid combinations on foliage and immature fruit color of *Capsicum annum* L. *JOURNAL OF HEREDITY*, *99*(2), 105-111.
- Lin, Y., Liu, P., Liang, W., Hu, Y., Xu, P., Zhou, J., Pu, J., & Zhang, H. (2018). Luteolin-4'-O-glucoside and its aglycone, two major flavones of *Gnaphalium affine* D. Don, resist hyperuricemia and acute gouty arthritis activity in animal models. *PHYTOMEDICINE*, *41*, 54-61.
- Lite, C., Guru, A., Juliet, M., & Arockiaraj, J. (2022). Embryonic exposure to butylparaben and propylparaben induced developmental toxicity and triggered anxiety-like neurobehavioral response associated with oxidative stress and apoptosis in the head of *zebrafish* larvae. *ENVIRONMENTAL TOXICOLOGY*, *37*(8), 1988-2004.
- Liu, C., Pan, J., Yin, Z., Feng, T., Zhao, J., Dong, X., & Zhou, Y. (2022). Integrated transcriptome and metabolome analyses revealed regulatory mechanisms of flavonoid biosynthesis in *Radix Ardisia*. *PEERJ*, *10*, e13670.
- Liu, L., Wang, Y., He, P., Li, P., Lee, J., Soltis, D., & Fu, C. (2018). *Chloroplast genome* analyses and genomic resource development for epilithic sister genera *Oreotrophe* and *Mukdenia* (Saxifragaceae), using genome skimming data. *BMC GENOMICS*, *19*(1), 1-17.
- Liu, M., Burgos, A., Ma, L., Zhang, Q., Tang, D., & Ruan, J. (2017). Lipidomics analysis unravels the effect of nitrogen fertilization on lipid metabolism in tea plant (*Camellia sinensis* L.). *BMC PLANT BIOLOGY*, *17*(1), 1-10.
- Liu, Z., Bruins, M. E., de Bruijn, W. J. C., & Vincken, J. (2020). A comparison of the phenolic composition of old and young tea leaves reveals a decrease in flavanols and phenolic acids and an increase in flavonols upon tea leaf maturation. *JOURNAL OF FOOD COMPOSITION AND ANALYSIS*, *86*, 103385.
- Lou, S., Lai, Y., Huang, J., Ho, C., Ferng, L., & Chang, Y. (2015). Drying effect on flavonoid

- composition and antioxidant activity of immature kumquat. *Taiwanese JOURNAL OF AGRICULTURAL CHEMISTRY AND FOOD SCIENCE*, 171(15), 356-363.
- Lu, C. F., Li, Y. J., Cui, Y. M., Ren, J. S., Qi, F. T., Qu, J. P., Huang, H., & Dai, S. L. (2021). Isolation and Functional Analysis of Genes Involved in Polyacylated Anthocyanin Biosynthesis in Blue Senecio cruentus. *FRONTIERS IN PLANT SCIENCE*, 12, 640746.
- Lu, X. Y., Chen, Z., Gao, J. L., Fu, S. L., Hu, H. R., & Ren, J. (2020). Combined metabolome and transcriptome analyses of photosynthetic pigments in red maple. *Plant physiology and biochemistry: PPB*, 154, 476-490.
- Luiza, K. B., Nascimento, D. S. M., Diniz, D. S. F., Thayres, D. S. L. K., Santos, S. L., Jose, D. A. C., Ayala, V. G., & Rodrigues, M. A. (2022). Flavonoids, anthocyanins, betalains, curcumin, and carotenoids, sources, classification and enhanced stabilization by encapsulation and adsorption. *FOOD RESEARCH INTERNATIONAL*, 153, 110929.
- Luo, C., Huang, W., Sun, H., Yer, H., Li, X., Yang, L., Yan, B., Wang, Q., Wen, Y., Huang, M., & Huang, H. (2021). Comparative *chloroplast genome* analysis of Impatiens species (Balsaminaceae) in the karst area of China: insights into genome evolution and phylogenomic implications. *BMC GENOMICS*, 22, 1-18.
- Luo, Z., Duan, T., Yuan, S., Chen, S., Bai, X., & Zhang, D. (2015). Reproductive isolation between sympatric sister species, *Mussaenda kwangtungensis* and *M. pubescens* var. *alba*. *JOURNAL OF INTEGRATIVE PLANT BIOLOGY*, 57(10), 859-870.
- Ly, S. N., Garavito, A., De Block, P., Asselman, P., Guyeux, C., Charr, J., Janssens, S., Mouly, A., Hamon, P., & Guyot, R. (2020). *Chloroplast genomes* of Rubiaceae: Comparative genomics and molecular phylogeny in subfamily Ixoroideae. *PLOS ONE*, 15(4), e232295.
- M, B. H. (2004). 'The stress of dying': the role of heat shock proteins in the regulation of apoptosis. *JOURNAL OF CELL SCIENCE*, 117(Part 13), 2641-2651.
- Ma, D., Reichelt, M., Yoshida, K., Gershenzon, J., & Constabel, C. (2018). Two R2R3-MYB proteins are broad repressors of flavonoid and phenylpropanoid metabolism in poplar. *PLANT JOURNAL*, 96(5), 949-965.
- Ma, Q., Poopal, R., Zhang, J., Chen, X., & Ren, Z. (2022). Real-time determination of water status upon simultaneous *zebrafish* exposure to sublethal concentrations of CuSO₄. *AQUATIC TOXICOLOGY*, 252, 106296.
- Mao, K., Lu, G., Li, Y., Zang, Y., Zhao, X., Qiu, Q., Qu, M., & Ouyang, K. (2022). Effects of rumen-protected creatine pyruvate on blood biochemical parameters and rumen fluid characteristics in transported beef cattle. *BMC VETERINARY RESEARCH*, 18(1), 35.
- Martens, S., Mateus, N., & Freitas, V. (2014). Special issue on anthocyanins. *PLANTA*, 240(5), 899.

- Mei, X., Wan, S., Lin, C., Zhou, C., Hu, L., Deng, C., & Zhang, L. (2021). Integration of Metabolome and Transcriptome Reveals the Relationship of Benzenoid-Phenylpropanoid Pigment and Aroma in Purple Tea Flowers. *FRONTIERS IN PLANT SCIENCE*, *12*, 762330.
- Mei, X., Zhou, C., Zhang, W., Rothenberg, D. O., Wan, S., & Zhang, L. (2019). Comprehensive analysis of putative dihydroflavonol 4-reductase gene family in tea plant. *PLOS ONE*, *14*(12), e227225.
- Montoro, P., Braca, A., Pizza, C., & De Tommasi, N. (2005). Structure-antioxidant activity relationships of flavonoids isolated from different plant species. *FOOD CHEMISTRY*, *92*(2), 349-355.
- Montoro, P., Braca, A., Pizza, C., & Nunziatina, D. T. (2005). Structure-antioxidant activity relationships of flavonoids isolated from different plant species. *FOOD CHEMISTRY*, *92*(2), 349-355.
- Murugesu, S., Khatib, A., Ahmed, Q. U., Ibrahim, Z., Uzir, B. F., Benchoula, K., Yusoff, N. I. N., Perumal, V., Alajmi, M. F., Salamah, S., & El-Seedi, H. R. (2019). Toxicity study on *Clinacanthus nutans* leaf hexane fraction using *Danio rerio* embryos. *TOXICOLOGY REPORTS*, *6*(C), 1148-1154.
- Nadia, S. (2022). *Zebrafish* as a Model for Neurological Disorders. *INTERNATIONAL JOURNAL OF MOLECULAR SCIENCES*, *23*(8), 4321.
- NavaneethaKrishnan, S., Rosales, J. L., & Lee, K. (2019). ROS-Mediated Cancer Cell Killing through Dietary Phytochemicals. *OXIDATIVE MEDICINE AND CELLULAR LONGEVITY*, *2019*, 9051542.
- Necşulea, A., & Lobry, J. R. (2007). A new method for assessing the effect of replication on DNA base composition asymmetry. *MOLECULAR BIOLOGY AND EVOLUTION*, *24*(10), 2169-2179.
- Nguyen, T. H., Le, H. D., Kim, T. N. T., The, H. P., Nguyen, T. M., Valérie, C., Jér Me, L., & Patrick, K. (2020). Anti-inflammatory and antioxidant properties of the ethanol extract of *Clerodendrum cyrtophyllum* Turcz in copper sulfate-induced inflammation in *zebrafish*. *ANTIOXIDANTS*, *9*(3), 192.
- Nipun, T. S., Khatib, A., Ahmed, Q. U., Nasir, M. H. M., Supandi, F., Taher, M., & Saiman, M. Z. (2021). Preliminary phytochemical screening, in vitro antidiabetic, antioxidant activities, and toxicity of leaf extracts of *Psychotria malayana* Jack. *PLANTS*, *10*(12), 10122688.
- Nyane, N. A., Tlaila, T. B., Malefane, T. G., Ndwandwe, D. E., & Owira, P. M. O. (2017). Metformin-like antidiabetic, cardio-protective and non-glycemic effects of naringenin: Molecular and pharmacological insights. *EUROPEAN JOURNAL OF PHARMACOLOGY*, *803*(0), 103-111.

- Pamanji, R., Yashwanth, B., Bethu, M. S., Leelavathi, S., Ravinder, K., & Rao, J. V. (2015). Toxicity effects of profenofos on embryonic and larval development of *Zebrafish* (*Danio rerio*). *ENVIRONMENTAL TOXICOLOGY AND PHARMACOLOGY*, 39(2), 887-897.
- Panagiota, K., & Manetas, Y. (2006). The importance of being red when young: anthocyanins and the protection of young leaves of *Quercus coccifera* from insect herbivory and excess light. *TREE PHYSIOLOGY*, 26(5), 613-621.
- Pannell, J. R. (2018). Gender specialisation and stigma height dimorphism in Mediterranean *Lithodora fruticosa* (Boraginaceae). *PLANT BIOLOGY*, 20(1), 112-117.
- Park, J. K., Kim, J., Moon Jin, Y., Ahn Eun, Y., Lee Eun, Y., Lee Eun, B., Cho, K., & Song Yeong, W. (2016). Altered lipoproteins in patients with systemic lupus erythematosus are associated with augmented oxidative stress: a potential role in atherosclerosis. *ARTHRITIS RESEARCH AND THERAPY*, 18(1), 306.
- Peng, Y., Wang, K., Cooney, J. M., Wang, T., Espley, R. V., & Allan, A. C. (2019). Differential regulation of the anthocyanin profile in purple kiwifruit (*Actinidia* species). *HORTICULTURE RESEARCH*, 6(1), 3.
- Pessina, A., Di Vincenzo, M., Francesca, M., Francesca, M., Fabiola, O., Basilio, R., Giorgia, G., & Oliana, C. (2021). Polydatin beneficial effects in *zebrafish* larvae undergoing multiple stress types. *INTERNATIONAL JOURNAL OF ENVIRONMENTAL RESEARCH AND PUBLIC HEALTH*, 18(3), 1116.
- Pham, T. X., & Lee, J. (2012). Dietary regulation of histone acetylases and deacetylases for the prevention of metabolic diseases (Review). *NUTRIENTS*, 4(12), 1868-1886.
- Plunkett, B. J., Espley, R., Dare, A. P., Warren, B. A. W., Grierson, E. R. P., Cordiner, S., Turner, J. L., Allan, A. C., & Albert, N. D. K. M. (2018). Myba from blueberry (*vaccinium* section *cyanococcus*) is a subgroup 6 type r2r3myb transcription factor that activates anthocyanin production. *FRONTIERS IN PLANT SCIENCE*, 9, 1300.
- Pompelli, M. F., Fran A, S. C., Tigre, R. C., De Oliveira, M. T., Sacilot, M., & Pereira, E. C. (2013). Spectrophotometric determinations of chloroplastidic pigments in acetone, ethanol and dimethylsulphoxide. *REVISTA BRASILEIRA DE BIOCENCIAS*, 11(1), 52-58.
- Qin, G., & Xu, R. (1998). Recent advances on bioactive natural products from Chinese medicinal plants. *MEDICINAL RESEARCH REVIEWS*, 18(6), 375-382.
- Qiu, J., Ren, C., Fan, J., & Li, Z. (2010). Antioxidant activities of aged oat vinegar in vitro and in mouse serum and liver. *JOURNAL OF THE SCIENCE OF FOOD AND AGRICULTURE*, 90(11), 1951-1958.

- Rai, A., Umashankar, S., & Rai, M. (2016). Coordinate Regulation of Metabolite Glycosylation and Stress Hormone Biosynthesis by TT8 in Arabidopsis. *PLANT PHYSIOLOGY*, 171(4), 2499-2515.
- Rajiv, C., Roy, S. S., Tamreihao, K., Kshetri, P., Singh, T. S., Sanjita, D. H., Sharma, S. K., Ansari, M. A., Devi, E. D., Devi, A. K., Langamba, P., Singh, H. N., Akoijam, R., Tania, C., & Sonia, C. (2021). Anticarcinogenic and antioxidant action of an edible aquatic flora *Jussiaea repens* L. using in vitro bioassays and in vivo zebrafish model. *MOLECULES*, 26(8), 2291.
- Rao, J., Peng, T., Li, N., Wang, Y., Yan, C., Wang, K., & Qiu, F. (2022). Nephrotoxicity induced by natural compounds from herbal medicines - a challenge for clinical application. *CRITICAL REVIEWS IN TOXICOLOGY*, 52(9), 757-778.
- Rattanakan, S., George, I., Haynes, P. A., & CA, G. R. C. (2016). Relative quantification of phosphoproteomic changes in grapevine (*Vitis vinifera* L.) leaves in response to abscisic acid. *HORTICULTURE RESEARCH*, 3, 16029.
- Ravichandran, R. (2002). Carotenoid composition, distribution and degradation to flavour volatiles during black tea manufacture and the effect of carotenoid supplementation on tea quality and aroma. *FOOD CHEMISTRY*, 78(1), 23-28.
- Ren, J., Liu, Z., Chen, W., Xu, H., & Feng, H. (2019). Anthocyanin Degrading and Chlorophyll Accumulation Lead to the Formation of Bicolor Leaf in Ornamental Kale. *INTERNATIONAL JOURNAL OF MOLECULAR SCIENCES*, 20(3), 603.
- Revathi, M., & Jagadeesan, G. (2022). Hepato-Protective effect of Betulinic acid and Rotundic acid on Mercuric Chloride Intoxicated Albino Wistar Rats. *RESEARCH JOURNAL OF PHARMACY AND TECHNOLOGY*, 15(3), 1189.
- Rezaei, M. K., Deokar, A., & Tar'An, B. (2016). Identification and Expression Analysis of Candidate Genes Involved in Carotenoid Biosynthesis in Chickpea Seeds. *Frontiers of Plant Science*, 7, 1867.
- Saeed, M., Naveed, M., Arif, M., Kakar, M., Manzoor, R., Abd El-Hack, M., Alagawany, M., Khandia, R., & Munjal, A. (2017). Green tea (*Camellia sinensis*) and L-theanine: Medicinal values and beneficial applications in humans - A comprehensive review. *BIOMEDICINE AND PHARMACOTHERAPY*, 95(1), 1260-1275.
- Seitz, C., Ameres, S., & Forkmann, G. (2007). Identification of the molecular basis for the functional difference between flavonoid 3'-hydroxylase and flavonoid 3',5'-hydroxylase. *FEBS LETTERS*, 581(18), 3429-3434.
- Sharma, A., Mazumdar, B., & Keshav, A. (2021). Valorization of unsalable Amaranthus tricolour leaves by microwave-assisted extraction of betacyanin and betaxanthin. *BIOMASS CONVERSION AND BIOREFINERY*, 13, 1251-1267.
- Shashni, B., Tamaok, J., Kobayashi, M., & Nagasaki, Y. (2023). Design of a new self-

- assembling antioxidant nanomedicine to ameliorate oxidative stress in *zebrafish* embryos. *ACTA BIOMATERIALIA*, 159, 367-381.
- Shaw, J., Lickey, E. B., Beck, J. T., Farmer, S. B., Liu, W., Miller, J., Siripun, K. C., Winder, C. T., Schilling, E. E., & Small, R. L. (2005). The tortoise and the hare II: Relative utility of 21 noncoding chloroplast DNA sequences for phylogenetic analysis. *AMERICAN JOURNAL OF BOTANY*, 92(1), 142-166.
- Shen, J., Jiang, C., Yan, Y., Liu, B., & Zu, C. (2017). Effect of increased UV-B radiation on carotenoid accumulation and total antioxidant capacity in tobacco (*Nicotiana tabacum* L.) leaves. *GENETICS AND MOLECULAR RESEARCH*, 16(1), 16018438.
- Shen, J., Zou, Z., Zhang, X., Zhou, L., Wang, Y., Fang, W., & Zhu, X. (2018). Metabolic analyses reveal different mechanisms of leaf color change in two purple-leaf tea plant (*Camellia sinensis* L.) cultivars. *HORTICULTURE RESEARCH*, 5(1), 7.
- Shen, R., Ma, Y., Jiang, L., Dong, J., Zhu, Y., & Ren, G. (2018). Chemical composition, antioxidant, and antiproliferative activities of nine Chinese proso millet varieties. *FOOD & AGRICULTURAL IMMUNOLOGY*, 29(1), 625-637.
- Shetty, A. J., Shyamjith, D., & Alwar, M. C. (2007). Acute toxicity studies and determination of median lethal dose. *CURRENT SCIENCE*, 93(7), 917-920.
- Shi, J., Zhang, X., Zhang, Y., Lin, X., Li, B., & Chen, Z. (2020). Integrated metabolomic and transcriptomic strategies to understand the effects of dark stress on tea callus flavonoid biosynthesis. *PLANT PHYSIOLOGY AND BIOCHEMISTRY: PPB*, 115, 549-559.
- Shi, Q., Li, X., Du, J., & Li, X. (2019). Anthocyanin Synthesis and the Expression Patterns of bHLH Transcription Factor Family during Development of the Chinese Jujube Fruit (*Ziziphus jujuba* Mill.). *FORESTS*, 10(4), 346.
- Shinozaki, K., Ohme, M., Tanaka, M., Wakasugi, T., Hayashida, N., Matsubayashi, T., Zaita, N., Chunwongse, J., Obokata, J., Yamaguchi-Shinozaki, K., Ohto, C., Torazawa, K., Meng, B. Y., Sugita, M., Deno, H., Kamogashira, T., Yamada, K., Kusuda, J., Takaiwa, F., Kato, A., Tohdoh, N., Shimada, H., & Sugiura, M. (1986). The complete nucleotide sequence of the tobacco *chloroplast genome*: its gene organization and expression. *THE EMBO JOURNAL*, 5(9), 2043-2049.
- Shylaja, G., Mythili, S., & Sathivelu, A. (2017). In vitro antioxidant and antibacterial activity of endophytic fungi isolated from *Mussaenda luteola*. *JOURNAL OF APPLIED PHARMACEUTICAL SCIENCE*, 7(8), 234-238.
- Song, L., Ma, Q., Zou, Z., Sun, K., Yao, Y., Tao, J., Kaleri, N. A., & Li, X. (2017). Molecular Link between Leaf Coloration and Gene Expression of Flavonoid and Carotenoid Biosynthesis in *Camellia sinensis* Cultivar 'Huangjinya'. *Frontiers in Plant Science*, 8, 803.

- Song, S., Tao, Y., Gao, L., Liang, H., Tang, D., Lin, J., Wang, Y., Jr, F. G. G., & Li, C. (2022). An Integrated Metabolome and Transcriptome Analysis Reveal the Regulation Mechanisms of Flavonoid Biosynthesis in a Purple Tea Plant Cultivar. *FRONTIERS IN PLANT SCIENCE*, 13, 880227.
- SoussiYanicostas, N. (2022). *Zebrafish* as a model for neurological disorders. *INTERNATIONAL JOURNAL OF MOLECULAR SCIENCES*, 23(8), 4321.
- Strähle, U., Scholz, S., Geisler, R., Greiner, P., Hollert, H., Rastegar, S., Schumacher, A., Selderslaghs, I., Weiss, C., Witters, H., & Braunbeck, T. (2012). *Zebrafish* embryos as an alternative to animal experiments—A commentary on the definition of the onset of protected life stages in animal welfare regulations. *REPRODUCTIVE TOXICOLOGY*, 33(2), 128-132.
- Sun, Q., Huang, J., Guo, Y., Yang, M., Guo, Y., Li, J., Zhang, J., & Xu, W. (2020). A cotton NAC domain transcription factor, GhFSN5, negatively regulates secondary cell wall biosynthesis and anther development in transgenic *Arabidopsis*. *PLANT PHYSIOLOGY AND BIOCHEMISTRY*, 146, 303-314.
- Sun, Y., Zhou, M., Luo, L., Pan, H., Zhang, Q., & Yu, C. (2023). Metabolic profiles, bioactive compounds and antioxidant activity of rosehips from Xinjiang, China. *LWT*, 174, 114451.
- Sunantha, K., Florencio, C. R., Thuengtung, S., & Ogawa, Y. (2022). Changes in bioactive compounds and antioxidant activity of plant-based foods by gastrointestinal digestion: a review. *CRITICAL REVIEWS IN FOOD SCIENCE AND NUTRITION*, 62(17), 4684-4705.
- Teame, T., Zhang, Z., Ran, C., Zhang, H., Yang, Y., Ding, Q., Xie, M., Gao, C., Ye, Y., Duan, M., & Zhou, Z. (2019). The use of *zebrafish* (*Danio rerio*) as biomedical models. *Animal Frontiers*, 9(3), 68-77.
- Velaithan, V., Okuda, K. S., Ng, M. F., Samat, N., Leong, S. W., Faudzi, S. M. M., Abas, F., Shaari, K., Cheong, S. C., Tan, P. J., & Patel, V. (2017). *Zebrafish* phenotypic screen identifies novel Notch antagonists. *INVESTIGATIONAL NEW DRUGS*, 35(2), 166-179.
- Velayutham, M., Ojha, B., Issac Praveen, K., Lite, C., Guru, A., Pasupuleti, M., Arasu Mariadhas, V., AlDhabi Naif, A., & Arockiaraj, J. (2021). NV14 from serine O-acetyltransferase of cyanobacteria influences the antioxidant enzymes in vitro cells, gene expression against H₂O₂ and other responses in vivo *zebrafish* larval model. *CELL BIOLOGY INTERNATIONAL*, 45(11), 2331-2346.
- Velayutham, M., Ojha, B., Issac, P. K., Lite, C., Guru, A., Pasupuleti, M., Arasu, M. V., Al-Dhabi, N. A., & Arockiaraj, J. (2021). NV14 from serine O-acetyltransferase of cyanobacteria influences the antioxidant enzymes in vitro cells, gene expression against H₂O₂ and other responses in vivo *zebrafish* larval model. *CELL BIOLOGY*

INTERNATIONAL, 45(11), 2331-2346.

- Vidyalakshmi, K. S., Nagarajan, S., Vasanthi, H. R., & Rajamanickam, V. (2009). Hepatoprotective and antioxidant activity of two iridoids from *Mussaenda "dona aurora"*. *Zeitschrift fur Naturforschung. C, JOURNAL OF BIOSCIENCES*, 64(5-6), 329-334.
- Vidyalakshmi, K. S., Vasanthi, H. R., & Rajamanickam, G. V. (2008). Ethnobotany, Phytochemistry and Pharmacology of *Mussaenda* Species (Rubiaceae). *EBL*, 2008(1), 469-475.
- Vieira, B. C., Bicalho, E. M., Munn-Bosch, S., & Garcia, Q. S. (2017). Abscisic acid regulates seed germination of *Vellozia* species in response to temperature. *PLANT BIOLOGY*, 19(2), 211-216.
- Việt, T. Q., & Trung, V. (2017). Thành phần hóa học của cây *Mussaenda pubescens* (Rubiaceae). *VIETNAM JOURNAL OF CHEMISTRY*, 55(3), 355.
- Wach, A., Pyrzyńska, K., & Biesaga, M. (2005). Quercetin content in some food and herbal samples. *FOOD CHEMISTRY*, 100(2), 699-704.
- Wan, L., Lei, Y., Yan, L., Liu, Y., Pandey, M. K., Wan, X., Varshney, R. K., Fang, J., & Liao, B. (2020). Transcriptome and metabolome reveal redirection of flavonoids in a white testa peanut mutant. *BMC PLANT BIOLOGY*, 20(1), 161.
- Wang, F., Chen, L., Chen, H., Chen, S., Liu, Y., & Santos-Buelga, C. (2019). Analysis of Flavonoid Metabolites in Citrus Peels (*Citrus reticulata* "Dahongpao") Using UPLC-ESI-MS/MS. *MOLECULES*, 24(15), 2680.
- Wang, H., Wang, J., Zhao, K., Fan, W., Zhu, Z., & Wang, H. (2019). Complete plastome sequence of *Mussaenda Hirsutula Miq* (Rubiaceae): An endemic shrub in South China. *Mitochondrial DNA Part B: Resources*, 4(1), 677-678.
- Wang, J. M., & Kang, W. Y. (2013). Aroma volatile compounds in *Mussaenda pubescens*. *CHEMISTRY OF NATURAL COMPOUNDS*, 49(2), 358-359.
- Wang, J., Hu, T., Wang, Y., Wang, W., Hu, H., Wei, Q., Yan, Y., & Bao, C. (2023). Metabolic and Transcriptomic Analyses Reveal Different Metabolite Biosynthesis Profiles between Purple and Green Pak Choi. *INTERNATIONAL JOURNAL OF MOLECULAR SCIENCES*, 24(18), 13781.
- Wang, K., Deng, Y., Zhang, J., Cheng, B., Huang, Y., Meng, Y., Zhong, K., Xiong, G., Guo, J., Liu, Y., & Lu, H. (2021). Toxicity of thioacetamide and protective effects of quercetin in *zebrafish* (*Danio rerio*) larvae. *ENVIRONMENTAL TOXICOLOGY*, 36(10), 2062-2072.
- Wang, N. A., Chen, S. A., Xie, L. A., Wang, L. A., Feng, Y. A., Lv, T. A., Fang, Y. A., & Ding, H. A. (2022). The complete *chloroplast genomes* of three Hamamelidaceae species: Comparative and phylogenetic analyses. *ECOLOGY & EVOLUTION*, 12(2), 1-21.

- Wang, S., Han, X., Yu, T., Liu, Y., Zhang, H., Mao, H., Hu, C., & Xu, X. (2022). Isoprocarb causes neurotoxicity of zebrafish embryos through oxidative stress-induced apoptosis. *ECOTOXICOLOGY AND ENVIRONMENTAL SAFETY*, 242, 113870.
- Wang, Y., Tian, J., Shi, F., Li, X., Hu, Z., & Chu, J. (2021). Protective effect of surfactin against copper sulfate-induced inflammation, oxidative stress and hepatic injury in zebrafish. *MICROBIOLOGY AND IMMUNOLOGY*, 65(10), 410-421.
- Wang, Y., Wang, H., Wu, S., Li, D., & Chen, S. (2017). Effect of Gelsemium elegans and *Mussaenda pubescens*, the Components of a Detoxification Herbal Formula, on Disturbance of the Intestinal Absorptions of Indole Alkaloids in Caco-2 Cells. *Evidence-based Complementary and Alternative Medicine*, 2017, 1-10.
- Wang, Z. G., Ying, X. G., Gao, P., Wang, C. L., Wang, Y. F., Yu, X. W., Chen, J., Wang, B., & Luo, H. Y. (2019). Anti-Inflammatory Activity of a Peptide from Skipjack (*Katsuwonus pelamis*). *MARINE DRUGS*, 17(10).
- Wang, Z., Sun, W., Yu, D., Zhao, Y., Xu, H., He, Y., & Li, H. (2018). Rotundic acid enhances the impact of radiological toxicity on MCF-7 cells through the ATM/p53 pathway. *INTERNATIONAL JOURNAL OF ONCOLOGY*, 53(5), 2269-2277.
- Warren, C. R. (2008). Rapid Measurement of Chlorophylls with a Microplate Reader. *JOURNAL OF PLANT NUTRITION*, 31(7), 1321-1332.
- Wei, C., Yang, H., Wang, S., Zhao, J., Liu, C. L. C., Gao, L., Xia, E., Lu, Y., Tai, Y., & She, G. (2018). Draft genome sequence of *Camellia sinensis* var. *sinensis* provides insights into the evolution of the tea genome and tea quality. *PROCEEDINGS OF THE NATIONAL ACADEMY OF SCIENCES OF THE UNITED STATES OF AMERICA*, 115(18), 4151-4158.
- Winkel-Shirley, B. (2001). Flavonoid biosynthesis. A colorful model for genetics, biochemistry, cell biology and biotechnology. *PLANT PHYSIOLOGY*, 126(2), 485-493.
- Zhao, W., Wang P., Xu R., Qin G., Jiang S., Wu H. (1995). Saponins from *Mussaenda pubescens*. *PHYTOCHEMISTRY*, 39(1), 191-193.
- Wu, L., Nie, L., Wang, Q., Xu, Z., Wang, Y., He, C., Song, J., & Yao, H. (2021). Comparative and phylogenetic analyses of the chloroplast genomes of species of Paeoniaceae. *SCIENTIFIC REPORTS*, 11(1), 14643.
- Wu, L., Nie, L., & Xu, Z. (2020). Comparative and Phylogenetic Analysis of the Complete Chloroplast Genomes of Three Paeonia Section Moutan Species (Paeoniaceae). *FRONTIERS IN GENETICS*, 11, 980.
- Wu, Y., Wang, W., Yao, G., Jiang, X., Zhang, Y., & Song, S. (2018). Antioxidant phenolic acids from the leaves of *Armeniaca sibirica*. *JOURNAL OF ASIAN NATURAL PRODUCTS RESEARCH*, 20(10), 969-976.

- Xie, J., Sun, Y., Cao, Y., Han, L., Li, Y., Ding, B., Gao, C., Hao, P., Jin, X., Chang, Y., Song, J., Yin, D., & Ding, J. (2022). Transcriptomic and Metabolomic Analyses Provide Insights into the Growth and Development Advantages of Triploid *Apostichopus japonicus*. *MARINE BIOTECHNOLOGY*, *24*(1), 151-162.
- Xiong, T., Zeng, J., Chen, L., Wang, L., Gao, J., Huang, L., Xu, J., Wang, Y., & He, X. (2024). Anti-Inflammatory Terpenoids from the Rhizomes of Shell Ginger. *JOURNAL OF AGRICULTURAL AND FOOD CHEMISTRY*, *71*(1), 424-436.
- Xu, C., Liang, L., Li, Y., Yang, T., Fan, Y., Mao, X., & Wang, Y. (2021). Studies of quality development and major chemical composition of green tea processed from tea with different shoot maturity. *LWT - FOOD SCIENCE & TECHNOLOGY*, *142*, 111055.
- Xu, H., Miao, X., Wang, W., Wang, G., & Li, Y. (2022). Transcriptome analysis reveals the early resistance of *zebrafish* larvae to oxidative stress. *FISH PHYSIOLOGY AND BIOCHEMISTRY*, *48*(4), 1075-1089.
- Xu, H., Miao, X., Wang, W., & Li, G. W. A. Y. (2022). Transcriptome analysis reveals the early resistance of *zebrafish* larvae to oxidative stress. *FISH PHYSIOLOGY AND BIOCHEMISTRY*, *48*(4), 1075-1089.
- XU, J., XU, R., LUO, Z., DONG, J., & HU, H. (1992). Mussaendosides M and N, New Saponins from *Mussaenda pubescens*. *JOURNAL OF NATURAL PRODUCTS*, *55*(8), 1124-1128.
- Xu, R., Zhao, W., Xu, J., Shao, B., & Qin, G. (1996). Studies on bioactive saponins from Chinese medicinal plants. *ADVANCES IN EXPERIMENTAL MEDICINE AND BIOLOGY*, *404*, 371-382.
- Xu, Y., Qiu, H., Liu, H., Liu, M., Huang, Z., Yang, J., Su, Y., & Yu, C. (2012). Effects of koumine, an alkaloid of *Gelsemium elegans* Benth., on inflammatory and neuropathic pain models and possible mechanism with allopregnanolone. *Pharmacology, BIOCHEMISTRY AND BEHAVIOR*, *101*(3), 504-514.
- Xue, S., Shi, T., Luo, W., Ni, X., Iqbal, S., Ni, Z., Huang, X., Yao, D., Shen, Z., & Gao, Z. (2019). Comparative analysis of the complete *chloroplast genome* among *Prunus mume*, *P. armeniaca*, and *P. salicina*. *HORTICULTURE RESEARCH*, *6*(1), 89.
- Yan, X., Pang, P., Qin, C., Mi, J., Yang, L., Yang, B., & Nie, G. (2023). Improvement of sea buckthorn (*Hippophae rhamnoides* L.) flavonoids on the antioxidant and immune performance of Yellow River carp (*Cyprinus carpio* L.) fed high-carbohydrate diet. *FISH & SHELLFISH IMMUNOLOGY*, *144*, 109289.
- Yan, Y., Liu, Q., Yan, K., Wang, X., & Xu, P. (2022). Transcriptomic and metabolomic analyses reveal how girdling promotes leaf color expression in *Acer rubrum* L. *BMC PLANT BIOLOGY*, *22*(1), 498.

- Yang, J., Yang, S., Li, H., Yang, J., & Li, D. (2013). Comparative *Chloroplast Genomes* of *Camellia* Species. *PLOS ONE*, *8*(8), 1.
- Yang, L., Yang, C., Li, C., Zhao, Q., Liu, L., Fang, X., & Chen, X. (2016). Recent advances in biosynthesis of bioactive compounds in traditional Chinese medicinal plants. *SCIENCE BULLETIN*, *61*(1), 3-17.
- Yao, X., Tang, P., Li, Z., Li, D., Liu, Y., & Huang, H. (2015). The First Complete *Chloroplast Genome* Sequences in Actinidiaceae: Genome Structure and Comparative Analysis. *PLOS ONE*, *10*(6), e129347.
- Ye, J., Ye, Y., Yin, J., Jin, J., Liang, Y., Liu, R., Tang, P., & CA, Y. X. (2022). Bitterness and astringency of tea leaves and products: Formation mechanism and reducing strategies. *TRENDS IN FOOD SCIENCE & TECHNOLOGY*, *123*, 130-143.
- Yen, L., Kousar, M., & Park, J. (2023). Comparative Analysis of *Chloroplast Genome* of *Desmodium stryacifolium* with Closely Related Legume Genome from the Phaseoloid Clade. *INTERNATIONAL JOURNAL OF MOLECULAR SCIENCES*, *24*(7), 6072.
- Yuan, H., Zhang, J., Nageswaran, D., & Li, L. (2015). Carotenoid metabolism and regulation in horticultural crops. *HORTICULTURE RESEARCH*, *2*, 15036.
- Yuan, S. Y. S., Chen, S. C. S., Deng, X. D. X., Duan, T. D. T., Luo, Z. L. Z., & Zhang, D. Z. D. (2017). Pollen–ovule ratios are strongly correlated with floral reciprocity, in addition to sexual system, in *Mussaenda* (Rubiaceae). *NORDIC JOURNAL OF BOTANY*, *35*(4), 395-403.
- Zhang, D., Gao, F., Jakovli, I., Zou, H., Zhang, J., Li, W. X., & Wang, G. T. (2020). PhyloSuite: An integrated and scalable desktop platform for streamlined molecular sequence data management and evolutionary phylogenetics studies. *MOLECULAR ECOLOGY RESOURCES*, *20*(1), 348-355.
- Zhang, D., Yuan, S., Xu, F., Zhu, F., Yuan, M., Ye, H., Guo, H., Lv, X., Yin, Y., & Lin, H. (2016). Light intensity affects chlorophyll synthesis during greening process by metabolite signal from mitochondrial alternative oxidase in *Arabidopsis*. *Plant, CELL & ENVIRONMENT*, *39*(1), 12-25.
- Zhang, M., Yang, Y., Yuan, H., Hua, J., Deng, Y., Jiang, Y., & Wang, J. (2020). Contribution of addition theanine/sucrose on the formation of chestnut-like aroma of green tea. *LWT - FOOD SCIENCE & TECHNOLOGY*, *129*, 109512.
- Zhang, Q., Wang, L., Liu, Z., Zhao, Z., Zhao, J., Wang, Z., Zhou, G., Liu, P., & Liu, M. (2020). Transcriptome and metabolome profiling unveil the mechanisms of *Ziziphus jujuba* Mill. peel coloration. *FOOD CHEMISTRY*, *312*, 8146.
- Zhang, Q., Wang, L., Wang, Z., Liu, Z., Zhao, Z., Zhou, G., Liu, M., & Liu, P. (2020). Variations of the nutritional composition of jujube fruit (*Ziziphus jujuba* Mill.)

- during maturation stages. *INTERNATIONAL JOURNAL OF FOOD PROPERTIES*, 23(1), 1066-1081.
- Zhang, Q., Zhai, J., Shao, L., Lin, W., & Peng, C. (2019). Accumulation of Anthocyanins: An Adaptation Strategy of *Mikania micrantha* to Low Temperature in Winter. *Frontiers in Plant Science*, 10, 1049.
- Zhang, Z., Zhang, Y., Wang, Y., Zhang, Q., Yan, X., Di, Y. D., He, H., & Hao, X. (2012). Three novel beta-carboline alkaloids from *Gelsemium elegans*. *FITOTERAPIA*, 83(4), 704-708.
- Zhao, M., Li, J., Zhu, L., Chang, P., Li, L., & Zhang, L. (2019). Identification and characterization of MYB-bHLH-WD40 regulatory complex members controlling anthocyanidin biosynthesis in blueberry fruits development. *GENES*, 10(7), 496.
- Zhao, W. Z. W., Wang, P. W. P., Xu, R. X. R., Qin, G. Q. G., Jiang, S. J. S., & Wu, H. W. H. (1996). Saponins from *mussaenda pubescens*. *PHYTOCHEMISTRY*, 42(3), 827-830.
- Zhao, W. Z. W., Wolfender, J. W. J., Hostettmann, K. H. K., Cheng, K. C. K., Xu, R. X. R., & Qin, G. Q. G. (1997). Triterpenes and triterpenoid saponins from *Mussaenda pubescens*. *PHYTOCHEMISTRY*, 45(5), 1073-1078.
- ZHAO, W. Z. W., XU, J. X. J., QIN, G. Q. G., XU, R. X. R., WU, H. W. H., & WENG, G. W. G. (1994). New Triterpenoid Saponins from *Mussaenda pubescens*. *JOURNAL OF NATURAL PRODUCTS*, 57(12), 1613-1618.
- Zhao, W. Z. W., Xu, R. X. R., Qin, G. Q. G., Vaisar, T. V. T., & Lee, M. L. M. (1996). Saponins from *Mussaenda pubescens*. *PHYTOCHEMISTRY*, 42(4), 1131-1134.
- Zhao, W., Xu, R., Qin, G., Wu, H., Jiang, S., & Yang, G. (1996). A New Phenolic Glycoside from *Mussaenda pubescens*. *NATURAL PRODUCT SCIENCES*, 2(1), 14-18.
- Zhao, W., Yang, G., Xu, R., & Qin, G. (1996). New Saponins from *Mussaenda pubescens*. *NATURAL PRODUCT LETTERS*, 8(2), 119-126.
- Zhao, X., Li, P., Zuo, H., Peng, A., Lin, J., Li, P., Wang, K., Tang, Q., Tadege, M., Liu, Z., & Zhao, J. (2023). CsMYBL2 homologs modulate the light and temperature stresses-mediated anthocyanin and catechins biosynthesis in tea plants (*Camellia sinensis*). *THE PLANT JOURNAL*, 16279.
- Zhao, X., Ren, X., Zhu, R., Luo, Z., & Ren, B. (2016). Zinc oxide nanoparticles induce oxidative DNA damage and ROS-triggered mitochondria-mediated apoptosis in *zebrafish* embryos. *AQUATIC TOXICOLOGY*, 180, 56-70.
- Zhao, X., Wang, S., Wu, Y., You, H., & Lv, L. (2013). Acute ZnO nanoparticles exposure induces developmental toxicity, oxidative stress and DNA damage in embryonic larval *zebrafish*. *AQUATIC TOXICOLOGY*, 136-137, 49-59.
- Zhao, Y., Sun, Z., Du, H., Bi, C., Meng, J., & Cheng, Y. (2022). A Novel Centerline Extraction

- Method for Overlapping Fish Body Length Measurement in Aquaculture Images. *AQUACULTURAL ENGINEERING*, 99, 102302.
- Zheng, X. T., Yu, Z. C., Tang, J. W., Cai, M. L., Chen, Y. L., Yang, C. W., Chow, W. S., & Peng, C. L. (2021). The major photoprotective role of anthocyanins in leaves of *Arabidopsis thaliana* under long-term high light treatment, Antioxidant or light attenuator. *PHOTOSYNTHESIS RESEARCH*, 149, 25-40.
- Zhou, C., Hu, L., Mu, R., Mei, X., Wu, X., Wang, C., & Zhou, X. (2022). Compound green tea (CGT) regulates lipid metabolism in high-fat diet induced mice. *RSC ADVANCES*, 12(37), 24301-24310.
- Zhou, C., Mei, X., Rothenberg, D. O., Yang, Z., Zhang, W., Wan, S., Yang, H., & Zhang, L. (2020). Metabolome and Transcriptome Analysis Reveals Putative Genes Involved in Anthocyanin Accumulation and Coloration in White and Pink Tea (*Camellia sinensis*) Flower. *MOLECULES*, 25(1), 190.
- Zhou, C., Zhou, X., Dai, T., Wen, Z., Guo, X., Song, Y., Long, L., Li, Y., & Mei, X. (2021). Chloroplast genome structure and phylogenetic position of *Lophatherum gracile*. *MITOCHONDRIAL DNA. PART B, RESOURCES*, 6(1), 26-28.
- Zhou, H., Cao, H., Zheng, Y., Lu, Z., Chen, Y., Liu, D., Yang, H., Quan, J., Huo, C., Liu, J., & Yu, L. (2020). Liang-Ge-San, a classic traditional Chinese medicine formula, attenuates acute inflammation in *zebrafish* and RAW 264.7 cells. *JOURNAL OF ETHNOPHARMACOLOGY*, 249, 112427.
- Zhou, Q., Sun, W., & Lai, Z. (2016). Differential expression of genes in purple-shoot tea tender leaves and mature leaves during leaf growth. *JOURNAL OF THE SCIENCE OF FOOD & AGRICULTURE*, 96(6), 1982-1989.
- Zoupa, M., Machera, K., & Legler, J. (2017). *Zebrafish* as an Alternative Vertebrate Model for Investigating Developmental Toxicity-The Triadimefon Example. *INTERNATIONAL JOURNAL OF MOLECULAR SCIENCES*, 18(4), 817.

BIOGRAPHY

Mr. Caibi ZHOU was born on August, 1986 in An Long County, GUIZHOU province, China. He received his Bachelor Degree of Tea Science from Yangtze University, China in Jun 2012. Then, he received his Master Degree of Tea Science from South China Agricultural University, China in Jun 2015. He started his career as an Experimental administrator and Research Assistant in Department of Tea science, College of Horticultural, South China Agricultural University, China from July 2015 - Jun 2016. Then, in the same year, he as a tea science teacher joined College of Biological Science and Agriculture, Qiannan Normal University for Nationalities. He was appointed as an assistant professor in December 2018, associate professor in December 2020, and professor in December 2022. In November, 2020, he pursued in a PhD program in School of Crop Production Technology, Institute of Agricultural Technology, Suranaree University of Technology, Nakhon Ratchasima, Thailand.

